Interaction between Vinyl Acetate-Ethylene Latex stabilized with Polyvinyl Alcohol and Portland Cement

vorgelegt von
M. Sc. Yu Jin
aus Wuhan, V.R. China

von der Fakultät VI – Planen Bauen Umwelt
der Technischen Universität Berlin
zur Erlangung des akademischen Grades

Doktor der Ingenieurwissenschaften
- Dr. -Ing. -

genehmigte Dissertation

Promotionsausschuss:

Vorsitzender: Prof. Dr. Frank U. Vogdt
Gutachter: Prof. Dr. habil. Oliver Weichold
Gutachter: Prof. Dr. habil. Dietmar Stephan
Gutachter: Dr. habil. Wolf-Dieter Hergeth

Tag der wissenschaftlichen Aussprache: 07.10.2015

Berlin 2016

Acknowledgements

First I would like to express my heartfelt gratitude to Prof. Dr. Dietmar Stephan for giving me the opportunity to conduct my doctoral work at the chair of building materials and construction chemistry at TU Berlin, especially I experienced a dark period before that. I acknowledge him for all the supervision, supports and valuable discussion throughout my thesis, as well as the confidence he placed on my work. I also owe my gratitude to my second supervisor Dr. Dieter-Wolf Hergeth from Wacker Chemie AG for his unreserved pass of knowledge. Many part of the thesis would not have been possible without his support and guidance. I benefit a lot from their supervisions and experienced considerable progress on how to conduct scientific work.

I also would like to thank DAAD (Deutscher Akademischer Austauschdienst) for financial assistance during my study. Personally, I deeply appreciate the support from David Hildebrand when he worked at DAAD.

I like to take this opportunity to express my thanks to the following people at the chair:

Jessica Grewe, Anja Städtke, David Dahnacke for their technical assistance; Agnieszka Kowalczyk from Kiwa for help on ICP; Annekathrin Aisch for all the administrative stuffs; Dr. Christian Lehmann for his guidance, especially on XRD; Gerrit Land for his help on isothermal calorimetry and TGA; Kai Amrhein, Ricarda Tänza, Sameena Kamaruddin, Dr. Sang-Yeop Chung, Dr. Mohamed Abd Elrahman, Henning von Daake, Clemens Ehm, Veronika Märkl, Claudia Schatz, Nick Schneider, Kasra Shafiei, Sandra Wiegel for the nice collegial atmosphere; in special, Kai Foth and Maria Grüneberger for all the help as well as those pleasant conversations.

I also like to take this opportunity to express my thanks to the following people at Wacker Chemie AG when I carried out my experiments there:

Dr. Ulf Dietrich, Dr. Ingo Müller, Stephan Hesel for the helpful discussions and advices; Alexander Kraft for the help on ESEM and AFm; Barbara Hager, Gabriele Weibel, Florian Braunsperger for their help in the lab.

Serina Ng, Mirko Gruber, Elina Dubina, Ahmed Habbaba, Oksana Storcheva, many thanks to their encouragement and help which make me survive through all the bad times in Munich. Likewise, all the good times with them are memorable. Yuanyuan Zhang, Jianwei Mao, Huiran Tang, Xiaohan Liu, Yue Liu, many thanks to their friendship to make my stay here such a pleasant experience.

Lastly, I would like to thank my parents for their understanding and always support, especially I go to a far distance where I am not able to pay my due services to them. I owe my gratitude to my parents in law for their understanding and support, especially they take the responsibility

to raise my son, as in my absence. I also owe my deeply gratitude to my lovely wife Xueye Zheng for all her sacrifice and love. Without all of you, this would have been possible.

Abstract

The purpose of this thesis was to investigate the interaction between the Vinyl-Acetate Ethylene (VAE) latex stabilised with Polyvinyl Alcohol (PVOH) and Portland cement. This interaction was divided into three stages: (1) colloidal interaction at the beginning, (2) hydration of cement in the presence of polymers, and (3) film formation of the latex in cementitious environment.

In the first stage, the colloidal interaction between two VAE latices stabilized by PVOH and Portland cement, including its main mineral phases, was investigated. The non-ionic VAE latex particles showed negative charge but had no affinity to Ca^{2+} by means of charge titration. Adsorption profiles were determined via the depletion method; the results indicated the analogous Langmuir type adsorption. The Zeta potential results showed a negligible effect of the VAE latex particles, indicating that the non-electrostatic interaction was dominant. Meanwhile, PVOH revealed preferential interaction with the aluminate phase. As a consequence, the strong interaction led to the flocculation of the latices in some extreme cases, e.g. in the C_3A suspension.

In the second stage, the divergent influence of the latex particles and PVOH on the hydration kinetics was confirmed by means of isothermal heat flow calorimetry, ICP-OES as well as in-situ XRD measurements. In accordance with the initial interaction, latex particles influenced the silicate phase hydration principally, while PVOH affected the aluminate hydration. Although the equilibrium concentration of SO_4^{2-} was lower in the presence of polymers during the first few hours, the strong 'sulfate depletion' peak in the heat flow calorimetry was subjected to the enhanced reaction between the aluminate and sulphate carrier, which was hindered by PVOH at the beginning.

In the third stage, the latex formed a film in the cementitious environment. Film formation was characterized in terms of its surface morphology, which was investigated by means of environmental scanning electron microscopy and atomic force microscopy. The coalescence of the polymer was indicated by its redispersibility. The latex films were stored under 85% relative humidity (R.H.), or coated on cement substrate under 50% R.H., or casted from the dispersions in synthetic cement pore solution (SCPS). Results showed that film formation was accelerated in the cementitious environment and that removal of PVOH in the vicinity of the latex particles by the interaction with cement was essential for polymer interdiffusion and coalescence.

Zusammenfassung

Das Ziel dieser Arbeit war, die Wechselwirkung zwischen der Vinyl-Acetat-Ethylen (VAE) Polymerdispersion mit Polyvinylalkohol (PVOH) als Schutzkolloid und Portlandzement zu untersuchen. Die Wechselwirkung wurde in drei Phasen unterteilt: (1) kolloidale Wechselwirkung am Anfang, (2) Hydratation des Zements in Gegenwart von Polymeren, und (3) Filmbildung der Polymerdispersionen in zementhaltiger Umgebung.

In der ersten Phase wurde die kolloidale Wechselwirkung zwischen zwei VAE Dispersionen mit PVOH und Portlandzement untersucht. Die nichtionischen VAE Partikel wiesen negative Ladung, aber keine während der Ladungstitration nachweisbare Affinität zu Ca^{2+} auf. Die Adsorptionsprofile wurden mittels Verarmungsmethode gemessen und waren analog zum Adsorptionsprofil nach Langmuir. Dabei war die an Zementminerale adsorbierte Menge unabhängig von der Ladungsdichte. Außerdem zeigte das Ergebnis der Zeta-Potentialmessung eine vernachlässigbare Wirkung der Polymerpartikel, was auf eine Dominanz der nicht-elektrostatischen Wechselwirkung hinweist. PVOH hingegen wechselwirkt vorzugsweise mit der Aluminatphase. In einigen extremen Fällen führen die starken Wechselwirkungen zu einer Flockung der Polymerdisperisonen, z. B. bei der C_3A-Suspension.

In der zweiten Phase konnten mittels isothermer Wärmeflusskalorimetrie, ICP-OES und *in situ* XRD-Messungen die unterschiedlichen Einflüsse von Polymerpartikeln und PVOH auf die Hydratationskinetik nachgewiesen werden. Wie die Ergebnisse aus Phase (1) vermuten lassen, beeinflussten die Polymerpartikel hauptsächlich die Hydratation des Silikats, während PVOH Auswirkungen auf die Hydratation des Aluminats hatte. Obwohl die Gleichgewichtskonzentration von SO_4^{2-} in der Gegenwart von Polymeren in den ersten Stunden niedriger war, wurde der starke Sulfatpeak der der Wärmeflusskalorimetrie durch die verbesserte Reaktion zwischen Aluminat und Sulfatträger hervorgerufen, die zu Beginn durch PVOH behindert wurde.

In der dritten Phase wurde der Polymerfilm in zementhaltiger Umgebung gebildet. Die Filmbildung wurde in Bezug auf die Oberflächenmorphologie charakterisiert, die mittels *Environmental Scanning Electron Microscope* und Rasterkraftmikroskopie untersucht wurde. Dabei wurde das Zusammenwachsen des Polymers auf seine Redispergierbarkeit hingewiesen. Die Polymerfilme wurden unter 85% relativer Feuchte (r. F.) aufbewahrt, bei 50% als Schicht auf den Zementstein aufgebracht oder aus den Dispersionen in synthetischen Porenlösung gegossen. Die Ergebnisse zeigten, dass die Filmbildung in zementhaltiger Umgebung beschleunigt wurde und das Entfernen von PVOH aus der Umgebung der

Polymerpartikel durch die Wechselwirkung mit Zement unerlässlich für den Prozess des Zusammenwachsens des Polymers war.

Abbreviation and Symbols

Γ	Adsorption amount
ε	Dielectric constant
ε_0	Permittivity of free space
ζ	Zeta potential
η	Dynamic viscosity
θ	Surface coverage
μ	Mobility
μ_e	Electrical mobility
ρ	Density
σ	Surface charge density
Ψ	Surface potential
A	Hamaker constant
a	Radius of spherical particles
c_i	Molarity of the i th ion
k_B	Boltzmann constant
N_A	Avogadro's number
R	Gas constant
z_i	Valence of the i th ion
AFM	Atomic Force Microscopy
AMPS	2-Acrylamido-2-methylpropane sulfonic acid
BET	Brunauer-Emmett-Teller
C	Coulomb
c	Concentration
DP	Degree of Polymerization
DLVO	Derjaguin-Landau-Verwey-Overbeek
DSC	Differential Scanning Calorimetry
E	Ethylene
ESEM	Environmental Scanning Electron Microscopy
FTIR	Fourier Transfer Infrared spectroscopy
h	Hour
IAP	Ion activity products
ICP-AES	Inductively Coupled Plasma - Atomic Emission Spectroscopy
MFFT	Minimum Film Formation Temperature

min	Minute
mol	Molar
mV	Millivolt
M_w	weight-average molecular weight
p/c	Polymer cement ratio
PCC	Polymer Cement Concrete
PCD	Particle Charge Detector
PDADMAC	Poly(diallyldimethylammoniumchloride)
PMC	Polymer Modified Cement
p/m	Polymer mineral ratio
PS	Polystyrene
PSD	Particle Size Distribution
PVA	Poly(Vinyl Alcohol)
PVAL	Poly(Vinyl Alcohol)
PVOH	Partially hydrolyzed poly(vinyl acetate -co- vinyl alcohol)
R_H	Hydrodynamic radius
rpm	Revolutions per minute
SCPS	Synthetic Cement Pore Solution
SEM	Scanning Electron Microscopy
SI	Saturation Indices
T_g	Glass transition temperature
TGA	Thermogravimetric Analysis
TOC	Total Organic Carbon
VA	Vinyl Acetate homopoylmer
VAE	Vinyl Acetate-Ethylene copolymer
VDW	Van der Waals force
VeoVa	Vinyl versatate
w/c	Water cement ratio
w/m	Water mineral ratio
w/s	Water solid ratio
XRD	X-ray Diffraction

Nomenclature of cement chemistry

In cement chemistry, chemical composition of the mineral phase is presented in a short form. It is based on the abbreviation of the oxides by employing the first letter, instead of the element symbols. All elements are represented in their highest oxidation state.

Name (mineral name)	Composition	Abbreviation
Calcium oxide (lime)	CaO	C
Silicon dioxide (silica)	SiO_2	S
Aluminum oxide (alumina)	Al_2O_3	A
Iron oxide	Fe_2O_3	F
Sulfur trioxide	SO_3	$\overline{S}$
Water	H_2O	H
Dicalcium silicate (belite)	$2CaO \cdot SiO_2$, Ca_2SiO_4	C_2S
Tricalcium silicate (alite)	$3CaO \cdot SiO_2$, $Ca_3(SiO_4)O$	C_3S
Tricalcium aluminate (aluminate)	$3CaO \cdot Al_2O_3$, $Ca_3Al_2O_6$	C_3A
Tetracalcium aluminoferrite (ferrite)	$4CaO \cdot Al_2O_3 \cdot Fe_2O_3$, $Ca_2(Al,Fe)O_5$	C_4AF
Calcium silicate hydrate	$xCaO \cdot ySiO_2 \cdot zH_2O$, variable	C-S-H
Calcium aluminate hydrate	$xCaO \cdot yAl_2O_3 \cdot zH_2O$, variable	C-A-H
Calcium hydroxide (portlandite)	$Ca(OH)_2$	CH
Calcium sulfate dihydrate (gypsum)	$CaSO_4 \cdot 2H_2O$	$C\overline{S}H_2$
Calcium sulfate hemihydrate (bassanite)	$CaSO_4 \cdot 0.5H_2O$	$C\overline{S}H_{0.5}$
Calcium sulfate (anhydrite)	$CaSO_4$	$C\overline{S}$
Aluminate ferrite tri- (ettringite, if X is SO_4^{2-})	$[Ca_6Al_2(OH)_{12}](X)_3 \cdot 26H_2O$	AFt
Aluminate ferrite mono-	$[Ca_2Al(OH)_6]_2(X)_n \cdot m \cdot H_2O$	AFm

Note: Fe^{3+} could replace Al^{3+} partially and forms solid solution in AFt or AFm structure. For AFm phase, X could be anions such as OH^-, Cl^- (n = 2) or SO_4^{2-}, CO_3^{2-} (n = 1); for AFt phase, monovalent anion is hardly accommodated to the structure.

Table of contents

1 Introduction

Cementitious material is the most widely used man-made materials in the world. However, this material has some weaknesses, such as low tensile strength, high permeability, low chemical resistance, amongst others. For this purpose, synthetic polymer has been used to improve its weakness for many years [1,2]. Polymer cement concrete (PCC) or labelled as polymer modified cement (PMC) is thereof a composite material thereof with two binders: cement and polymer. Polymer in the context here is narrowly defined as polymer emulsion or its derivative form redispersible polymer powder [3]. Compared to ordinary cementitious material, PMC improves workability of the fresh material as well as the elastic modulus, adhesion, impact resistance, and abrasion resistance, of the hardened end product [4].

PMC has various applications in the construction field. These include, but are not limited to, floor screed, water proofing, tile adhesive, decorative finish and repair mortar for the concrete structure, and so forth [1]. Though the formulations of PMC in these applications are complex, the synergetic effect from the combination of cement and polymer is the key for the desired performance. This composite is an invaluable element in the development of sustainable construction materials [3] and mechanistic investigations, particularly related to the microstructure of PMC have been intensively carried out [5-9]. Despite of the extensive research, the main outcomes from such work generally depicted a general model where the influence of polymers on the cement hydration is shown, as accompanied by film formation. The physicochemical nature of the polymers that drives the mechanisms is however ignored. As a result, interpretation of mechanisms driving the change in rheology [10,11], differences in the ability to undergo film formation [12,13], and alteration on hydration kinetics [14,15] of the composite materials are often left unnoticed or hypothesized. Therefore, there is a need to decrease this gap in knowledge to meet future demand.

Recently, further specific research has been performed in this area, whereby investigations were conducted to understand the interaction between cement and polymer, especially in colloidal systems [16-19]. The advantage of these studies is apparent as physicochemical interaction among them can be comprehensively elaborated. On the other hand, the disadvantage is the demanding nature of such experimental work, where case by case studies must be performed due to the variety of the polymers.

In the literature [20-22], a commonly employed polymer – poly(vinyl acetate -co- ethylene) (VAE, abbreviated as EVA in these literatures) – in the adhesive and construction industries has not sufficiently understood. The uniqueness of this polymer is the incorporation of polyvinyl alcohol (poly(vinyl acetate -co- vinyl alcohol), accurately), which acts as a protective colloid, especially

in its powder form [23]. This polymer is made up of a combination of the macromolecule particle and poly(vinyl acetate -co- vinyl alcohol), while the polyvinyl alcohol is either adsorbed/grafted on the particle or dissolved in the medium [24–26]. The presence of poly(vinyl acetate -co- vinyl alcohol) endues the polymer high mechanical properties as well as its tackiness [27]. Additionally, the film formed by the VAE copolymer stabilized with polyvinyl alcohol can be dispersible in water, if it contains sufficient amounts of polyvinyl alcohol, polyacrylamide, starch, or dextrins [28]. However, due to its water solubility, undesired redispersion may occur and be fatal in some cases, e.g. adhesion failure by water immersion.

Since there is a gap between the physicochemical nature of the VAE polymer and the microstructure of the polymer modified cement, this work is aimed at comprehensively understanding the interaction between the VAE polymer and Portland cement. This work is divided into 6 chapters, whereby the interactions of these polymers in their colloid state, alteration on hydration kinetics and film formation in the cementitious environment are studied, with emphasis on the physicochemical properties of the polymer. Chapter 2 focuses on the background of this work, including the raw materials and their interaction with water, i.e. film formation and cement hydration. Besides, current knowledge of the interaction between the polymer and cement will be introduced afterwards. In chapter 3, characterization of the raw materials as well as the methods will be presented. In chapter 4, surface and electrical properties of the polymer as well as initial adsorption in a diluted colloid system are discussed, and the initial interaction mechanism is speculated from the results. Based on the initial interaction in the colloid system, the influences of the polymer on the hydration kinetics of Portland cement are discussed in chapter 5. In this chapter, the influence of different polymers on ion composition in cement pore solution, and hydration products are monitored. In order to reveal the effect of the interaction on the film-forming, a polymer film formed in the cementitious environment is simulated and studied by means of ESEM and AFM in chapter 6, while its relation to redispersibility is also indicated. Finally, a conclusion and short outlook from this work will be given in chapter 7.

2 Scientific Background

In this chapter, an overview of the physical and chemical properties of polymer and cement is provided. In particular, their interactions with water, i.e. film formation or cement hydration respectively, will be highlighted. Finally, a state-of-the-art study concerning the interaction between the polymer and cement is introduced.

2.1 Latex

2.1.1 Latex particles

2.1.1.1 Introduction

The terms 'latex', 'polymer dispersion', 'emulsion polymer', 'emulsion' are used as the synonymous [29]. According to IUPAC, latex or polymer dispersion is recommended as its name and defined as 'colloidal dispersion of polymer particles in a liquid' [30]. In general, any particle that has some liner dimension between 10^{-9} m (1 nm) and 10^{-6} m (1 μm) is considered as a colloid [31].

1 ml polymer dispersion contains
ca. 1.000.000.000.000.000 particles

1 particle contains
ca. 1 – 10.000 macromolecules

1 macromolecule consists of
100 – 1.000.000 monomer units
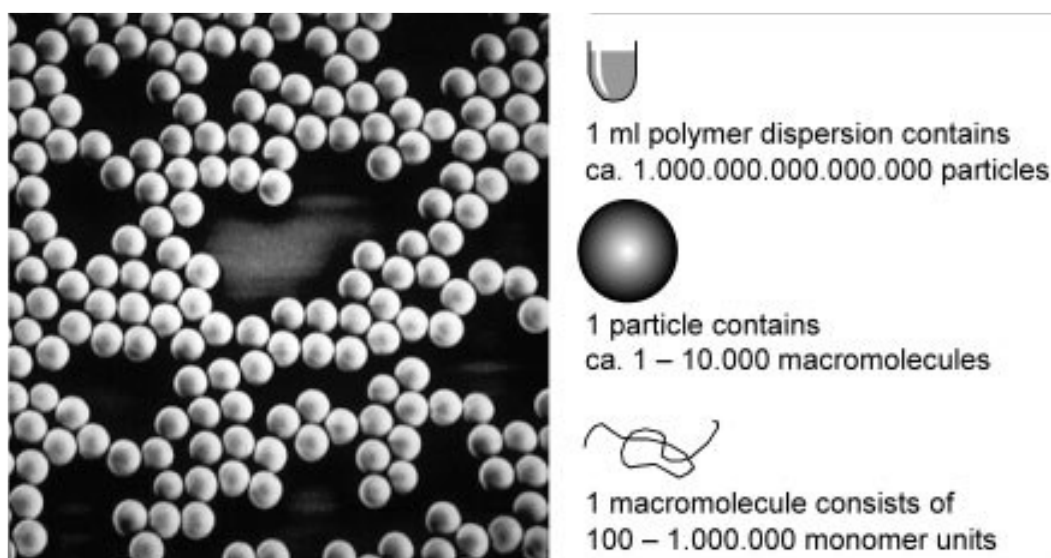
Figure 2.1 Illustration of latex by its hierarchies [29]

Normally, a latex possesses a solid content of 40-60 wt.-%, in which, 1 mL latex contains ~ 10^{15} particles while one particle is composed of 1-10000 macromolecules, as illustrated in Figure 2.1. The inner particle structure could be observed by cryo-SEM via fracturing, as reported by Ma *et al*. (Figure 2.2) [32]. Latex particles have various morphologies, including simple homogeneous spherical particles, core-shell type, or much more complex structure, such as raspberry or moon-like [33–35]. Nevertheless, as a complex system, complexity of a latex arises in part from its nature as lyophobic sols and in part from the polymeric nature of the

disperse phase [36]. In other words, colloidal properties as well as composed polymer are two significant characteristics of the latex.
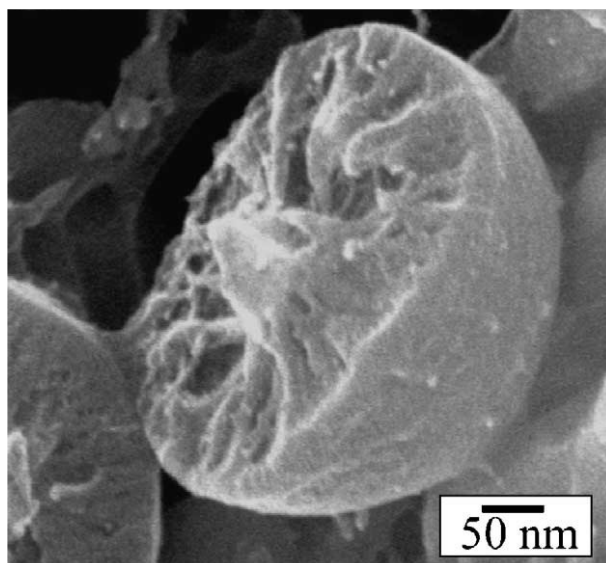

Figure 2.2 Cryo-SEM image of an acrylic latex particle that was fractured [32]

2.1.1.2 Colloid

When defining colloids, one of the most important features of colloidal particles is the dimension. Colloidal particles come in all shapes and sizes. Among which, monodisperse spheres with a well-defined mean particle size are not only uniquely easy to characterize, but are also very rarely encountered. In practice, particles are either characterized by a high degree of symmetry like a sphere, or asymmetry like an ellipsoid [31]. Actually, most common particle size methods measure an equivalent spherical diameter (ESD) [37]. This is the diameter the particle would have if it was a sphere and can be based on volume to yield an equivalent volume diameter or surface to yield a sphere having equivalent surfaces. Normally, a concise representation of particle size is required, expressed as the average diameter. Table 2-1 defines some common average diameters.

Table 2-1 Definition of particle average diameter [37]

Average	Symbol	Definition (number basis)
Number average	d_n	$\dfrac{\sum_i n_i d_i}{\sum_i n_i}$
Weight average	d_w	$\dfrac{\sum_i n_i d_i^4}{\sum_i n_i d_i^3}$
Z-average	d_z	$\dfrac{\sum_i n_i d_i^5}{\sum_i n_i d_i^4}$

Surface average	d_s	$\dfrac{\sum_i n_i d_i^3}{\sum_i n_i d_i^2}$
Volume average	d_v	$\left(\dfrac{\sum_i n_i d_i^3}{\sum_i n_i}\right)^{1/3}$
Sauter	d_{32}	$\dfrac{d_v^3}{d_s^2}$

Where n_i is the number of particles with diameter d_i.

Colloidal systems tend to show a degree of size dispersity, i.e. distribution of different particle diameters [38]. The relative magnitude of the number, surface and volume are given by the sequence $d_n < d_s < d_v$, for the polydisperse system [31]. Colloidal particles are protected via repulsive forces against flocculation or agglomeration / coagulation. Generally, there are four stabilization categories of a colloidal system, as illustrated in Figure 2.3. A more detailed description of electrostatic and steric effects is given below.
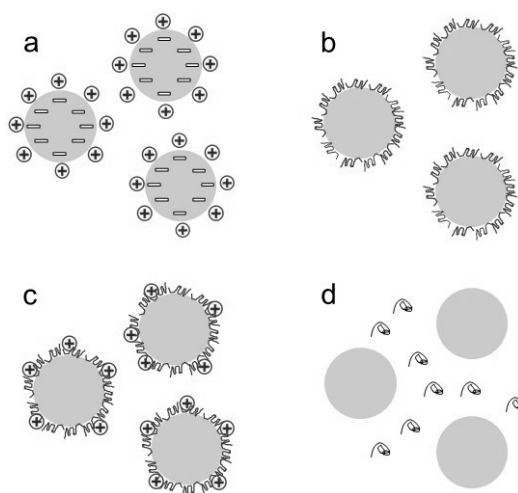

Figure 2.3 Stabilization categories of colloidal systems: a) electrostatic; b) steric; c) electrosteric; d) depletion (redrawn according to the literature [39])

Electrostatic stabilization: the particle surface is charged by the dissociation of surface functional groups, or adsorption of ionic groups, or isomorphous substitution. The free ions on the other hand, are distributed in the vicinity of the charged surface, which is described by the Stern-Gouy-Chapman model, known as the electrical double layer. This stabilization mechanism was elaborated well by the Derjaguin-Landau-Verwey-Overbeek (DLVO) theory [40,41], whereby the repulsive electrical double layer and attractive Van der Waals forces were combined together (illustrated in Figure 2.4). Based on that theory, a colloid is kinetic stable rather than thermodynamic stable, which can be illustrated by the dispersions of lyophobic particles in low ionic strength [31].
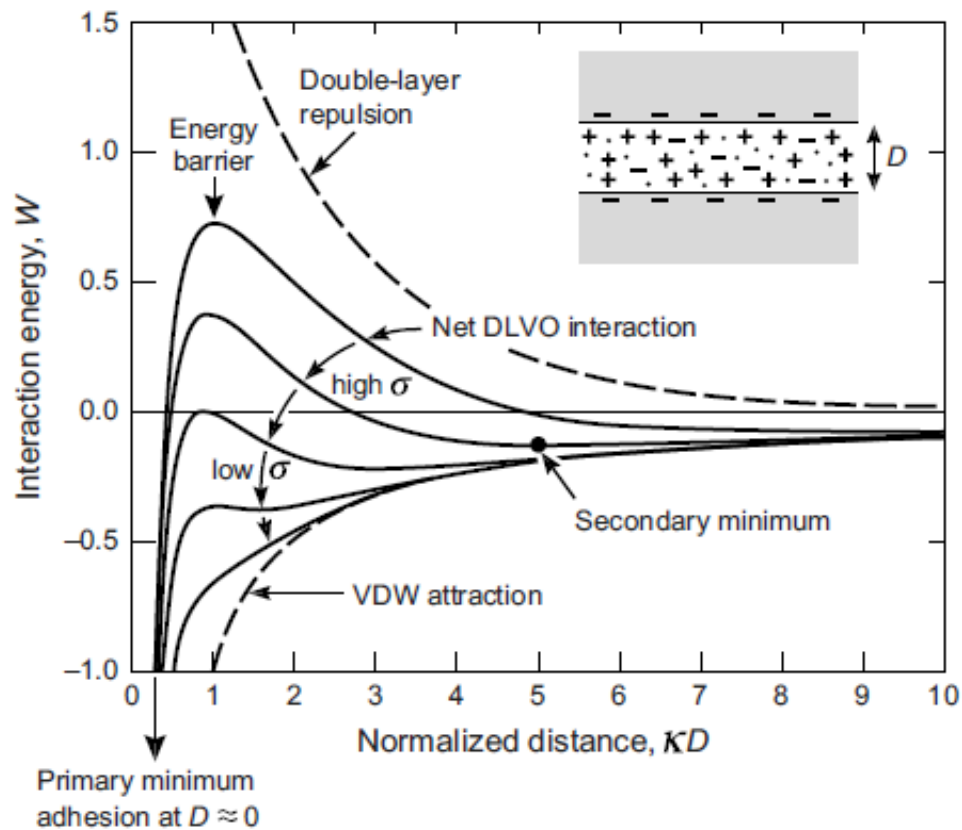
Figure 2.4 Schematic energy versus distance profiles of the DLVO interaction (between two planar surfaces; VDW: Van der Waals) [42]

With an increase in electrolyte concentration, the stability of a colloid decreases, as estimated by critical coagulation concentration (ccc). The compression of the double layer, which is characterized by the Debye length (κ^{-1}) is followed by a net attractive interaction energy [41], resulting in the coagulation of the dispersed particles. Moreover, the valence of the counterions has a principal effect on the stability of the colloid, known as Schulze-Hardy Rule. Therefore, electrostatic stabilization alone is insufficient when the colloid is employed in a medium with high electrolyte concentration, e.g. cement pore solution [43,44]. In fact, Goto [45] studied several commercial latices commonly used in cement applications; none could be stabilized by electrostatic force alone.

Steric stabilization: the stabilization of colloidal particles against flocculation, which is imparted by non-ionic macromolecules [46]. The addition of polymer to a dispersion can stabilize or destabilize the dispersion, depending on the nature of interactions between the polymer and the solvent [31]. Hunter [47] described four typical effects of polymer on the stability of the colloidal dispersions. They are: 1) bridging flocculation at low polymer concentration, 2) steric stabilization at medium polymer concentration, 3) depletion flocculation at medium to high polymer concentration and 4) depletion stabilization at high polymer concentration. If the polymer chains are demixed from the solvent, polymer depletion between the dispersed

particles may occur. However, this demixing process is thermodynamically unfavourable in good solvents, inducing depletion stabilization [31]. In other words, polymer stabilized colloids could be affected by the polymer concentration as well as the state of the solvent, while the latter was described by Flory-Huggins theory [48]. In poor solvents, polymer induced stabilization could be eliminated, since polymer-polymer interaction is attractive in this condition [49,50]. Generally, with the increase in salt ions, colloidal stability should decrease with decreasing polymer solvency, though there are some exceptions [51].

If the colloid is stabilized by polyelectrolytes, a combination of the electrostatic effect as well as the effect that arises solely from the polymeric nature occurs, effect which is referred to as electrosteric stabilization [31].

2.1.1.3 Polymer

The size and shape of polymers are intimately connected to their properties. Generally, the structure of polymers is described and can be characterized at four level structurally: primary structure with a precise sequence of the individual atoms of the polymer chain; secondary structure with molecular shape or conformation of the polymer chain (e.g. linear, comb, branched, etc.); tertiary structure with shaping or folding of the polymer (crosslinking, lamellar, etc.); and quaternary structure with the overall shape of tertiary structures [52]. In general, a polymer is classified into natural and synthetic, organic and inorganic [52]; whereas, only synthetic organic polymers will be discussed in this section. For latex polymer, molecular mass and molecular mass distribution, chemical composition and its distribution, intramolecular microstructure such as tacticity, sequence distribution etc. are significant [53]. In other words, the primary structure of the macromolecule is the main concern when it comes to the characterization of the latex polymer.

One of the important characterizations of a polymer is its chemical composition of the repeating units. For chain-growth polymers, a copolymer refers to that composed of two kinds of repeat units, while a homopolymer is composed of only one repeat unit. Similarly, there are also terpolymer and multicomponent copolymer with more than three repeat units [54]. Accordingly, distribution patterns can be obtained in copolymers starting from two kinds of repeat units, as illustrated in Figure 2.5.
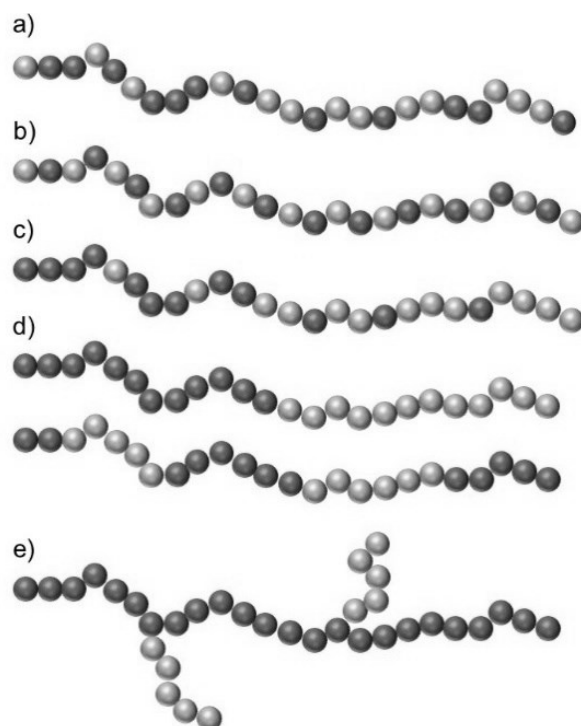
Figure 2.5 Distribution patterns of the copolymer: a) statistical or random; b) alternating; c) gradient; d) diblock (up) or segmented (down); e) graft and branched (redrawn according to the literature [55])

These microstructures, which can be achieved via different polymerization processes as well as kinetic factors (e.g. reactivity), can have a determining influence on copolymer properties [55], of which the monomer reactivity ratio is an essential parameter. Table 2-2 presents some typical monomer reactivity ratios. The inherent reactivity ratio is influenced by the reaction conditions, e.g. temperature, solvent, etc [55]. Herein, if $r_1>1$, the radical $M_1\bullet$ adds monomer M_1 in preference to M_2; if $r_1<1$, $M_1\bullet$ adds M_2 in preference to M_1, and vice versa. Therefore, alternating structures by $r_1\rightarrow0$ and $r_2\rightarrow0$, random structures by $r_1\cdot r_2\rightarrow1$ and blocky structures by $r_1\cdot r_2>1$ are promoted respectively [56]. Therefore, the sequence distribution within the copolymer can be crudely estimated from the reactivity ratios. Other fine intramolecular structures of the macromolecule including tacticity is discussed in section 2.1.2.

Table 2-2 Some typical monomer reactivity ratios in radical copolymerization [57]

Comonomers		r_1	r_2	T (°C)
M_1	M_2	(reactivity of M_1)	(reactivity of M_2)	
Acrylic acid	n-Butyl methacrylate	0.24	3.5	50
1,3-Butadiene	Styrene	1.4	0.58	50
Ethylene	Vinyl acetate	0.79	1.4	130
		1.0	1.0	N/A*
Methyl acrylate	Styrene	0.8	0.19	60
Vinyl acetate	Vinyl Versatate VV10	0.99	0.92	60**

*: In ref. [58] / ** in ref. [59]

Synthetic polymer also contains macromolecules with various degrees of polymerization, which is ascribed by polydispersity index (PDI) with respect to molecular weight or degree of polymerization (DP) [56]. The molar mass, which is defined by various averages and especially the molar mass distribution, determines a large range of properties of the polymer [53]. Polydispersity is given by the ratio of weight average molecular weights (M_w) and number average molecular weight (M_n), from which information on the molar mass distribution is provided (equations 2-1 - 2-3).

$$M_n = \sum_i x_i M_i = \frac{\sum_i n_i M_i}{\sum_i n_i} = M_0 \frac{\sum_i i n_i}{\sum_i n_i} \qquad \text{2-1}$$

$$M_w = \sum_i w_i M_i = \frac{\sum_i i n_i M_i}{\sum_i i n_i} = \frac{\sum_i n_i M_i^2}{\sum_i n_i M_i} = M_0 \frac{\sum_i i^2 n_i}{\sum_i i n_i} \qquad \text{2-2}$$

$$PDI = \frac{M_w}{M_n} \qquad \text{2-3}$$

Where

i	degree of polymerization or i-mer
M_0	molecule weight of the repeat unit
M_i	associated molecular weight of i-mer
n_i	number of i-mer
x_i	number fraction or mole fraction of i-mer
w_i	weight fraction or mass fraction of i-mer

The dry content of polymer dispersions only contributes approximately 4 wt.-% of total polymer production, about 7.5 million tons by the year of 2001 [29]. Emulsion polymerization has developed into a widely used process for the production of synthetic latex / polymer dispersions [60]. This kind of polymerization refers to a unique process employed for radical chain polymerizations, which involves the polymerization of monomers in the form of emulsions (i.e., colloidal dispersions) [57]. The advantage of the process is that it is capable of producing high molecular weight polymers at low viscosity, while its disadvantage is the presence of stabilizers in the final products.

Vinyl acetate homo- and copolymers, polyacrylates and styrene butadiene copolymers are the major categories of synthetic latices [29]. Emulsion copolymers of vinyl acetate (VAc) are increasingly used in numerous applications due to the advantageous combination of good durability and wide availability at low cost [58]. Polyvinyl acetate emulsion is less valuable and usually requires plasticization, either external plasticizer like *o*-phthalic diesters or an internal one such as comonomers, e.g. vinyl esters, the fumaric and maleic diesters or the acrylic esters [61]. Ethylene copolymerized with VAc under normal circumstances enters the polymer backbone only and provides neither bulky nor long chain side group. Its primary contribution to the plasticization is by increasing intra-chain mobility, making the backbone more flexible [61]. As a result, the VAE copolymer offers considerable advantages over PVAc due to its lower glass transition temperature (T_g), which is mainly related to the ethylene content [62]. VAE copolymer characterization has been studied intensively [63–66]. However, as an industrial important emulsion polymer, only a few kinetic investigations on VAE emulsion have been published [67]. Nevertheless, Scott *et al*. carried out a series of studies on semi-batch emulsion copolymerization of VAE [67–69], discussing the influence of redox initiator system, co-solvent, temperature, VAc feed rate, emulsifier type and pressure on the microstructure of the copolymer. These industrially significant VAE emulsions are currently stabilized via both surfactant and partially hydrolyzed polyvinyl alcohol (PVOH), which could also affect the polymer structure and hence its final physical properties [70]. The continuous emulsion copolymerization process has a significant influence on the physical properties of VAE emulsion polymer, i.e. its polymer structure has been altered thereof [71].

2.1.2 Protective colloid - Polyvinyl Alcohol (PVA)

Polyvinyl alcohol (abbreviated as PVA instead of PVAL normally) is widely used industrially as a protective colloid in the emulsions of VAc homopolymer and copolymers [27]. PVA stabilized latices show better emulsion fluidity such as Newtonian flow or structural viscosity, superior wet primary tackiness as adhesives, good mechanical film properties such as higher tensile strength and creep resistance, excellent mechanical stability, and higher freeze-thaw

stability compared to latices stabilized with low molecular weight surfactants [72]. Accordingly, the performance of the emulsion stabilized by PVA is largely dependent on the fine chemical structure of PVA used in polymerization [73].

2.1.2.1 Structure of polyvinyl alcohol

PVA is commercially manufactured by the alkaline hydrolysis of poly(vinyl acetate) [74]. Its physical properties such as melting and glass transition temperature, solubility and mechanical properties are greatly dependent on the two major parameters: molecular weight and hydrolysis degree [74,75]. For ease of elaboration, PVA is defined as the fully hydrolyzed polymer (i.e. degree of hydrolysis $\geq 96\%$ [76]) or general description while PVOH is assigned to the partially hydrolyzed one in the following description, though they are synonymous [77]. Despite the industrial interest on molecular weight and hydrolysis degree, the intra- and intermolecular structure affects the polymer properties, e.g. glass transition temperature and degree of crystallization, etc. [76]. Amiya *et al*. [78] has proposed a microstructure model for the PVOH macromolecule, in which vinyl acetate and double bond residues were presented as well (Figure 2.6). In this work, they employed ^{1}H-NMR to determine tacticity, 1,2 glycol linkage as irregular structures, end groups, short branches and polyene structure of the polymer.
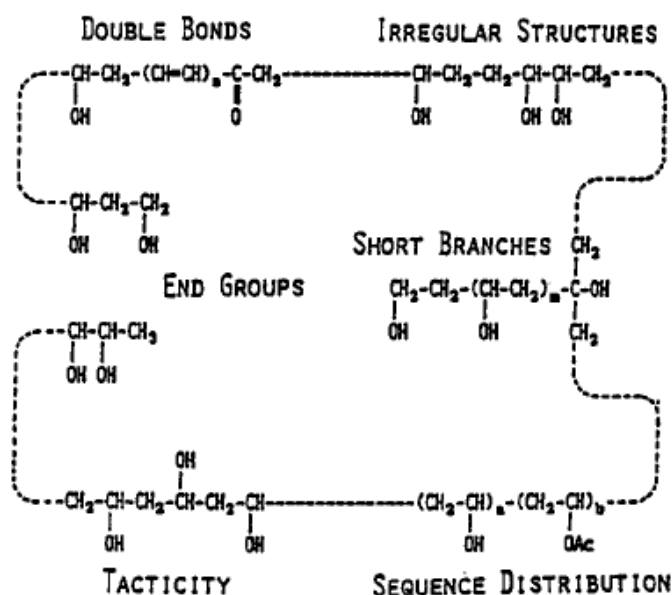

Figure 2.6 Proposed microstructure model of PVOH macromolecule [78]

Three categories of the polymer tacticity are shown in Figure 2.7. Moritani *et al*. [79] studied the tacticity of PVAs synthesized under various conditions and found that atactic stereoregularity was dominant, with exception of synthesis employing vinyl tert-butyl ether in toluene. In the case of partially hydrolyzed polyvinyl alcohol, the intramolecular distribution sequence of vinyl alcohol and vinyl acetate was emphasized [80–82]. Toppet *et al*. [82] developed a technique by employing both ^{13}C and ^{1}H NMR to determine the sequence distribution. They concluded that

tacticity of commercial PVOHs could be roughly estimated as: mm (isotactic triad, Ac-Ac-Ac) = 0.20, rr (syndiotactic triad, O-Ac-O) = 0.30, mr (heterotactic triad, O-Ac-Ac) = 0.50. However, Budhlall *et al*. [80] found small but significant differences in the degree of blockiness among PVOHs. Based on that, they [81] found that PVOH adopt different conformations in aqueous solutions, depending on the molecular weight and degree of blockiness. These different conformations are expected to play a significant role during the emulsion polymerization of vinyl acetate latex.
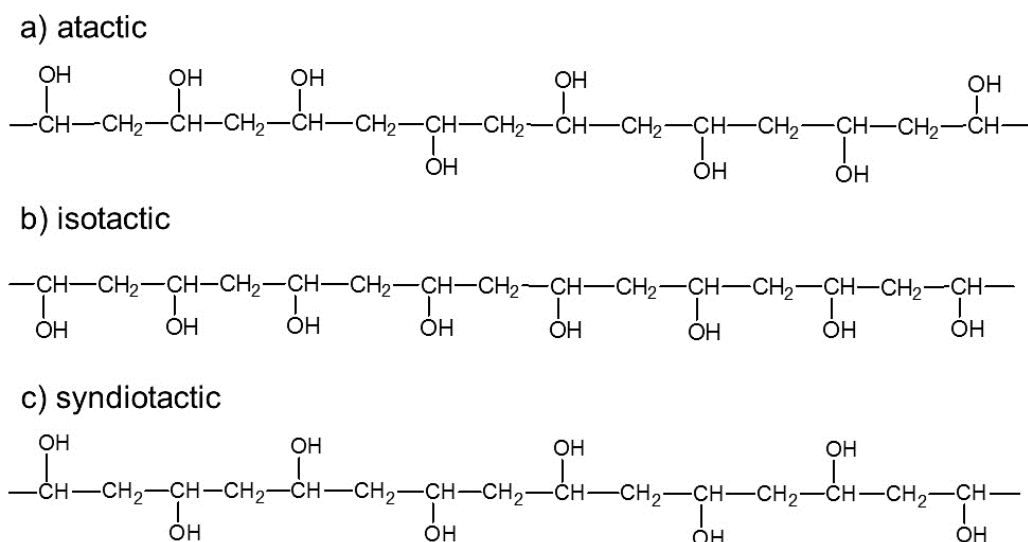
a) atactic

b) isotactic

c) syndiotactic

Figure 2.7 Tacticity of PVA

2.1.2.2 Polyvinyl alcohol as protective colloid

Stable latices can be made with protective colloid alone. Partially hydrolyzed (87-89 mole %) polyvinyl alcohol is commonly used as protective colloids in the industrial emulsion polymerization of VAc, which fulfills the dual function of emulsifying the monomer and stabilizing the latex particles [59]. PVOH has long been identified as a major cause which results in highly variable quality to final latex [25]. Noro [73] studied the microstructure of PVOH and its relation to PVAc properties. There, it was found that PVOH with blocky intramolecular structure increased the viscosity of the emulsion and improved its freeze-thaw stability. Gilmore *et al*. conducted a theoretical calculation coupled with experimental verification to determine the effect of PVOH on the kinetic of emulsion polymerization of PVAc [25,83]. They found that PVOH grafting onto PVAc did not play a significant role during particle nucleation and suggested that chemical grafting may follow physical adsorption (Figure 2.8). González *et al*. [84] developed a technique using acetonitrile selective solubility to separate grafted and linear PVOH, of which the ratio of the grafted and the linear was 22:78. Erget *et al*. [26] further developed this technique by employing ultracentrifugation but obtained a ratio about 46:54, indicating the influence of other conditions to PVOH grafting. Carrà *et al*. [24] used a similar technique to determine the

different types of PVOHs in the PVAc latex. They found that PVOH blockiness did not greatly influence polymerization kinetics or grafted fraction. Moreover, the grafted fraction was lower than physically adsorption, while the latter increased with the blockiness. Similarly, Budhlall found that total amount of grafted PVOH was independent of the degree of the blockiness [85].
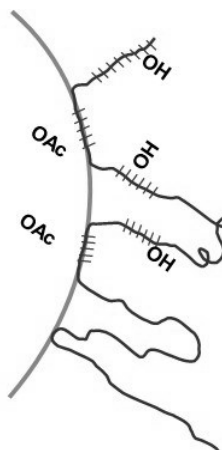

Figure 2.8 Adsorption of PVOH onto the surface of a latex particle, showing trains, tails and loops conformation (redrawn according to the literature [25])

2.2 Film formation of latex

It is generally accepted that the film formation process can be described in four states [86]. These states may neither occur sequentially [87] nor are universal in all cases [88,89]. Nevertheless, it commonly starts as an aqueous polymer dispersions that finally condenses and forms a homogeneous film, which is schematically illustrated in Figure 2.9.
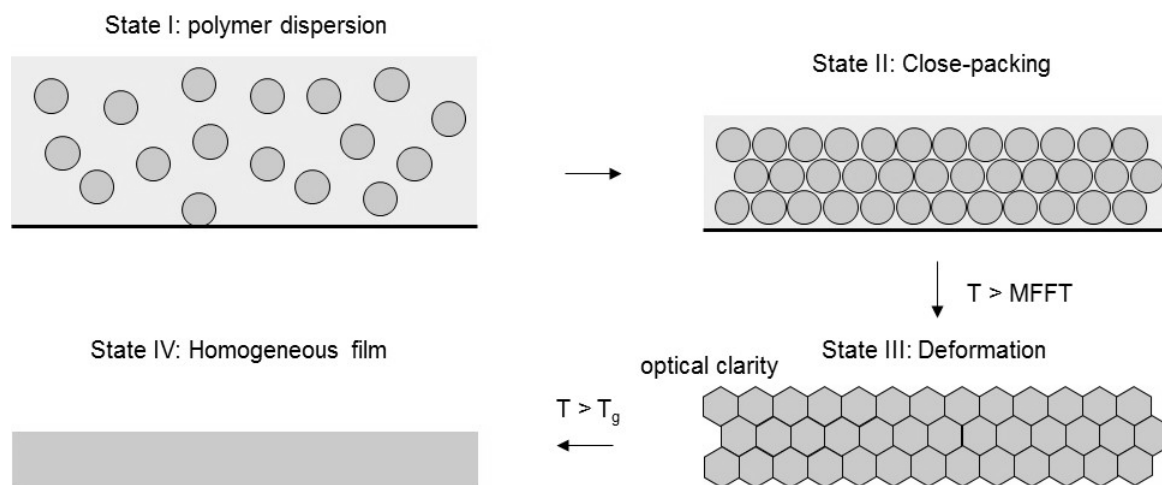

Figure 2.9 Schematic of the process of film formation (redrawn according to literature [86]);

From states I to II, latex particles approach each other in the aqueous phase as water evaporation. Ludwig *et al.* [90] found there to be no concentration gradients in the vertical

direction but profound influence on the water content in horizontal direction upon drying at ambient condition. Rottstegge et al. [91,92] investigated the dynamics of water during the drying process. Part of the water is shown to be immobilized either at the surfactant interface or inside the latex polymer, by which the hydrophilic polymer is plasticized. While the solvent evaporates, the saturation of the particles results in close contact until surface tension is overcome and deformation starts to occur.

For such a deformation to occur, there must be a driving force for compaction. Five mechanisms were proposed as the driving forces of deformation: 1) wet sintering, 2) dry sintering, 3) capillary deformation, 4) receding water front and 5) sheets deformation, whereby each mechanism was observed under suitable experimental conditions [93]. Minimum film formation temperature (MFFT) refers to the onset of film formation, meaning the point of optical clarity and mechanical integrity in a drying latex coating [94]. This parameter gives the information about particle deformation, by which Sperry et al. [95] found that wet MFT was lower than the dry MFFT for hydrophilic polymers due to water plasticization. They argued that capillary force had little effect on particle deformation for hydrophobic polymer. In contrary, Lin et al. [96] found that condensed water in the interstitial of particle boundaries enhanced the capillary pressure and concluded that capillary pressure was the dominant driving force for particle deformation. Besides, Ludwig et al. [90] stated that particle deformation was incomplete if ambient temperature was around the MFFT. Jensen et al. [97] found that small particle sizes could reduce the MFFT. If the temperature is well above T_g, the rate determining step in film formation is the process of evaporation; otherwise it relates to particle deformation [98]. With regards to the various techniques for the study of the film-forming process, electron microscopy is the prominent tool to investigate particle deformation and, in some cases, coalescence [32,98–102]. Accordingly, environmental scanning electron microscopy (ESEM) is a powerful tool, since this technique enables the study of wet and insulating materials in their original state [102].

In the last state, the deformed polymer will interdiffuse across the boundaries of the polymer domain and coalescence as a whole. In polymers, the motion of the centre-of-mass of a molecule does not occur until temperatures above the glass transition temperature, T_g, when the polymer is in the molten state [86]. Wang et al. [103] studied the effect of the molecular weights of polymers on their diffusion across interfaces, and a relation between the diffusion coefficient and molecular weight was found to be about $D \sim M^{-2.3}$ between the diffusion coefficient and molecular weight was found. The diffusion coefficient is also strongly dependent on temperature, while at room temperature only low value of about 5×10^{-18} m^2/s was observed for the investigated polymer.

Nevertheless, film formation of latices stabilized with a protective colloid which are widely used in the adhesive or construction industries [104], has been less well reported. Kast [105] investigated OsO_4 stained ultramicrotome section of vinyl acetate/ethylene (VAE) copolymer film and found that PVOH formed a continuous network throughout the film, by which latex polymer particles were separated. Budhlall *et al*. [106] used Atomic Force Micoscopy (AFM) to investigated PVAc latex film incorporated with different PVOHs. They found the surface morphology of the films to be strongly dependent on the degree of blockiness and molecular weight of PVOHs, i.e. PVOH in a medium could migrate to the surface during water evaporation, resulting in a hills-valley structure depending on the unbound amount of PVOH. Du Chesne *et al*. [28] added sodium dodecylsulfate (SDS) and non-ionic ethoxylated fatty alcohols (Genapol T250) into the VAE latex. They found that polymer particle interdiffusion was feasible due to the break-up of the surrounding PVOH membrane. Baueregger *et al*. [13] investigated both the polymer dispersions and its powder form of VAE and SBR, finding that the presence of kaolin in the powders accelerated the film-forming process.

2.3 Portland cement

2.3.1 Cement

Portland cement is made by heating a mixture of limestone and clay, or other materials of similar bulk composition and sufficient reactivity, ultimately to a temperature of about 1450 °C. Partial fusion occurs and nodules of clinker (schematic illustration in Figure 2.10 with cement nomenclature) are produced. The clinker is mixed with a few percent of calcium sulfate carrier as a set retarder and finely ground to make the cement powder [107].

Figure 2.10 Schematic illustration of cement clinker particle (adopted from literature [108])

Portland cement powder has a wide particle size distribution (PSD), from about 0.1-100 µm. Holzer et al. [109] used volume equivalent spherical diameter (VESD) to compare the shape of smaller (0.4-2 µm) and larger (20-60 µm) particles. They found that both ranges of particles presented prolate shapes. However, the smaller particles were more prolate than the larger ones, with a greater average length and average length to width ratio. Erdoğan et al [110] used a X-ray computed tomography to study the relation between particle shape and mineralogy. Cement with high amount of belite tended to have a higher equi-axed shapes at the length scale of 20-60 µm. They also found that actual cement particle size tended to be smaller than that measured by laser granulometry.

The clinker typically has a composition in the region of 67 wt.-% CaO, 22 wt.-% SiO_2, 5 wt.-% Al_2O_3, 3 wt.-% Fe_2O_3 and 3 wt.-% other components, and normally contains four major phases, called Alite (C_3S), Belite (C_2S), Aluminate (C_3A) and Ferrite (C_4AF). [107]. In the last few decades, quantitative phase analysis of anhydrous Portland cements by X-ray powder diffraction (XRPD) and whole profile fitting methods such as the Rietveld method have become standard practice in cement phase characterization [111–115]. Though amorphous phase [113] and reproducibility [114] could affect the accuracy of the results, it is far less labour-intensive than the microscope point counting (MPC) method [112]. However, the MPC method could provide surface phase fraction which is of interest in early cement hydration [116], where, aluminate (C_3A) and especially gypsum presented a much higher surface fraction than their weight fraction. Scrivener [117] also found that the proportions of interstitial phases exposed on the surfaces of the particles were significantly greater than those by volume in the bulk material.

2.3.2 Minerals

The polymorph structure of tricalcium silicate ($3CaO·SiO_2$, C_3S) has been refined by many researchers and C_3S doped with foreign ions such as Mg is needed to stabilize the structure at ambient temperature [118–123].

Dicalcium silicate ($2CaO·SiO_2$, C_2S) is another main constituent phases of cement mineral. It is usually consist of five polymorphs [107], among which only γ form is stable at room temperature. However, in the presence of small amount of impurities as low as 0.1 wt.-%, the β form is stable and the conversion from ß to γ is prohibited in cement clinker [124].

Pure tricalcium aluminate ($3CaO·Al_2O_3$, C_3A) does not exhibit polymorphism. The structure is built from Ca^{2+} ions and rings of six AlO_4 tetrahedra of formular $Al_6O_{18}^{18-}$ [125]. The aluminate present in cement clinker is a solid solution of C_3A with several foreign oxides like MgO, SiO_2, Fe_2O_3, Na_2O and K_2O. Only when doped with Na_2O will the symmetry of this mineral will change from cubic to orthorhombic. The influence of Na_2O amount on C_3A symmetry is summarized as below [126]:

0-1.9 wt.-%	Na_2O	cubic
1.9-3.7 wt.-%	Na_2O	cubic + orthorhombic
3.7-4.6 wt.-%	Na_2O	orthorhombic
4.6-5.9 wt.-%	Na_2O	monoclinic

The composition of the ferrite phase can be described by a limited solid solution between $Ca_2Fe_2O_5$ and $Ca_2Al_{1.33}Fe_{0.67}O_5$ with $Ca_2(Al_xFe_{1-x})_2O_5$ (C₄AF), $0<x<0.7$ [126].

Gypsum is added to the cement clinker during the grinding, where the heat produced can cause partial conversion of gypsum into hemihydrate ($CaSO_4 \cdot 0.5H_2O$) or γ-$CaSO_4$ [107]. Here, hemihydrate refers to ß-$CaSO_4 \cdot 0.5H_2O$, while its α-form is only made under saturated steam. Further dehydration could result in the formation of soluble anhydrite (γ-$CaSO_4$, but not truly anhydrous) at ~ 120 °C, while insoluble anhydrite (β-$CaSO_4$) is formed above 200-300 °C [127].

2.4 Interaction between latex and cement

Ohama [1] firstly proposed an interaction model between latex and cement. In this model, the cement hydration generally precedes the polymer film formation process by the coalescence of polymer particles in polymer latices. In due course, a co-matrix phase is formed between both the hydrated cement and the formed polymer film. The co-matrix phase is generally formed according to the simplified model shown in Figure 2.11. More recently, researchers have been more focused towards the microstructure development of polymer modified cement and the attributed improvement in mechanical properties as a function of polymer film formation [5,6,9]. In initial alkaline cement suspension, latex possessing a carboxylate ester undergoes alkaline hydrolysis or so-called saponification [128]. Thus, physical and chemical interactions between latex and cement are expected, once the two components are mixed and have evolved with time.
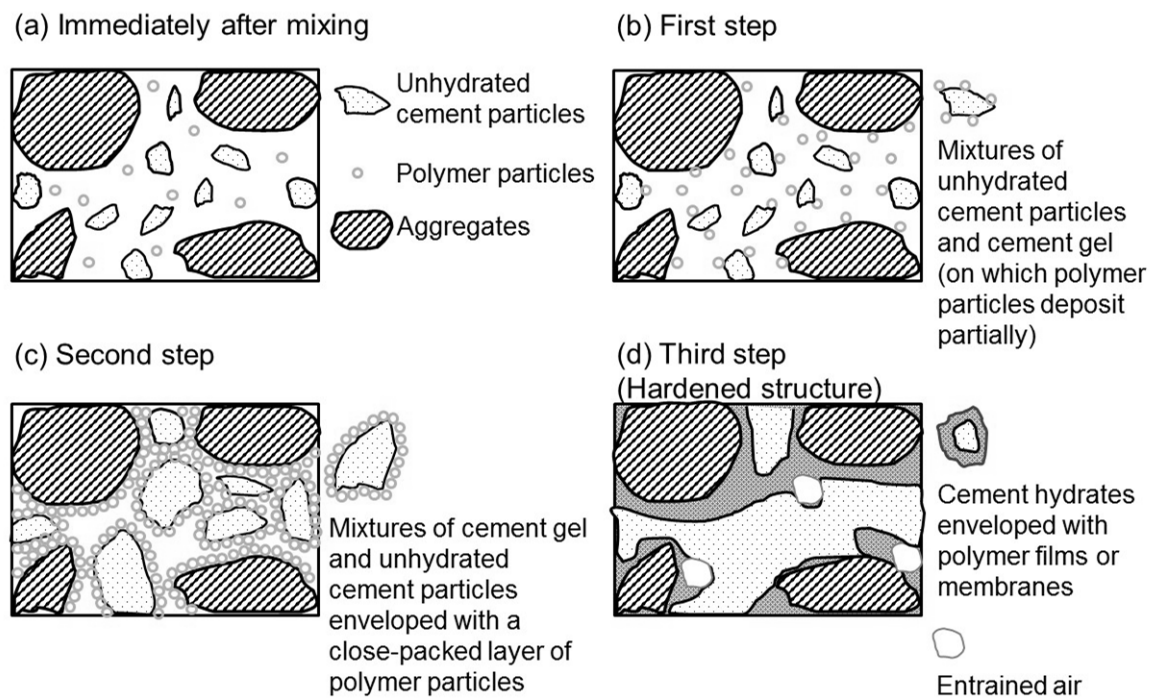
(a) Immediately after mixing

Unhydrated cement particles

Polymer particles

Aggregates

(b) First step

Mixtures of unhydrated cement particles and cement gel (on which polymer particles deposit partially)

(c) Second step

Mixtures of cement gel and unhydrated cement particles enveloped with a close-packed layer of polymer particles

(d) Third step (Hardened structure)

Cement hydrates enveloped with polymer films or membranes

Entrained air

Figure 2.11 Ohama model of formation of polymer cement co-matrix (redrawn after the literature [1])

Atkins *et al*. [129] studied polyvinyl acetate (PVAc) polymer powder, acrylic ester dispersions, polyvinylidene chloride (PVDC) dispersions, polystryrene acrylate (SA) dispersions and polystyrene butadiene (SBR) dispersions with Portland cement. They found that SBR had little chemical interaction with the cement, whereas PVAc and SA were either fully or partially hydrolyzed in cement pore solution. Larbi *et al*. [130] investigated the interaction between SA or PVDC dispersions and pore solution. They found that all the polymer dispersions influenced the ions concentration in the pore solution: SA dispersions decreased Ca^{2+} concentration while increasing both the SO_4^{2-} and OH^- concentration; PVDC dispersions decreased Ca^{2+} and OH^- in the long term. Pöllmann *et al*. [131] investigated the saponification of different polymer powders in cement based material, finding that styrene acrylate copolymer exhibited lower saponification than vinyl acetate-versatate copolymer and vinyl acetate ethylene at high pH. [16] Merlin *et al*. [19] investigated a methyl methacrylate (MMA) and butyl acrylate (BA) latex with non-ionic surfactant and found the latex adsorbed on cement minerals. Boutti *et al*. [18] investigated a low fraction of SA latex with cement and they concluded that there was no evidence of a latex-cement interaction. Plank *et al*. [17] studied the interaction between anionic or cationic latex and cement. They found that a charged latex particle adsorbed onto the surface of cement minerals. Ma *et al*. [132] also observed the adsorption of anionic polyacrylate latex on cement. Kaufmann *et al*. [16] determined the interaction between cationic polyacrylate latex, vinyl acetate latex, two VAE latex and vinyl acetate/vinyl versatate/butyl acrylate terpolymer latex and cement by means of zeta potential. They speculated that adsorption

between latex and cement mineral surface was weak, considering that the addition of polymer dispersions to cement leads to minor changes of the charge situation only.

Nevertheless, many researchers found that latex modifies hydration kinetics, though there has been variation in chemical composition, surfactant types or different additives [6,14,15,20–22,129,133]. In summary, the interaction between latex and cement can be generally divided into three phases: interaction in colloid state (adsorption if any), alteration on hydration kinetics due to physicochemical interactions and film formation in cement environments (Figure 2.12).
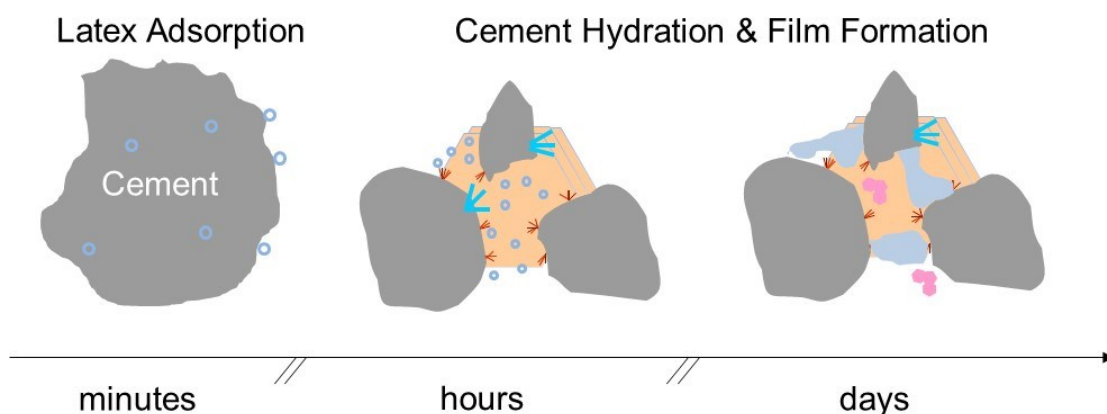
Figure 2.12 Schematic illustration of Interaction between latex and cement

2.4.1 Adsorption of latex polymer at solid/liquid interface

Adsorption can be defined as 'an increase in the concentration of a dissolved substance at the interface of a condensed phase and a liquid phase due to the operation of surface forces' [134]. When this condensed phase is solid, it is referred to as the adsorbent and the adsorbed material the adsorbate. In consideration of the adsorption processes, there are two aspects that must be addressed: 1) thermodynamic – the effect of the adsorption process on the final equilibrium interfacial energy of the system and 2) kinetics – the rate at which the adsorption process occurs [135].

Possibly the most favoured approach to the theoretical aspects of all adsorption systems is the study of the isotherm, in which the amount adsorbed is plotted against the pressure or concentration in the external phase, at constant temperature, and usually under equilibrium conditions [136]. Limousin *et al*. [137] reviewed and interpreted four main types of isotherm, as illustrated in Figure 2.13.
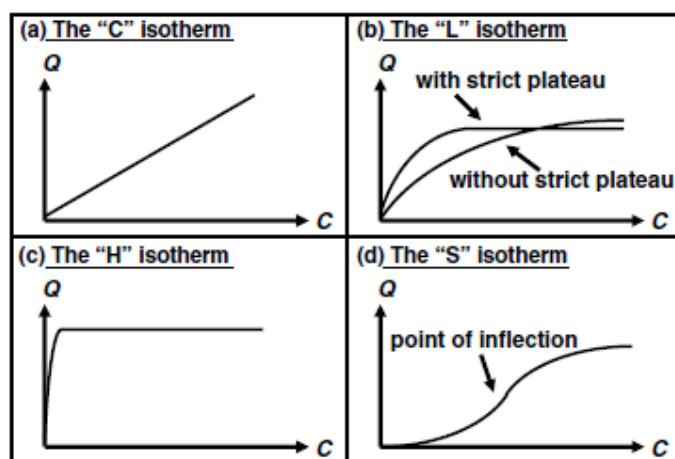
Figure 2.13 The four main types of adsorption isotherm [137]

The 'C' isotherm means that the ratio between the concentration of the compound remaining in solution and adsorbed on the solid is the same at any concentration. However, the simplicity of this isotherm must not justify its use without verification. The 'L' isotherm means that the ratio between the concentration of the compound remaining in solution and adsorbed on the solid decreases when the solute concentration increases, which suggests a progressive saturation of the adsorbate. This isotherm is usually divided into two sub-groups, one with a strict asymptotic plateau and the other without any plateau. The 'H' isotherm could be considered as a particular case of the 'L' isotherm, where the initial slope is very high. The 'S' isotherm shows a sigmoidal shape with a point of inflection. This type has two causes: 1) solute–solute attractive forces at the surface may cause cooperative adsorption which leads to the S-shape and 2) the sorption of a solute may be inhibited by a competing reaction within the solution, such as a complexation reaction with a ligand [138].

The type 'L' and 'H' isotherms can be assigned to the Langmuir or Freundlich isotherms [138]. Compared to the empirical Freundlich isotherm, the Langmuir isotherm is both theoretically easy to understand and widely applicable to experimental data [31]. The adsorption isotherm can be easily derived with following assumptions:

1) all the adsorption sites are assumed to be identical;
2) each site retains one molecule of the adsorbate;
3) all the sites are energetically and sterically independent

Then, the equilibrium constant could be written as:

$$K' = \frac{a_2^i a_1^b}{a_1^i a_2^b}$$
2-4

Where,

K' equilibrium constant of adsorption/desorption

a_2^i activity of solute or adsorbate at solid/solvent interface

a_1^b activity of solvent in the bulk solution

a_1^i activity of solvent at solid/solvent interface

a_2^b activity of solute in the bulk solution

If the activity of both solute and solvent by the mole fraction x are replaced, Equation 2-4 can be written as:

$$K' = \frac{x_2^i a_1^b}{x_1^i a_2^b} \qquad\qquad 2\text{-}5$$

Since $x_1^i + x_2^i = 1$, Equation 2-5 is rearranged to:

$$K' = \frac{x_2^i a_1^b}{(1 - x_2^i) a_2^b} \;\rightarrow\; x_2^i = \frac{K' a_2^b / a_1^b}{K' a_2^b / a_1^b + 1} \qquad\qquad 2\text{-}6$$

In dilute solutions the activity of the solvent is essentially constant, so the ratio K'/a_1^b can be defined to equal a new constant K, and the equation becomes:

$$x_2^i = \frac{K a_2^b}{K a_2^b + 1} \qquad\qquad 2\text{-}7$$

If the x_2^i is replaced by the fraction of maximum surface coverage θ and a_2^b is substituted by solute concentration c, the equation could be written as a more common form:

$$\theta = \frac{Kc}{Kc + 1} \qquad\qquad 2\text{-}8$$

However, many systems that definitely do not conform to the Langmuir assumptions – the adsorption of polymers for example – nevertheless display an experimental isotherm fitted with Langmuir isotherm [31]. Accordingly, the constant in Equation 2-8 is empirical without physical significance thereof. In general, one can assume that the adsorption of polymer at the interface will be monomolecular, since the thickness of the first polymer layer will make attraction for a second layer negligible [135]. In the case of latex particle, this monolayer adsorption is also valid generally, where adsorption is defined in a broad sense as both deposition (irreversible adsorption) and adhesion (chemical contact) [139].

For nonionic water soluble polymers, hydrogen-bonding and solvation forces are important. Though Pattanayek *et al.* [140] successfully established a model using hydrogen bonding to predict the adsorption of non-ionic polymers. However, various conditions may alter the adsorption behavior [141–144]. Chibowski *et al.* [141] studied the influence of residual acetate group of PVOH on adsorption to TiO_2. The hydrophobic acetate group presented a high affinity to

the TiO_2 particle surface but less relevance to pH in the range of 3-10. Backfolk *et al*. [142] studied the PVOH adsorption on silica surface at pH = 8.5 and found negligible adsorption. They also found that pre-adsorbed sodium polyacrylate or sodium polyphosphate increased PVOH adsorption. Santiya *et al*. [143] found that the adsorption of PVOH on alumina increased with pH in the range of 3-11. However, in the presence of polyacrlic acid, the adsorption of PVOH decreased significantly. Labidi *et al*. [144] studied the adsorption of PVA on calcite at pH 7-10 and found that adsorption increased in the presence of sodium oleate, i.e. the PVA-surfactant interaction enhanced PVA accumulation in the vicinity of the mineral surface.

With respect to latex adsorption, a more accurate description of the irreversible interaction is random sequential adsorption (RSA) [145]. Johnson *et al*. [146] verified the RSA theory by employing AFM to investigate the adsorption of a positively charged latex particles adsorbed on mica surface. There, it was found that the compression of the electrostatic double layer of the particles reduced the excluded area, i.e. an increase in the adsorbed amount of latex particles and surface coverage. Filby *et al*. [147] studied the adsorption between carboxylated latex and various minerals and found that the adhesion between them fitted well with DLVO theory, even when the hydration force was not taken into consideration. Adamczyk [148] also discussed the role of electrostatic interaction on particle adsorption and concluded that the electrical double layer affected the interaction range, maximum coverage, and deposition kinetics etc. Besides, he and his coworkers [149] investigated the influence of heterogeneous surfaces on particle adsorption, by covering freshly cleaved mica sheets with colloid iron oxide (i.e. Hematite). They found that the initial adsorption rate increased abruptly with the hematite covered surface. Similarly, Shen *et al*. [150] theoretically investigated the adsorption of a negatively charged particle on a negative planar surface in the presence of a positively charged square patch with regard to the chemical heterogeneity of the surfaces. They found that a critical patch size (commonly at the nanoscale) is required for the adsorption at a given ionic strength. Moreover, this critical size decreases with the increase in ionic strength.

2.4.2 Hydration kinetics of cement

The reaction of various types of cements and their components with water is an exothermic process. Measurement of the total heat and rate of heat development provides information on the kinetics of hydration [151]. The exothermic process could be roughly divided into: I – initial period; II – induction period; III – acceleration period; IV – deceleration period [152]. As a complex system, the hydration of the mineral phases of cement is ongoing under different kinetics at ambient temperature [153].
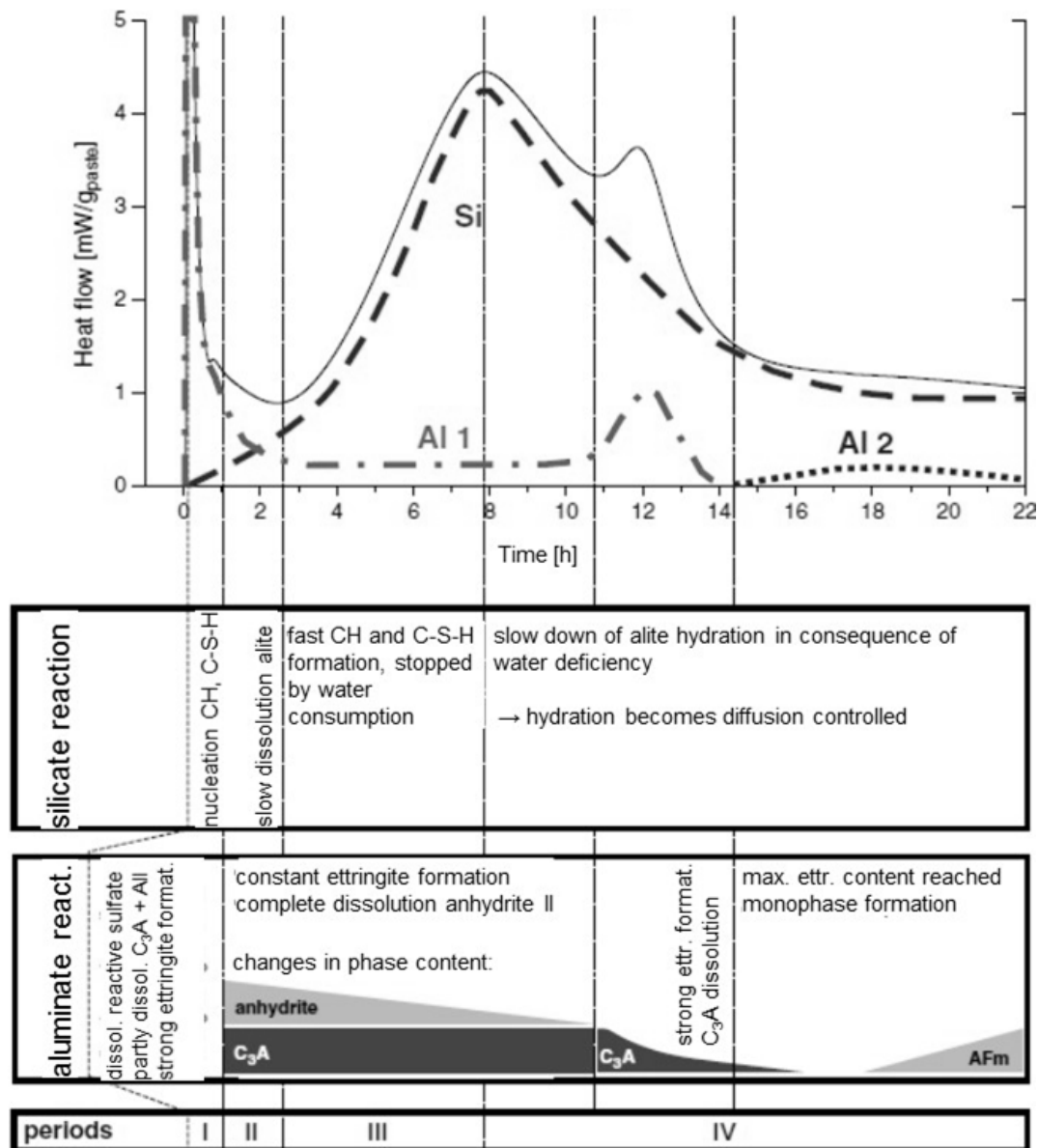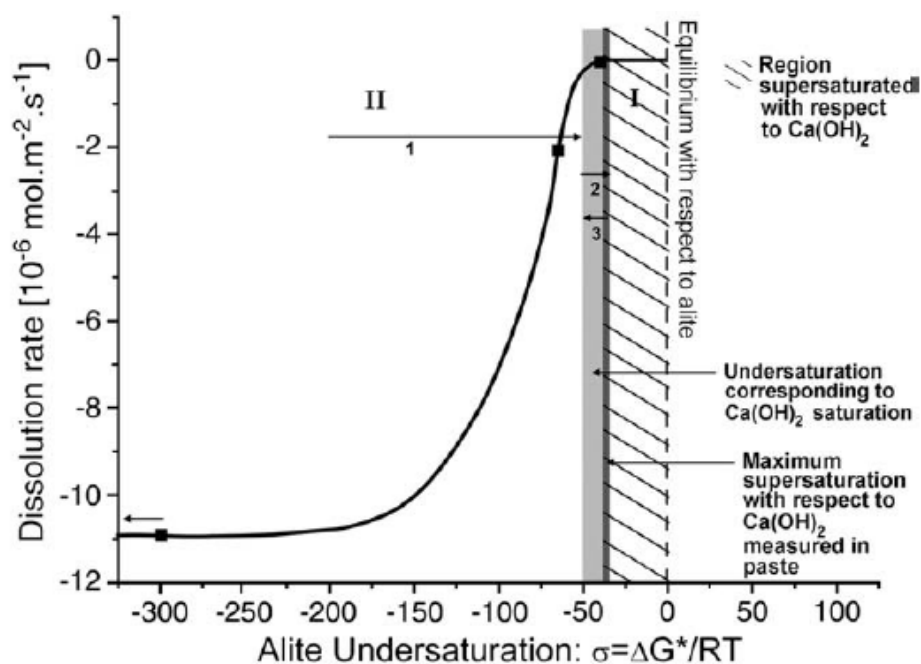
Figure 2.14 Interpretation of the total heat flow during early hydration of Portland cement (reedited the text after Hesse *et al*. [154])

Hesse *et al*. [154] developed a new approach to deconstruct the total heat flow during the early hydration (in Figure 2.14). They correlated the quantitative in-situ XRD method [155] with the enthalpy of involved mineral phases to calculate the heat evolution from silicate and aluminate reaction, respectively. Further, Jansen *et al*. [156] assigned the heat flow to three mechanisms principally: silicate reaction (sum of dissolution of alite and precipitation of C-S-H phase and portlandite), the dissolution of C_3A, and the precipitation of ettringite. They also divided the acceleration and deceleration periods into relatively distinct stages referred to as silicate reaction peak (the main exothermic peak) and sulfate depletion peak (or shoulder described by Taylor [107]) respectively.

Upon contact with water, a series of rapid reactions [157] begins which involves mainly the clinker interstitial phases (i.e. the aluminates and aluminoferrites, alkali sulphates, and free lime), plus the calcium sulphates (gypsum, hemihydrate and / or anhydrite) which have been interground with the cement. The aluminate phases (including the aluminoferrites in most cases) react very rapidly and exothermically, giving a flush of calcium and aluminate ions into solution. In the initial dissolution, protons are transferred from water molecules to the surface oxide compound of C_3S, accompanied by partially dissolution of Ca^{2+} and $H_2SiO_4^{2-}$ [158]. Simultaneously, ettringite precipitates within seconds [159], showing a preferred location on the clinker surface with an agglomeration tendency [160]. The initial precipitation of ettringite could be considered as the result of its low solubility product, which has been intensively investigated by Matschei *et al*. [161] with the $CaO-Al_2O_3-SiO_2-CaSO_4-CaCO_3-H_2O$ system. Following the first rapid reaction, the slow-down of the hydration or induction period has been the subject of considerable debate over the years with many proposed hypotheses [157]. In a recent reviews on the mechanism of cement hydration [152,153], two main hypotheses were discussed. The metastable barrier, however, was suspected and challenged with recent simulation of thermodynamics of C_3S hydration [162]. In contrast, dissolution theory applied to alite hydration [163] seems to be a promising interpretation for the driving mechanism. In this hypothesis, the slow-down of alite dissolution rate was accounted for by the near equilibrium state, while the rate-controlling process was highly related to undersaturation degree (shown in Figure 2.15). Nicoleau *et al*. [163] developed a sophisticated experimental set-up to study the dissolution rate of C_3S and C_2S and verified the hypothesis of dissolution theory proposed by Juilland *et al*. [163]. Nevertheless, Gartner [164] questioned this hypothesis and stated that the difference between the concentration of the solution when the dissolution rate slows down and the equilibrium solubility of C_3S calculated from bulk thermodynamics, is extremely large compared to the difference seen in other minerals. Moreover, unlike simplified ions concentration in C_3S-lime system, the cement system is much more complex. Thus, Nicoleau *et al*. [165] investigated the ion-specific effects on C_3S dissolution and found that divalent Ca^{2+} and especially SO_4^{2-} had a significant influence on surface charge and therefore the solubility. Further, they found that the Si-O-Al covalent bond was formed in low alkaline conditions and was stabilized by calcium ions in the coordination sphere of aluminum ions. Although the mechanism causing the acceleration of hydration is still not agreed due to the simultaneous occurrence of portlandite precipitation and C-S-H growth [153], it is generally accepted to be a nucleation and growth mechanism [152]. At the end of acceleration period, the primary peak is achieved and the deceleration was considered to be related to the formation of hydration layer; further reaction was controlled by diffusion [152].

Figure 2.15 Schematic representation of the rate of dissolution of alite as a function of the undersaturation [163]

As mentioned above, a shoulder or more definite peak could show after the primary exothermic peak due to renewed formation of ettringite [107]. Minard *et al*. [166] studied the C_3A hydration in the presence of gypsum. They found that the rate of formation of ettringite mainly depended on the specific surface of C_3A, indicating that the rate was limited by C_3A dissolution. Pourchet *et al*. [167] investigated C_3A hydration in the presence of gypsum or hemihydrate, finding that higher supersaturation degree and nucleation frequency of ettringite were obtained with hemihydrate. Quennoz *et al*. [168] studied the hydration of the C_3A-gypsum system and found that the dissolution of C_3A was controlled by the sorption of sulfate ions. Also, a broadening of exothermic peak of C_3A hydration in the presence of gypsum was observed at w/s =1. In the presence of alite, Quennoz *et al*. [169] observed the significant modification of heat evolution by enhancing the sulfate depletion peak and attributed this to the reaction between C_3A and sulfate desorbed from the silicate phase. Similarly, in the presence of PVOH, Jansen *et al*. [170] also observed an enhanced sulfate depletion peak of the heat evolution profile of a Portland cement hydration.

However, due to the large variation in the type of latex available, their influence on hydration kinetics is made even more complex, especially in cases where there was limited information based on latex characterization [15,129]. Atkins *et al*. [129] investigated several latices and found that heat evolution was reduced in the presence of the latices. Goto [45] investigated several latices with different charge type or copolymer compositions, finding that the degree of hydration at a given time was reduced with increasing concentration of latex, except for one

non-ionic VAE/Veova latex. Silva *et al*. [15] investigated the cement hydration in the presence of EVA polymer powder in diluted suspensions by soft-XRD and found that the formation of acicular ettringite was retarded for several hours.

2.4.3 Film formation in cement environment

In cement paste, electrolytes, high humidity and a charged surface can influence the film formation to some extent [9,39,171]. Gretz *et al*. [171] investigated the film formation of negatively charged styrene acrylate latex in deionized water or synthetic cement pore solution and found that the presence of electrolytes delayed the film formation and resulted in more fractured film. Beeldens *et al*. [9] found that the relative humidity influenced the film formation of high T_g polymer by direct relation with the drying rate. Gretz [39] also found that at low p/c ratios (~ 0.08), no film formation was observed for, for which polymer adsorption on cement minerals should be responsible.

3 Materials and Methods

In order to reveal the possible interaction described in chapter 2.4, experiments were carried out according to the procedures given in Figure 3.1.

Latex characterization

- Chemical composition → FTIR / TGA
- Glass transition temperature → DSC
- Free PVOH content → Ultracentrifugation
- Surface tension → Wilhemy plate
- Particle Size Distribution → Laser granulometry
- Surface charge → Particle charge titration

Cement mineral characterization

- Phase composition → XRD with Rietveld refinement
- Specific surface area → BET / Blaine test
- Particle size distribution → Laser granulometry

Initial interaction of latex /PVOH with cement in colloid state

In diluted state (w/c ≈ 9)

- Charge density → Particle charge titration
- Adsorption on minerals → Turbidity (UV/Vis spectrometer) / TOC
- Electrokinetic → Zeta potential (electroacoustic)

Hydration kinetics of cement affected by latex / PVOH

In concentrated state (w/c = 0.5)

- Rate of hydration → Isothermal calorimetry
- Ions composition → ICP-OES
- Hydration products → In-situ XRD

Film formation of latex stabilized with PVOH in cement environment

latex film

- Minimum Film-forming temperature → Kofler bank
- Stability in the pore solution → PSD via lasergranulometry
- Morphology → ESEM / AFM
- ✓ 80 % relative humidity
- ✓ on cement substrate
- ✓ in **S**ynthetic **C**ement **P**ore **S**olution

Figure 3.1 Flow chart of objectives of this study and related characterization methods

3.1 Characterization methods

All experiments were conducted in deionised water (conductivity ~ 0.055 µS/cm at 25 °C) produced by TKA MicroPure.

3.1.1 Laser granulometry

Laser granulometry was conducted via Mastersizer 2000 from Malvern, in which the particle sizes of range from 20 nm to 2000 µm could be measured. For latex, the dispersions were diluted to 0.1 wt.-% by deionized water; for the cement or clinker phase, it was measured in isopropanol as a medium, subjected to ultrasonic dispersion for 30 s. The particle size distribution curve was calculated automatically by computer software based on the Mie scattering theory.

3.1.2 Particle charge titration

The streaming potential of latices as a function of pH was determined by titration with either 0.1 mol/L HCl or NaOH to a 10 mL diluted latex dispersion (c = 0.1 wt.-%). Its dependence on the cationic ion concentration was determined by titration with 0.1 mol/L NaCl, KCl and $CaCl_2$ solution to a 10 mL diluted latex dispersion (c = 0.1 wt.-%), either in deionized water or in alkaline solution (adjusted by NaOH solution to pH = 12.5) using Mütek PCD 03 from BTG Instruments. The particle charge densities of the latices were determined by titratiing 15 mL of 0.1 wt.-% polymer dispersions against 0.01 mol/L cationic PDADMAC (polydiallyldimethylammonium chloride). This corresponds to a charge amount of 0.01 eq/L. With the volumetric consumption of PDADMAC solution, which is needed to reach the Isoelectric Point (IEP) of the streaming potential, the amount of charge can be calculated.

3.1.3 Differential scanning calorimetry (DSC)

To determine the glass transition temperature (T_g) of a latex polymer, aqueous polymer dispersions were dropped on a clean stainless steel plate. For evaporation of the water, dry film was transferred to a drying cabinet for at least 24 hours. Then, 10 mg of the sample was cut and weighed in an aluminium pan with a pinhole lid. Sample measurement was conducted by DSC 1 from Mettler-Toledo at a heating rate of 10 K/min from -70 to 160 °C. T_g was determined from the second heating curve (shown in Figure 3.2). If no specification is given, the T_g of the latex polymer is defined as the middle point of the transition zone.
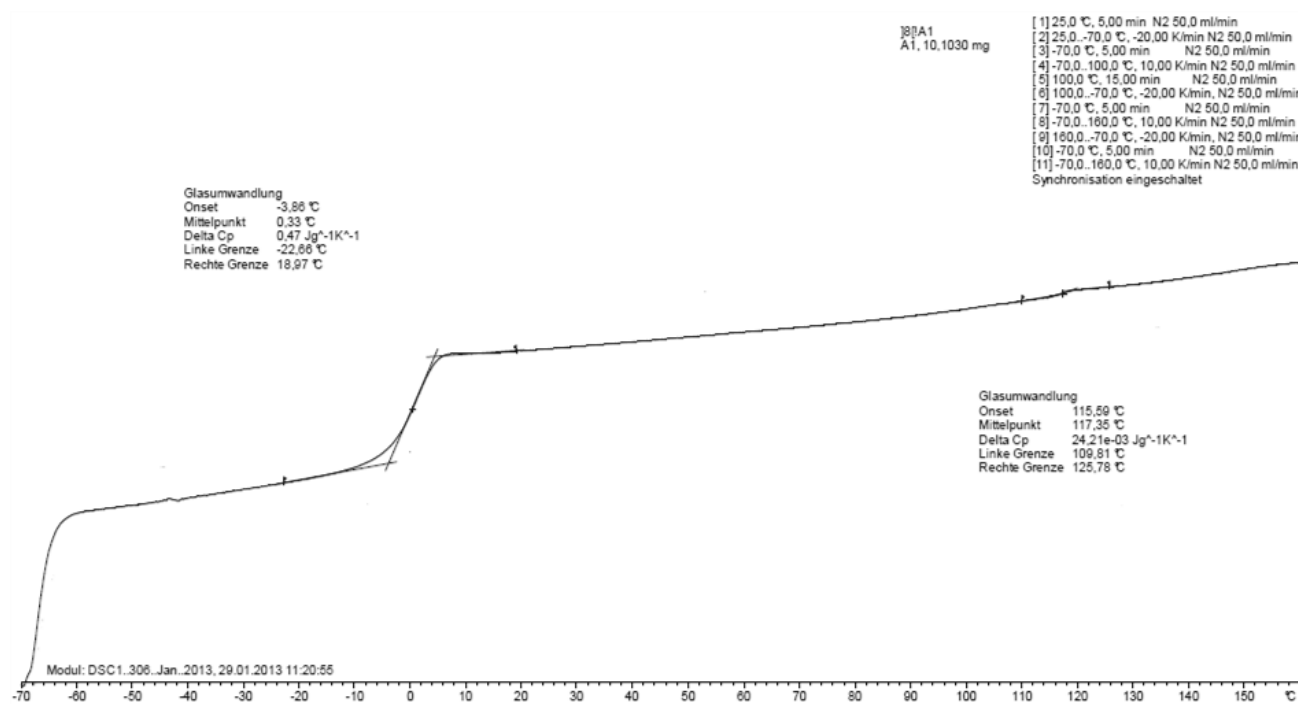
Figure 3.2 DSC curve of the latex polymer

3.1.4 Thermogravimetric analysis (TGA)

Thermogravimetry was conducted via TGA/DSC 1 from Mettler Toledo: the temperature interval is 38 – 1000 °C, with heating rate of 10 K/min under N_2 gas. For sample preparation, 10 wt.-% polymer dispersions were centrifuged at 40,000 rpm for 2 hours and the sediment was taken out and dried in the oven at 50 °C.

3.1.5 Surface tension (Wilhelmy plate method)

All solutions or dispersions were stirred for a minimum of 30 min prior to the measurement. Equilibrium surface tension was measured with a thermostated Krüss K11 tensiometer. The tensiometer was calibrated using deionised water prior to all measurements. The solution or dispersions were poured into a petri dish, which was then placed into an insulated metal jacket. Surface tension was measured using the Wilhelmy plate method. After each measurement, the plate was rinsed with deionised water and flamed to dry to remove any trace contaminants.

3.1.6 Kofler bank

The minimum film forming temperature (MFFT) was determined using a MFT Thermostair Kofler heating bench from Coesfeld Material Test. The heating surface was covered with aluminum foil before each measurement. Polymer dispersions (~50 wt.-%) were then distributed evenly using a film applicator (bed height 400 µm) over the entire length of the

Kofler bank. The temperature range was set from -5-15 °C for low T_g VAE polymer and 0-20 °C for high T_g VAE polymer. MFFT can be read (in Figure 3.3) from the point at which a transparent, crack-free film was observed.

Figure 3.3 Films on Kofler bank

3.1.7 Brunauer-Emmett-Teller method (BET)

Surface area determinations based on the Brunauer, Emmett, and Teller (BET) model were performed for minerals using a Sorptomatic 1990® from CE Instruments, Austin, Texas USA. According to the BET method, the surface area of a sorbent may be calculated from the N_2-isotherm observed at the boiling point of nitrogen. By analysing the adsorption and desorption curves within the relative pressure ranges [p/p_0] of approximately 0.05 and 0.33, the volume of the sample is determined and corresponds to the quantity of nitrogen necessary for a monomolecular layer.

3.1.8 Blaine test

The Blaine test was carried out via an electronic Blaine instrument from Testing Bluhm & Feuerherdt GmbH, Berlin/Germany. Prior to the measurement, the real density of the powder was determined by a helium pycnometer. ~3 g powder was weighed and transferred to a stainless-steel measuring cell with one sieve mesh and two filter papers. Then, the powder was compacted with the attached piston according to DIN EN 196-6. After the cell was fixed, the measurement was automatically conducted by the computer program and the specific surface area was calculated based on the air permeability through the powder.

3.1.9 Fourier-transfer infrared spectrometry (FTIR)

FTIR was conducted via Nicolet 6700 from Thermo Fisher Scientific under air. For latex characterization, one drop of polymer dispersions was coated in a small square stainless plate and heated to 40 °C until dry. The sample was subsequently placed on an Attenuated Total Reflection (ATR) accessory and the measurements were conducted from 400 to 4000 cm^{-1}. The air background was subtracted by the software automatically.

3.1.10   UV-vis spectrophotometry (adsorption isotherm)

18.00 g polymer dispersions with different concentrations ranged from 0-5 wt.-% were prepared. Subsequently, in order to separate the fine mineral particles from the polymer dispersions, a three-step method was carried out according to Merlin *et al.* [19] with some minor modifications. First, 9.00 g polymer dispersion was mixed with 1.00 g mineral for 1 min by a vortex mixer (step 1); secondly, the tube of polymer/mineral mixture was stood upright for 10 min (step 2); thirdly, the supernatant was decanted and stood for a further 20 min when non-ionic latex were employed or centrifuged at 100 g force in the presence of anionic latex (step 3). The second supernatant was recovered with the addition of 0.5 ml of 30 wt.-% HCl. After that, the second supernatant was diluted to the same volume as the other untreated half polymer dispersions. The procedure is illustrated in Figure 3.4.

$$D = \frac{C_{original} - C_{supernatant}}{C_{original}}$$
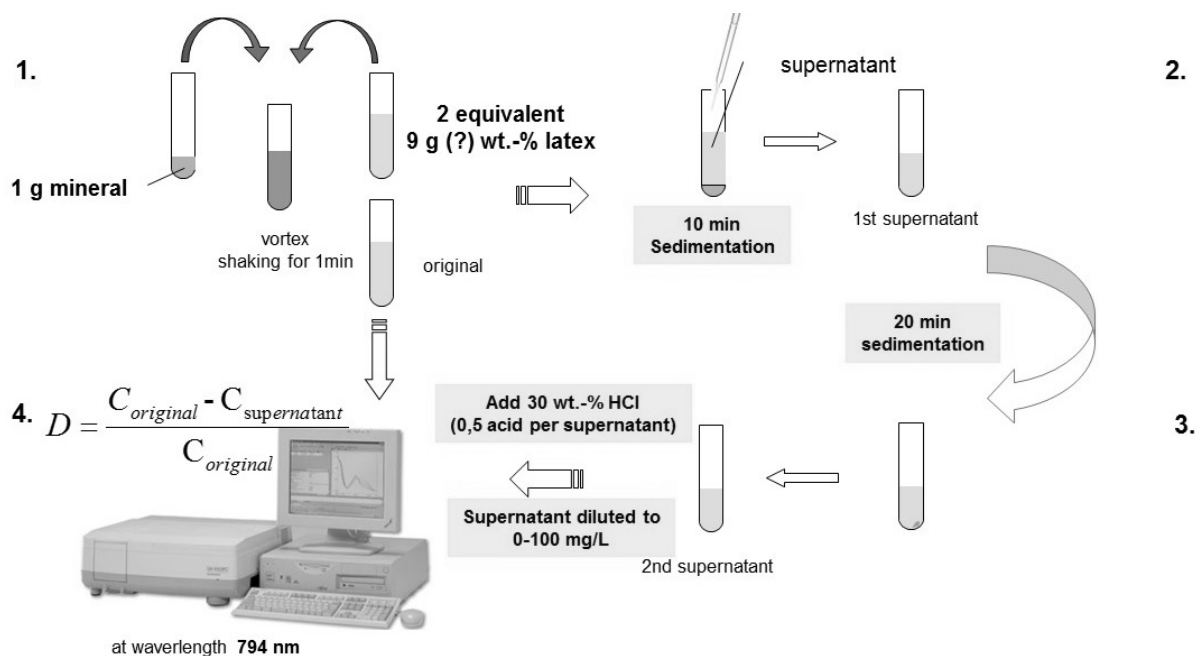
Figure 3.4 Steps for the determination of the adsorption isotherm

Turbidity was measured with a Shimadzu UV 1650 PC spectrometer at a single wavelength of 800 nm (non-ionic latex) or 850 nm (anionic latex), since most of the light is scattered forward while the wavelength is similar or larger than the particle size (as illustrated in Figure 3.5). The absorption, which is defined as the difference between incident and transmitted light intensities, showed precise linear correlation with latex concentration (Figure 3.6).
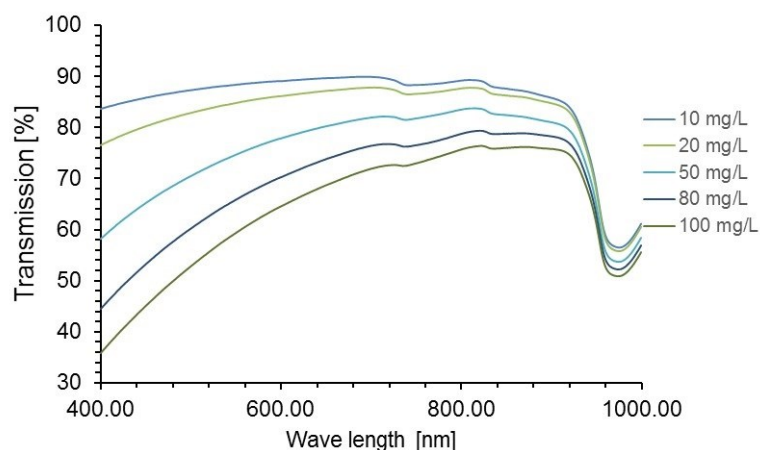
Figure 3.5 Scattered light intensity as a function of latex concentration
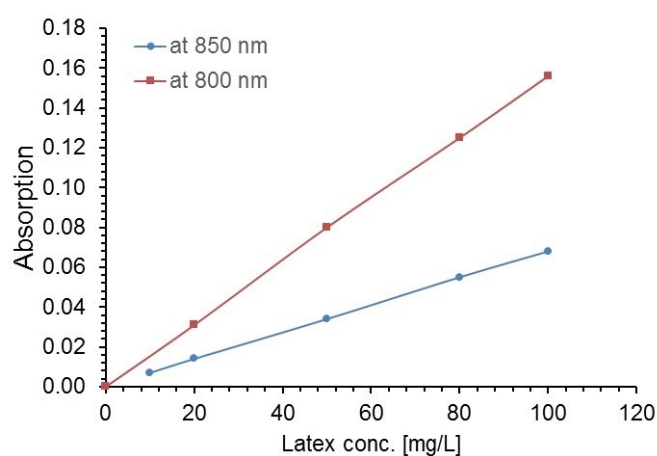
Figure 3.6 Linear relationship between concentration and absorption

Finally, depletion was calculated directly based on the ratio between the value of the supernatant and that of untreated polymer dispersions (step 4).

3.1.11   Total organic carbon (TOC) (adsorption isotherm)

PVOH adsorption was investigated only on the clinker phases. 2.7 g polymer solution with different concentrations ranging from 0-0.20 wt.-% were prepared. Then, the solution was mixed with 0.3 g mineral for 1 min and centrifuged for another 15 min at 3,000 g force. The supernatant was extracted by a syringe and filtered with a 0.4 µm syringe filter. 20 µl of 30 wt.-% HCl was added to the filtrate and diluted to 20 ml. The final solution was measured by TOC-L from Shimadzu. The filtrates, as well as known PVOH concentrations were also measured for the calculation of PVOH depletion.

3.1.12   Zeta potential (electroacoustic method)

Unlike other techniques, Zeta potential determined by the electroacoustic method can be measured at very high solid concentrations. In this study, the Zeta potential was measured

using DT310 from Dispersion Technology. The Zeta potential was calculated from the colloidal vibration current (CVI) that was induced by ultrasound propagation through the suspension. The principle of this method as well as its applications were described in detail elsewhere [172]. Though this method is able to measure high solid ratio specimen, high water/cement ratio suspensions were performed in accordance with adsorption protocol.

The actual ratio between cement and polymer dispersions was equal to 9. Polymer concentrations ranged from 0-1 wt.-%. Regarding the high ionic background of cement suspensions, filtration via a Buchner funnel was measured to subtract the background (i.e. ionic vibration current) from the CVI. The Zeta potential was calculated by the software based on the recorded electric signal.

3.1.13   Isothermal calorimetry

10 g cement was filled into 10 mL plastic vials, mixed with the specific amount of diluted latex or PVOH at a <u>w/c ratio of 0.5</u>. It was homogenized for 1 min by vortex vibration and the fresh sample was placed into the isothermal calorimeter from C3 Prozess und Analysentechnik GmbH, Haar/Germany. The temperature was set to 20 °C. Heat flow data logging was recorded for 48 hours with an interval of 30 s.

3.1.14   ICP-AES (for ions concentration)

ICP-AES, also referred to as Inductively Coupled Plasma Optical Emission Spectrometry (ICP-OES) was employed to analyze the ions' composition in cement pore solution. Solution samples were measured via Spectro ciros vision from SPECTRO Analytical Instruments GmbH.

Latex or PVOH was firstly diluted to achieve a <u>w/c ratio of 0.5</u>. The polymer dispersions or solutions were mixed with 40 g cement manually for 1 min. The pore fluid was extracted at different intervals by vacuum filtration using qualitative filter paper (pore size of 4-7 µm) and the pHs of the extracts were measured immediately. The fluid was further filtered by a 0.22 µm PVDF syringe membrane and acidified to pH ~ 2 with 30 wt.-% HCl. The whole procedure is illustrated in Figure 3.7. The clear solution was stored in sealed 50 ml plastic tubes and put into a refrigerator (~ 3~5 °C) until analysis. For Ca, S, Na, K elemental analysis, further dilution of a factor of 20 was applied to keep the concentration of those elements below 200 mg/L (20 mg/L for Ca).
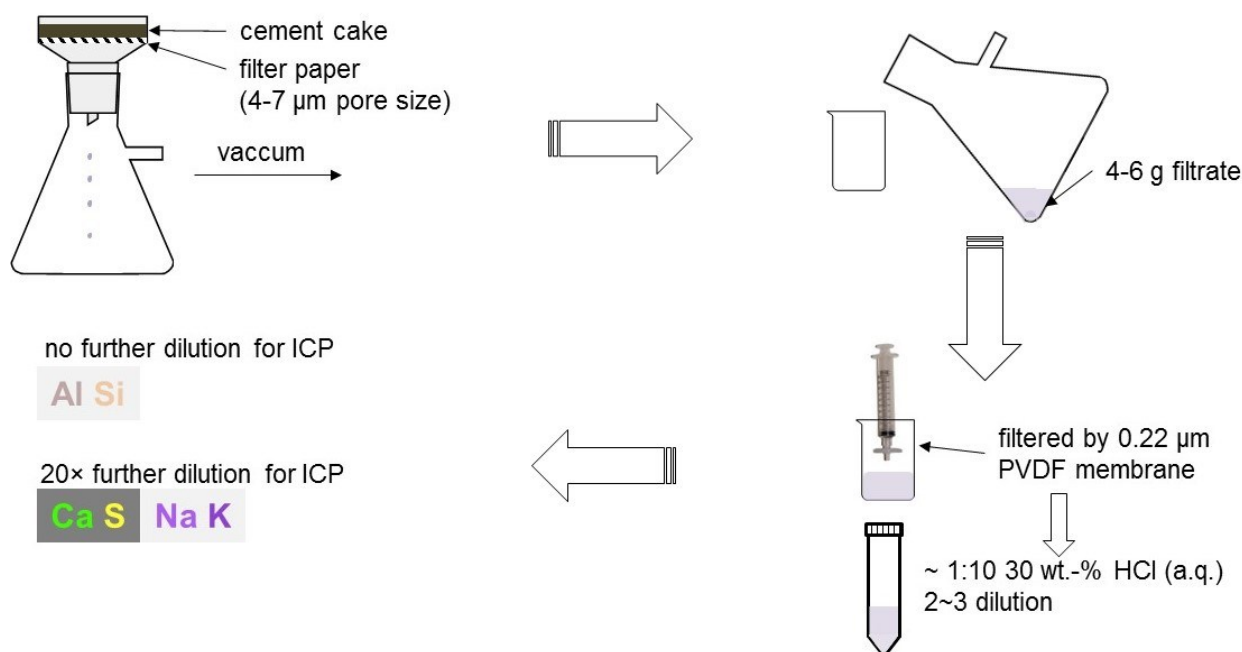
Figure 3.7 Procedures for the filtration of the cement pore solution

The average ion concentration was achieved from 3~5 repeat experiments. The reproducibility and accuracy are shown in Figure 3.8, with the standard deviation being approximately ± 10-15% for major ion species in the solution. As presented, dilution of the original solution may increase the error. Also, the variation of ambient temperature may affect the dissolution. Furthermore, the filtrate amount was varied, which may result in the deviation of the calculated concentration (in Figure 3.9).
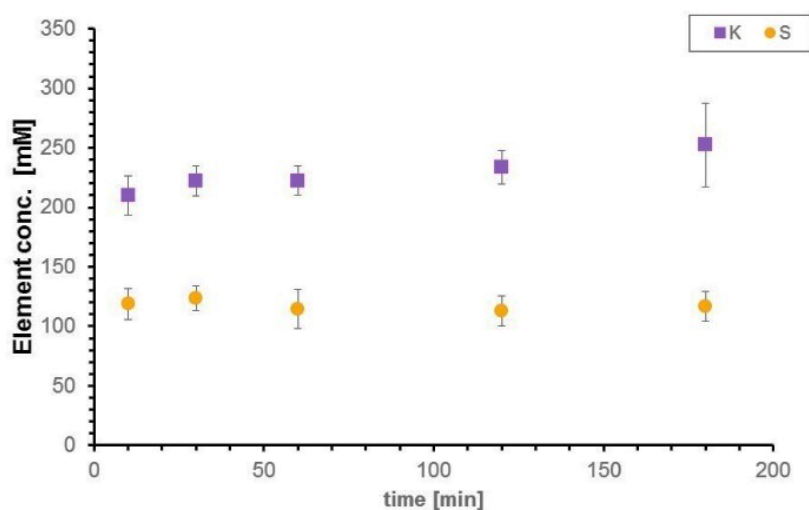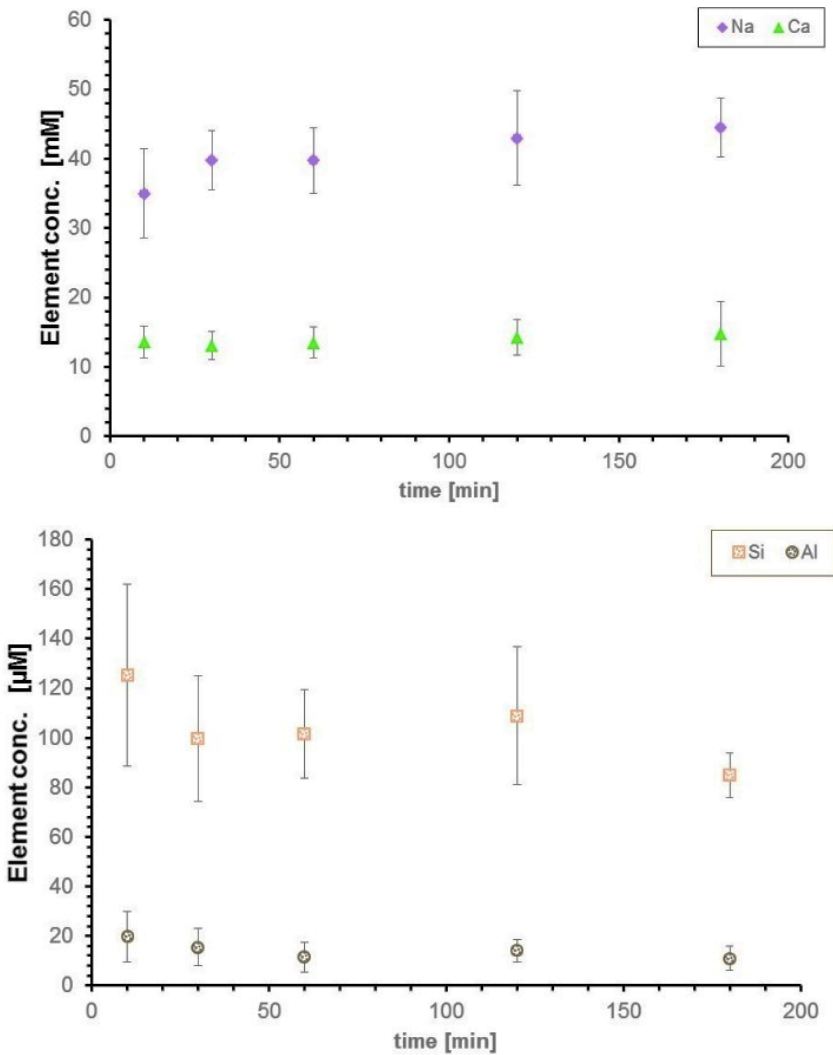
Figure 3.8 Ion concentration of the cement pore solution
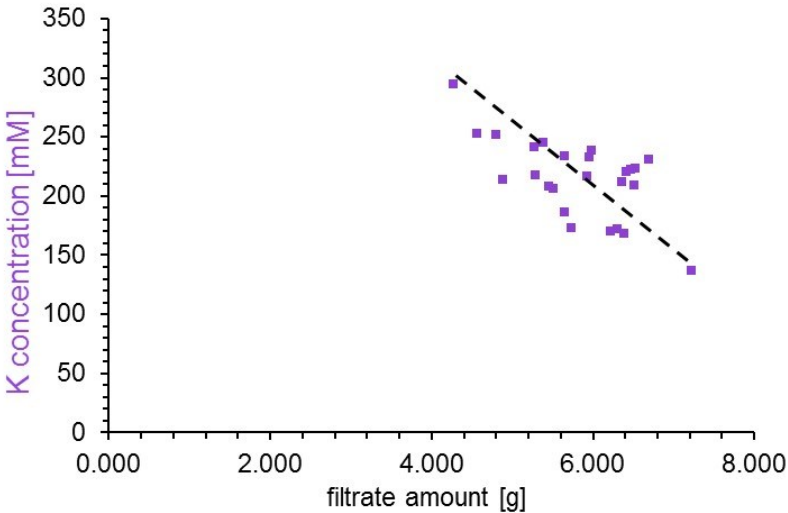
Figure 3.9 Relation between measured concentrations and filtrate amounts

3.1.15   X-ray diffraction (XRD)

Cement powder was measured at room temperature on a Bruker AXS D8 instrument, utilizing a Bragg-Bretano geometry. Step size was set to 0.017 ° 2θ and accumulated time per step of 29.8 s. The X-ray tube (Cu K$_\alpha$) operated at a voltage of 45 kV and a current of 40 mA. A nickel filter was setup for the incident beams, and an aperture slit of 0.5° was utilized. The scan range was set from 6-70° 2θ. Rietveld refinement of the X-ray diffractogram was analyzed by using the TOPAS 4.0 software.

For the cement paste, in-situ XRD measurement was conducted via PANalytical Empyrean with an interval of 15 min for 24 hours, 2θ degree ranged from 5-65° at a voltage of 40 kV and a current of 40 mA. Samples were prepared at a w/c of 0.5 by vortex vibration for 1 min. The fresh sample was covered by a Kapton™ film to inhibit water evaporation and the sample holder was connected to a Peltier stage to keep the ambient temperature at 20 °C.

3.1.16   Environmental scanning electron microscopy (ESEM)

For wet samples, 20 µL of the sample was deposited on a concave Al disk sample holder. For observation of microstructure of the latex film, the sample was transferred into a Quanta 200 F (FEI, Eindhoven/Netherlands) ESEM equipped with a peltier cooling stage and a gaseous secondary electron detector. The Al disk was placed on the cooling stage in the chamber at < -2 °C. A gentle pump-down sequence was performed automatically by the software to prevent water evaporation while reducing the chamber pressure. Once the water vapor purging cycle was completed, a water vapor pressure of 6.5 – 7.5 mbar was set for wet samples. To allow high resolution imaging, the pressure was lowered to dehydrate the surface layer for a very short time. Wet samples were investigated under water vapor pressure from 3.0-5.0 mbar. Imaging was carried out at accelerating voltages of 20.0 kV, and at working distances of 6-8 mm. To minimize the influence of the electron beam, the imaging area was shifted ~ 20 µm from the focus area.

For dry samples, small pieces were cut from long side of the dry film and fixed to the Al disk sample holder by adhesive tabs. Then, the reduced water vapour pressure condition (1.0 to 2.0 mbar) was applied. Imaging was carried out at accelerating voltages of 10.0 kV, and at working distances of 8-11 mm.

3.1.17   Atomic force microscopy (AFM)

AFM images were obtained in ScanAsyst™ mode using a Dimension Icon from Bruker, Billerica, MA/USA. This ScanAsyst™ mode is based on PeakForce™ tapping mode but with advanced algorithms to monitor image quality and to make the appropriate parameter

adjustments. The PeakForce™ tapping mode operates in a similar fashion to the tapping mode but differs from it in that it operates in a non-resonant mode [173]. In this study, "ScanAyst Air" cantilevers made of silicon nitride with the length about 100 μm were used, which oscillated well below the resonance at around 70 kHz. AFM tips used here were rectangular silicon with a nominal spring constant of only 0.4 N·m^{-1}. For image acquisition, a "PeakForce" amplitude of about 150 nm was set.

3.2 Chemicals and Materials

All chemicals and materials were used without further purification.

3.2.1 Chemicals

Chemicals used in this study are listed in Table 3-1.

Table 3-1 Chemicals

No.	Name	Type	Properties
1	$CaSO_4 \cdot 2H_2O$	Sigma-Aldrich	ACS reagent, >98%
2	Na_2SO_4	Sigma-Aldrich	ACS reagent, powder
3	K_2SO_4	Sigma-Aldrich	ACS reagent, powder
4	KOH	Sigma-Aldrich	ACS reagent, pellets
5	$CaCO_3$	Sigma-Aldrich	ACS reagent, ≥98%
5	$CaCl_2 \cdot 2H_2O$	Sigma-Aldrich	ACS reagent, ≥99%
7	HCl (aq)	Sigma-Aldrich	≥30 wt.-%
8	KCl	Merck	ACS reagent, powder
9	NaCl	Merck	ACS reagent, ≥98%

3.2.2 Polymer

Three kinds of VAc based latices were used in this study: two Vac/E copolymer latices (latex A and B) with different ethylene content and one VAE latex (latex C) containing traces of 2-Acrylamido-2-methylpropane sulfonic acid (AMPS, as the trademark of the Lubrizol Corporation). The latter was induced in order to compare either the influence of different physicochemical properties (e.g. particle size, surface charge, etc.), or the effect of PVOH. However, the emphasis of this work was only related to non-ionic VAE latex A and B, which were stabilized with non-ionic PVOH. A schematic illustration of its microstructure is presented in Figure 3.10, organized according to literature [24,25]. All the latices were synthesized via semi-batch emulsion polymerization with redox initiator and provided by Wacker Chemie AG,

Burghausen/Germany. Moreover, another 20 wt.-% PVOH solution (88 mol% hydrolysis, Mw ~ 27K Da, R_H ~ 4 nm) was provided by Wacker Chemie, for the purpose of elaborating the potential influence of PVOH on the interaction with the cement minerals. For the ease of clarification, the phrase 'latex polymer' in this work denotes only the polymer whose constituent is the latex particle. 'Latex' refers to the mixture of latex particles and PVOH in the case of a non-ionic latex.
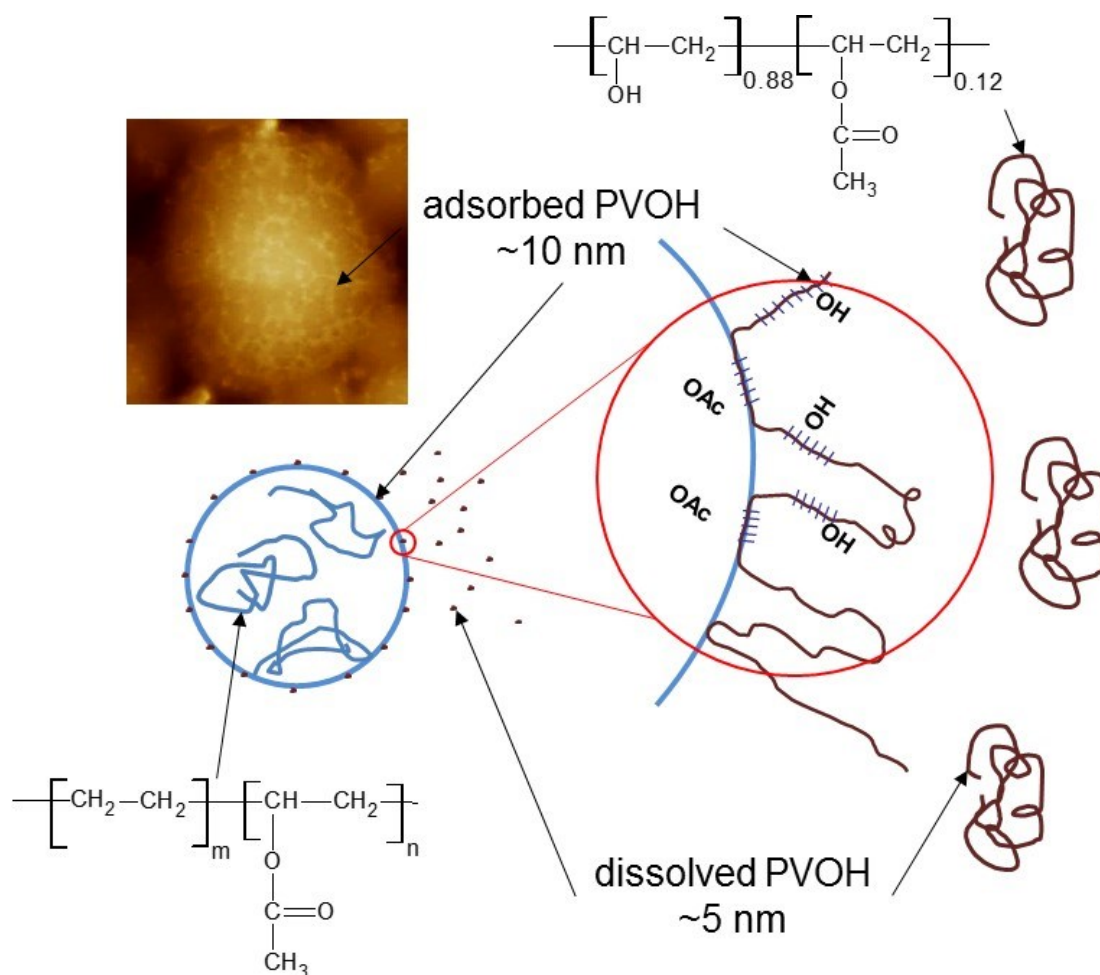

Figure 3.10 Schematic illustration of the VAE latex stabilized with PVOH [24,25]

Information about latex polymer composition is given by the FTIR spectrum in Figure 3.11, showing a typical vinyl acetate-based polymer composition. The absorption peaks at about 3454 cm^{-1} can be attributed to O-H stretching; 2932 cm^{-1} to C-H asymmetric stretching of CH_3 or CH_2; 2857 cm^{-1} to C-H symmetric stretching of CH_3 or CH_2; 1728 cm^{-1} to C=O stretching; 1433 cm^{-1} to CH_2 in-plane bending or scissoring; 1370 cm^{-1} to C-H (CH_3) symmetric stretching and 1226 cm^{-1} to C(=O)-O stretching; 1017 cm^{-1} to out of plane –CH bending; and 942 cm^{-1} to O-H out-of plane bend [174]. The relative absorption of CH_2 at 2932 cm^{-1} to C(=O)-O at 1226 cm^{-1} is approximately 1:4 for latex polymer A and 1:6 for latex polymer B, indicating that latex

polymer A contains more methylene group but less VAc group. This is also in accordance with their compositions.
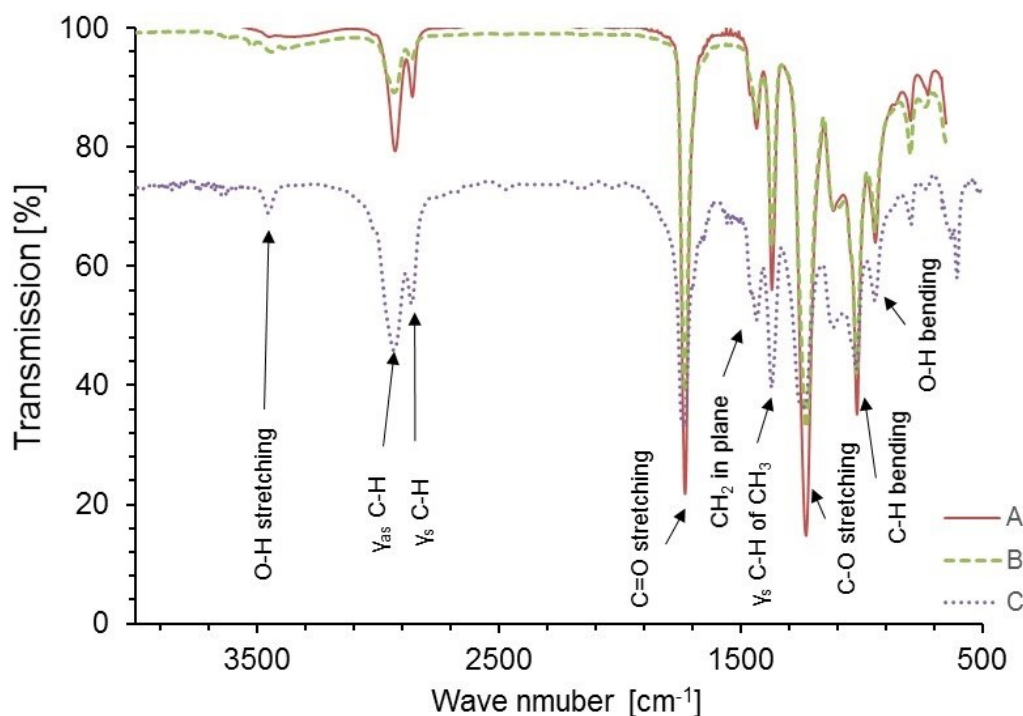
Figure 3.11 FTIR spectrum of investigated latices

The general physical properties of the latices are listed in Table 3-2. Individually, MFFT is more related to latex film, which refers to the lowest possible temperature at which film formation can occur as determined by visual observation of cracks or whitening [175]. Nonetheless, the property is the indicator of the lower temperature range over which a latex can be used in applications [94].

Table 3-2 Characterization of latex polymer (provided by Wacker Chemie AG)

Latex	Monomer ratio [wt.-%]	Solid [wt.-%]	PVOH [wt.-%]	Specific surface area [m²/g]	Surface tension [mN/m]	T_g [°C]	MFFT [°C]
A	80:20	55.5	4.3	7.14	48.3	0	<0
B	93:7	57.7	5.5	7.13	47.3	22	6
C	/	53.2	/	14.8	37.6	10	<0

In Table 3-2, the weight ratio of monomers was determined by the weight loss due to pyrolysis of VAc group [176]. Even though the latex was centrifuged, it was impossible to remove all adsorbed PVOH. Figure 3.12 presents the PVOH amount in serum, showing nearly no difference between the original and the dialyzed latex (see section 3.3.1). This result indicated an adsorption-desorption equilibrium between the particle surface and PVOH. It was thus

inevitable that partially adsorbed PVOH was still incorporated in the sediment even after ultracentrifugation (~40,000 g force for 2 hours), resulting in an overestimated VAc content together with the grafted PVOH in the copolymer.
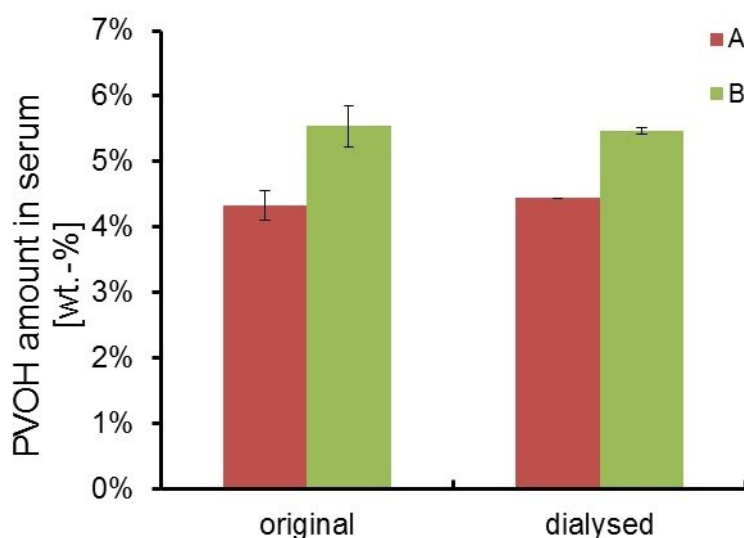
Figure 3.12 PVOH amount in serum by weight of latex solid after ultracentrifugation

Alternatively, when the empirical Fox equation (Equation 3-1) is used, T_g of the copolymer can be approximately calculated from T_g of their homopolymers [56], using the weight fraction of the monomers and vice versa.

$$\frac{1}{T_g} = \frac{w_1}{T_{g,1}} + \frac{w_2}{T_{g,2}}$$
                                                                                   3-1

Where,

T_g Glass transition temperature of the copolymer [K]

w Weight fraction of monomer in the copolymer [w/w]

$T_{g,1}$ Glass transition temperature of the homopolmyer of monomer 1 [K]

In order to determine the weight fraction, T_g of the homopolymer must be known. Here, T_g of polyethylene and polyvinyl acetate was taken as -95 °C and 42 °C respectively [56]. Then, calculated VAc:E ratio is 80:20 for latex A and 91:9 for latex B. Besides, the composition of latex polymer C could be postulated as 85:15 on the same principle.

As a colloid, PSD of the latices is an essential parameter. PSD of the investigated latices was given by means of laser granulometry based on Mie scattering theory (Figure 3.13). Anionic latex C showed narrow PSD as well as fine particles. On the other hand, PVOH stabilized latex A and B showed very similar broad PSD, with a distinguished bimodal distribution. The specific surface area was obtained directly from the theoretical model based on laser granulometry.
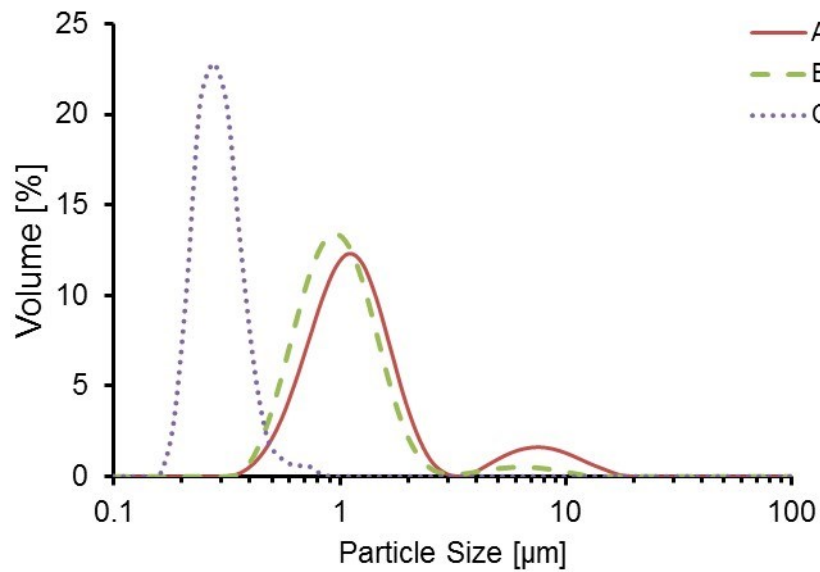
Figure 3.13 PSD of investigated latices

From ESEM images, the bimodal distribution of particle size was more evident (Figure 3.14). Large particles had a typical diameter of 1.5 µm, while small particles were 0.7 µm or less. Importantly, this observation was not the same as that obtained from laser granulometry, since volume weighted particle size distribution is more sensitive to the particle diameter, i.e. a large particle contributes the volume fraction more by its radius cubed. In Figure 3.15, the particle size of latex C possesses a diameter of 300 ± 100 nm, which fitted the result obtained by laser granulometry well.
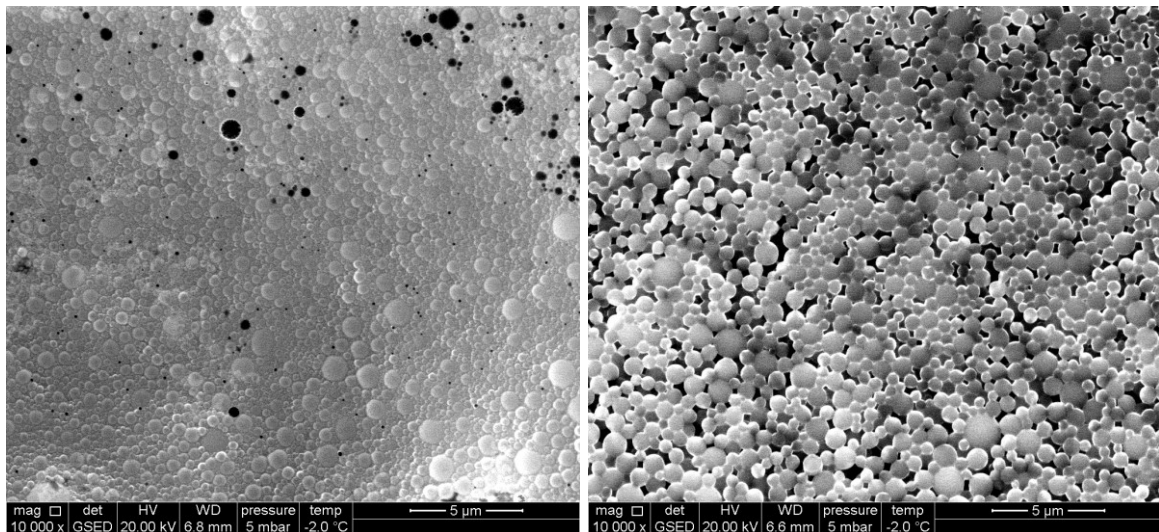
Figure 3.14 ESEM image of latex A (left) & B (right) (Note: black spots were voids)

| mag □ | det | HV | WD | pressure | temp | ━━ 5 µm ━━ |
| 10 000 x | GSED | 20.00 kV | 8.0 mm | 3 mbar | -2.0 °C | |
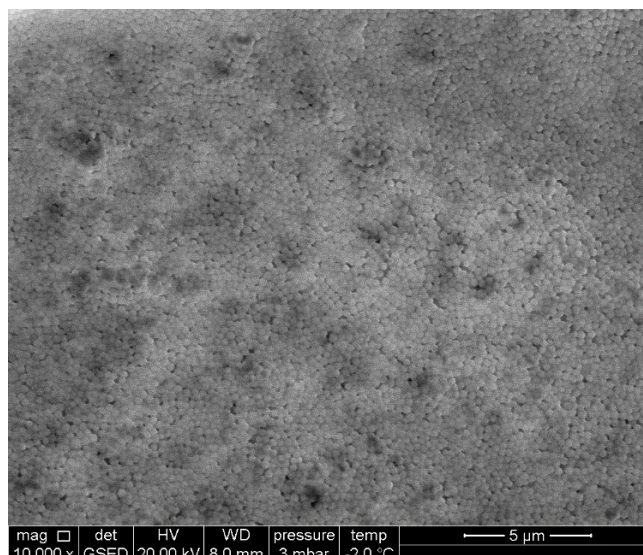
Figure 3.15 ESEM image of latex C

In this study, VAE latex was stabilized with non-ionic PVOH, but the redox initiator or other dissociable substances may impart some charge to the overall surface. It is well known that the surface charge of latex particles varies with pH. Obviously, this effect will impact the interaction with other charged particles. Thus, pH dependence of the electrokinetic surface charge was measured by means of a particle charge detector (PCD). As shown in Figure 3.16, at the start point, the non-ionic latices showed a negative surface at pH 4-4.5. With the increase or decrease of pH, the streaming potential of all the latices decreased. Though the absolute value cannot be quantitatively interpreted [177], the streaming potential at pH = 12 indicates that latices A and B possess a slightly negative surface charges in alkaline conditions. This may be attributed to the initiator on the particle surface, the deprotonation of the PVOH corona, or the alkaline hydrolysis of VAc groups. Nevertheless, the negative charge of the surface may contribute to the interaction with the charged mineral surface.
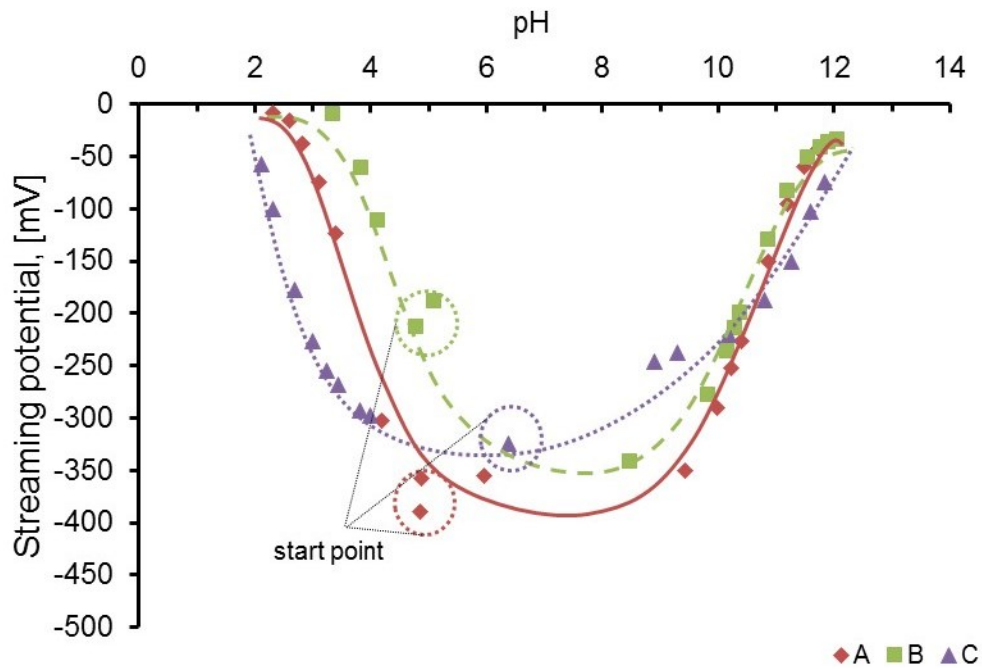
Figure 3.16 pH dependent streaming potential of the latices (0.1 wt.- %)

3.2.3 Cement minerals

The Portland cement used in this study was CEM I 42.5 R from Schwenk Zement. The quantitative phase analysis was conducted by Rietveld refinement based on powder diffraction pattern of the cement, which showed a little variation of the mineral phases (Table 3-3).

Table 3-3 Mineral phases of Portland cement [wt.-%]

Batch #	C_3S (m)	α-C_2S	β- C_2S	C_4AF	C_3A (c)	$C\bar{S}$	calcite	dolomite
1	55.39	1.51	11.98	7.74	8.31	5.26	5.46	0.76
2	59.94	2.89	6.54	9.23	7.90	3.55	3.88	2.55

C_3S (m) denotes monoclinic polymorph of the alite, and C_3A (c) denotes cubic crystal lattice of the aluminate phase. The pure clinker phases C_3S and C_3A were provided by Wacker Chemie, Burghausen / Germany. The specific surface area of the minerals is presented in Table 3-4.

Table 3-4 Specific surface area by different methods

Mineral	BET [m^2/g]	Blaine [m^2/g]	Laser granulometry [m^2/g]
cement	1.01	0.40	0.22
C_3S	0.77	0.35	0.39
C_3A (cubic)	0.91	/	0.37

The particle size distribution of the minerals was characterized by laser granulometry using a general model, as shown in Figure 3.17. Since cement particles are non-spherical, this

diameter should not be confused with volume equivalent spherical diameter [110], where the latter is applied to spherical particles like latex particles. Nevertheless, this PSD stated a general overview of the particle sizes, which were in the range of 1-100 µm.
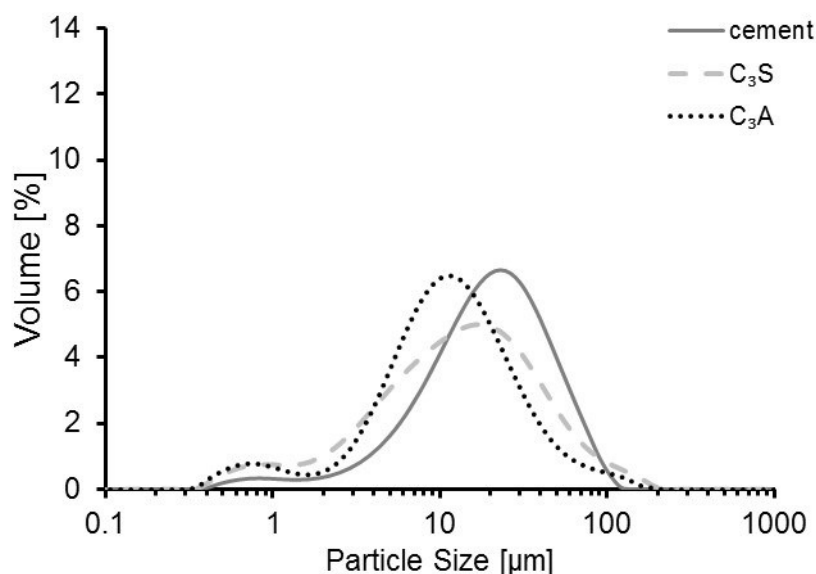
Figure 3.17 Particle size distribution of the investigated minerals dispersed in isopropanol

3.3 Sample preparation

3.3.1 Latex film formation

To investigate the influence of high humidity, undiluted latex was casted on a glass slide (75 mm × 25 mm × 1 mm) by film applicator with a thickness of 400 µm. Then, the glass slides were sealed in a Petri dish. To achieve 85% R.H. in the atmosphere, saturated KCl solution was filled in the petri dish which was beneath the glass slide. For samples with lower PVOH content than the original, latices were dialysed in running deionized water for 3 days by a membrane cut off from 100K Da; for samples with higher PVOH content, additional 5 wt.-% PVOH with M_w of 27K Da was added according to the solid content of the original latex.

The cement substrate was prepared two days before the film was applied, with a water cement ratio of 0.5. The cement slurry was poured onto a PVC board and stored under ambient conditions (23 ± 2°C, 50 ± 5 % R.H.). The film was coated on the hardened cement paste by a film applicator with a thickness of 400 µm, the specimens were stored under ambient conditions. For ESEM investigation, a small piece measuring around 2 cm × 2 cm was cut off from the film.

Latices were firstly dispersed in Synthetic Cement Pore Solution (SCPS) and diluted to 5 wt.-% with magnetic stirring for 15 min. SCPS (in Table 3-5, pH = 12.8) was prepared according to Gretz *et al*. [171]. Due to the low viscosity of the diluted dispersions, the film was dropped on a

PVC board by a pipette with 1 mL volume, covering an area about 10 cm². Films were left to dry under ambient conditions (23 ± 2 °C, 50 ± 5% R.H.).

Table 3-5 Composition of SCPS

	Concentration [g/L]	Concentration [mol/kg]
K	7.10	0.182
Na	2.25	0.098
Ca	0.40	0.010
S (sulfate)	2.75	0.086

To determine redispersibility, dry films were immersed into water for 10 min and then slightly rubbed using a finger. For redispersible films, it turned turbid immediately (Figure 3.18).

Figure 3.18 Redispersibility of the film and its relation to turbidity in water

3.3.2 Hydration of C_3A

The hydration of C_3A in the presence of PVOH with or without SO_4^{2-} was studied in order to determine the possibility of PVOH intercalated compound. For this purpose, C_3A was hydrated in saturated $Ca(OH)_2$ or $CaSO_4$ solution. In the absence of SO_4^{2-}, 2.5 g CaO, which was prepared by calcining $CaCO_3$ at 950 °C for 24 h, was dissolved in 400mL of deionized water. The suspension was stirred for 1 h and filtered to obtain a clear solution. Prior to C_3A addition, 1 g of a 20 wt.-% PVOH solution was mixed with the clear solution. Then, 1 g C_3A was added to the solution. This suspension was stirred for another hour. All the procedures were conducted at room temperature under argon using a mobile glove box (Figure 3.19). Afterwards, the suspension was centrifuged and the precipitate finally dried at 40 °C in vacuum. However, still little carbonation was observed by XRD. The precipitate was allowed to dry overnight and the powder was grounded in acetone and measured by XRD within 24 hours. If the hydration experiment were conducted in the presence of SO_4^{2-}, 2.5 g $CaSO_4 \cdot 2H_2O$ was used instead of CaO.
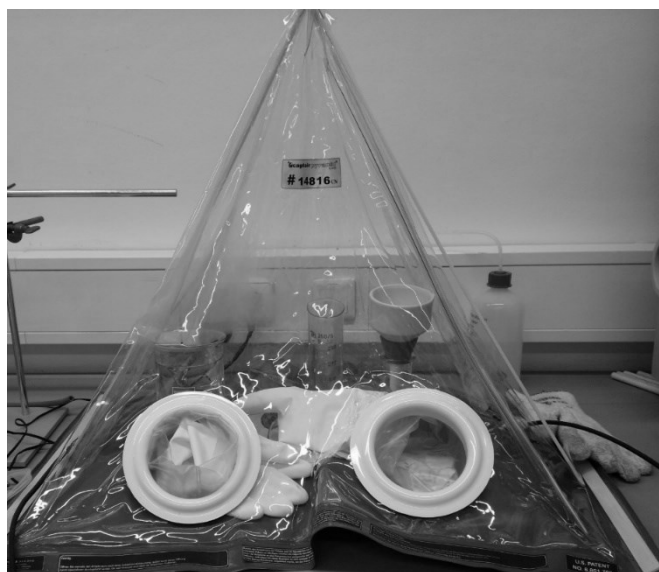
Figure 3.19 Mobile glove box for the C$_3$A hydration

4 Initial interaction between latex and cement

In cement suspension, dissolution of the minerals produces charged surfaces and ionic species in the interstitial solution. These charged surfaces, as well as the ions could interact with each other [178], or polyelectrolyte [179] through a process known as adsorption. Other than electrostatic force or ion-ion correlation, dispersion forces [180] (part of the Van der Waals forces) were also proposed as the origin of particle cohesion. While polymer colloids are introduced, this system is even more complex. However, adsorption isotherm, if any, can provide an overview about the interaction between latex and cement, regardless of the physical significance. Though only non-equilibrium as well as diluted conditions could be applied, adsorption isotherms indicate some specifics of both the mineral and polymer surfaces. The subsequent cement hydration and film formation processes can then be speculated.

4.1 Surface and electrokinetic properties of the latices

Generally, VAE latex stabilized by PVOH is nominally non-ionic, though it is not absolutely neutral due to the incorporated initiator and other dissociated species in the recipe. Thus, the influence of the ingredients on surface charge density of latex particles is interesting, especially with regards to possible interactions with ions presented in the cement pore solution and hence possible bridging effects by multivalent ion complexation. Charge titration by streaming current detector, in which colloidal charge can be altered by a controlled chemical dosage [181], can provide such useful information. Figure 4.1 presents the charge density of the latices in deionized water and alkaline solution. Surprisingly, latex C with acrylic acid monomer presented a comparable charge density with that of non-ionic latex A. However, if the particle size is taken into account (Figure 3.13), the surface of a single latex C particle would possess an apparently higher anionic charge than that of latex A, based on the inverse-square of the diameter ratio. Here, latices A and B were apparently not electrically neutral, as both latices possessed charges with latex A possessing a higher negative charge than latex B, indicating a higher amount of initiator or other electrolytes incorporated in its recipe. Under alkaline conditions, the determined negative charge density of all the latices increased, which could be attributed to the deprotonation of functional groups in the polymer chain or adsorbed PVOH. Alternatively, the influence of increased electrical conductivity in the bulk solution could not be excluded [182]. Nevertheless, latices A and B possessed a considerable amount of negative charges in alkaline conditions. In cement pore solution of an OPC, the high ionic strength [43,44] can compress the Debye length of the electrical double layer into the order of 1 nm [183]. Meanwhile, the radius of the PVOH coil in solution can be at least 5 nm [184]. When adsorbed onto the surface of VAE latex particles, the adsorbed thickness of PVOH could be more than

double its radius in solution [24]. Thus, detectable electrostatic force is negligible between hydrated cement surface and latex particles in the presence of PVOH corona. In this way, both latices A and B can be regarded as non-ionic latex in cement suspension.
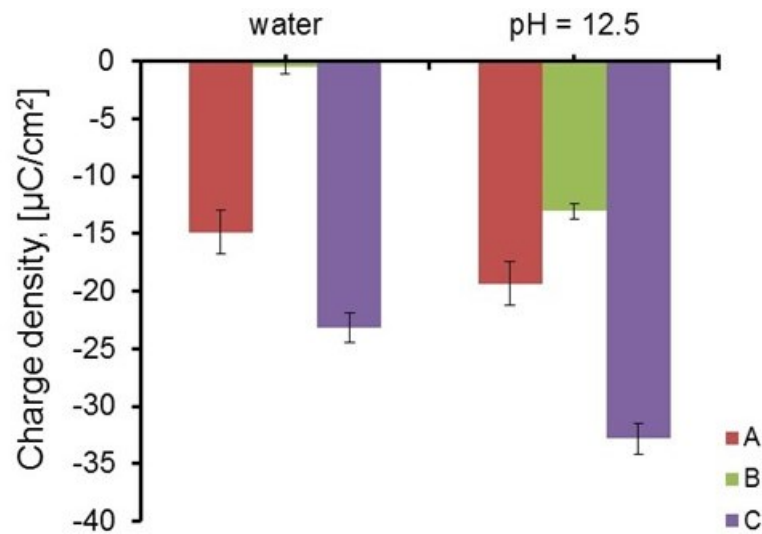

Figure 4.1 Particle charge density of latices while dispersed in neutral or alkaline medium

In cement pore solution, Ca^{2+} and high alkalinity are two main characteristics while dealing with possible interactions between the polymers colloids. Figure 4.2 shows the decrease in the streaming potentials of latices A and C in deionized water as a function of ionic strength induced by the salt solution titrant. Latex B behaved similar to latex A (not shown here), showing little affinity to Ca^{2+}. On the other hand, anionic latex C showed a high affinity to Ca^{2+}. This result implies that Ca^{2+} bridging may hardly occur between the surface of the non-ionic latex particle and the hydrating surface of cement grain.
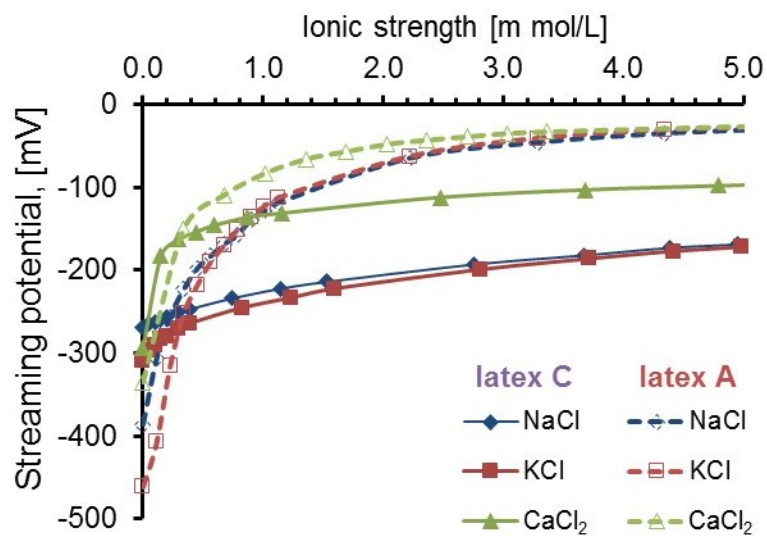
Figure 4.2 Streaming potential of diluted polymer dispersions as a function of ionic strength at deionized water

Under alkaline conditions (Figure 4.3), only anionic latex C showed affinity to Ca^{2+}. Non-ionic latex could hardly interact with the more cationic species since it went into a state of equilibrium with the approaching cations from the alkaline solution rapidly. This result revealed that Ca^{2+} bridging has less effect on the interaction between the surface of polymer particle and cement, especially in the presence of PVOH corona.
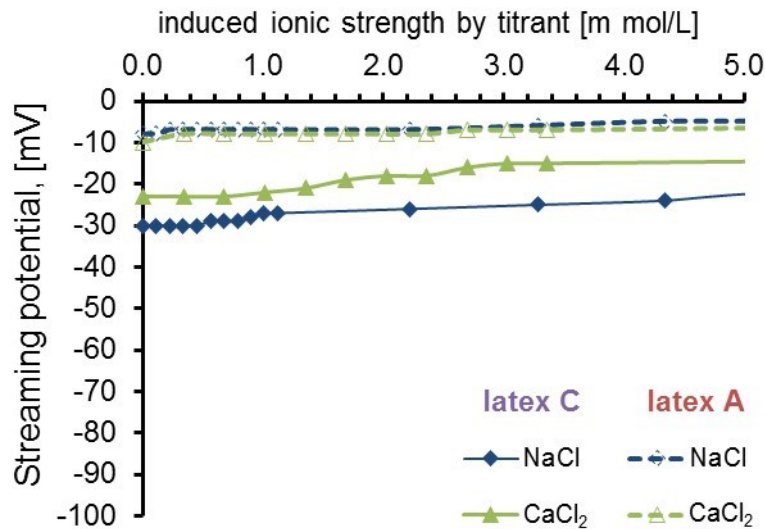
Figure 4.3 Streaming potential of diluted polymer dispersions as a function of cation concentration at pH =12.5 alkaline solution

4.2 Initial interaction between latex and cement minerals

The adsorption isotherm is mostly determined by the depletion method [185]. There are several possible reasons for the depletion of latex particles, which can result in the decrease in concentration of the supernatant. Adsorption, sedimentation, foaming or flocculation are some of the influence factors. If the colloid is well stabilized, as it is the case during the first hour, flocculation should be negligible (see Figure 6.3). Adsorption is the desired mechanism to be detected via the depletion method. However, it is impossible to avoid the fact that some latex particles will be trapped in the sediment in this study. In Figure 4.4, an almost constant depletion ratio was presented at high concentration for all the latices, implying adsorption as the non-dominant process under that condition. More precisely, this part of depletion can be accounted for by the incomplete separation of latex particles from cement sediment. Thus, depleted amount versus higher latex concentration (>2 wt.-%, equals to a polymer cement ratio of 0.18) was plotted. A good linear relation was found for all latices as shown in Figure 4.5.
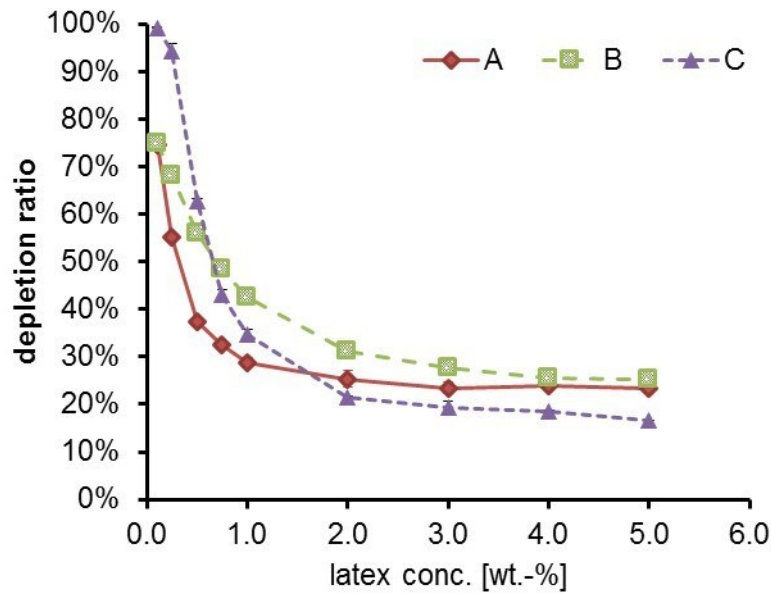
Figure 4.4 Depletion ratio of latices in the supernatant as a function of latex concentration
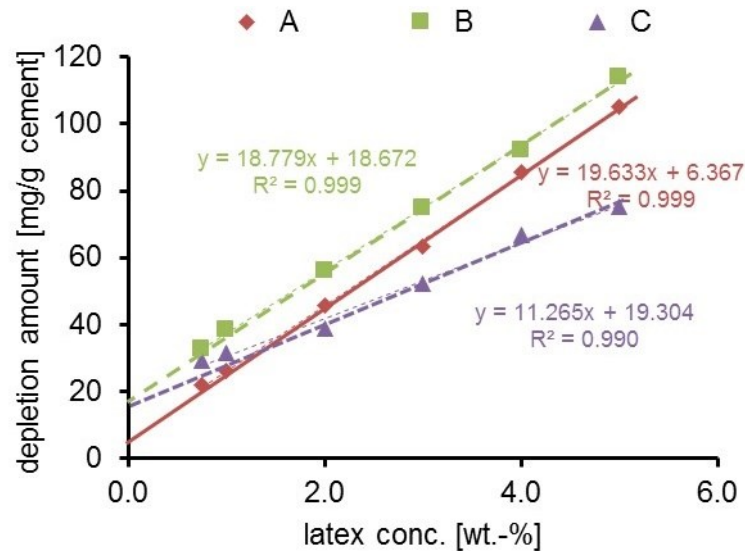

Figure 4.5 Linear regression of depletion amount versus latex concentration

If we assume that this linear trend in depletion was induced only by sedimentation, and subtract this value, a new relationship between the calculated adsorption amount and latex concentration can be attained, thereof presented in Figure 4.6. All latices reached saturated adsorption on the cement surface. At high latex concentrations, the saturation adsorption was thus presented by the intercept of the regression equation. A saturation amount of 19.3 mg/g cement for latex C, 18.7 mg/g cement for latex B and 6.4 mg/g cement for latex A could be assumed from the intercept, which fits well with the curves in Figure 4.6.

Obviously, the limitation of this regression is presented, since large subtraction especially at high concentrations can induce huge errors. Nevertheless, this semi-quantitative method remains effective at low latex concentrations, which covers the practical dosage in polymer

modified cement. The adsorption of anionic latex reached its saturation point at a polymer cement ratio of around 0.02-0.05 (equals to 0.25-0.5 wt.-% concentration), which was similar to the findings of the anionic latex adsorption on the Portland cement [17]. As expected, latex A had little interaction with the cement. Surprisingly, the adsorbed amount of latex B on cement was remarkably high. The mechanism of different adsorption behaviour for latices A and B was still indistinct. A possible explanation for this observation is that the different amounts or types of PVOH on the surface of VAE latex particles played an important role on surface forces.
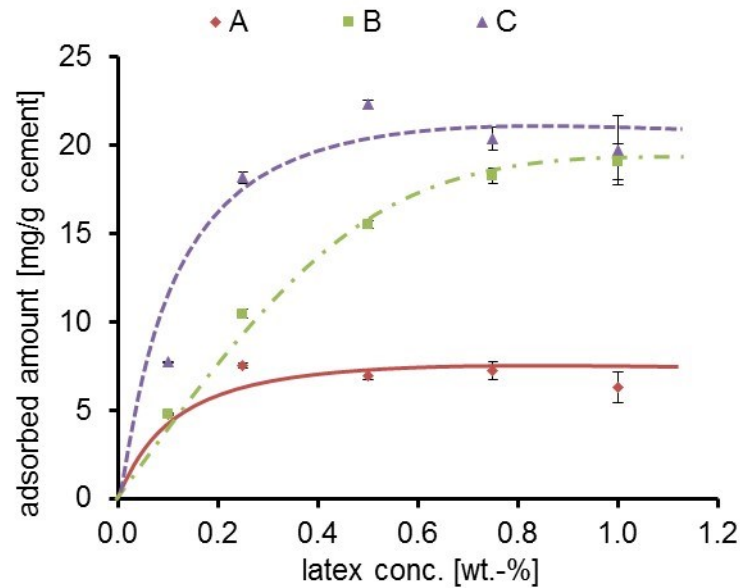
Figure 4.6 Calculated adsorption amount of latices on cement mineral

For further investigation of the relevance of polymer-cement interaction and their electrical properties, the Zeta potentials of cement suspensions, with titration of latex dispersions were conducted by means of the electroacoustic method. A Zeta potential of around 2 mV was found for the neat cement suspension. In Figure 4.7, the inversion of the Zeta potential with increasing dosage of latex C indicated that the surface properties of cement were altered by the adsorbed anionic latex particles. Meanwhile, the relatively stable value of -5 mV was found at around 0.50 wt.-% latex concentration, which was consistent with the adsorption measurements. For the two non-ionic latices, no distinguishable change in the Zeta potential was measured, suggesting that the latices are non-ionic and will exert negligible alteration on the electrokinetic properties of the cement surface.
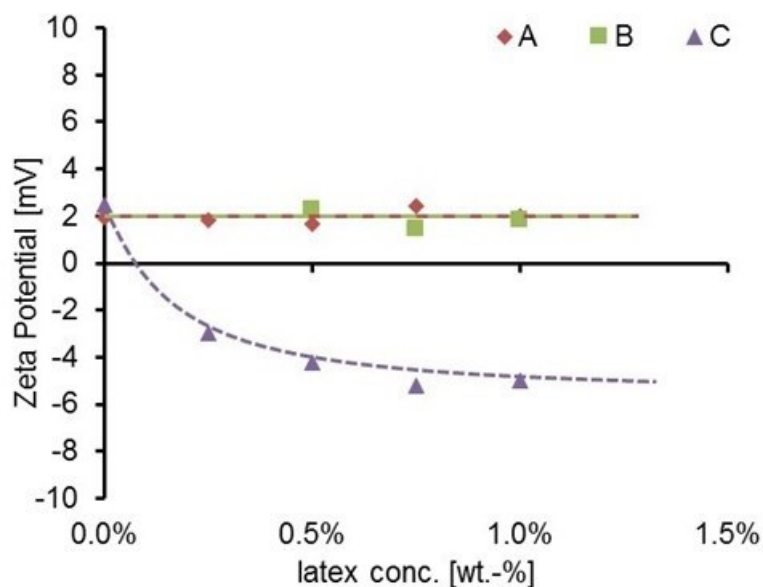
Figure 4.7 Zeta potential of cement-latex suspension (w/c ≈ 9) as a function of latex

concentration.

Depletion experiments on the hydrating clinker phase C_3A and C_3S were also carried out. Unfortunately, no reliable value could be obtained as the strong interactions between polymer and clinker phases led to the flocculation of the latex (Figure 4.8), when the polymer dispersions were mixed with C_3A. Therefore, determination of adsorption on C_3A was not feasible.

Figure 4.8 Flocculation of 0.25 wt.-% dispersions A after interaction with 1 g C_3A

Unlike C_3A, the adsorption of latices onto C_3S was similar to that on cement, when the adsorption was expressed as [mg/g mineral]. However, as per the interface phenomena, application of Specific Surface Area (SSA) is more reasonable. While discussing adsorption, it is difficult to determine the effective surface area since adsorption sites are varied for different adsorbates, as argued by Yamada [186]. Here, three kinds of SSA were determined, as shown in Table 3-4. For further illustration on the correlations to specific surface area, a simple calculation based on the surface occupancy was performed. For ease of calculation, one assumption is established, whereby the polydispersity of the adsorbed particles is equal to

original latex. This assumption was further confirmed by the PSD result (in Figure 4.9), where the PSD of the latex particles kept nearly the same before (original) and after interacting with cement (supernatant, as described in section 3.1.10).
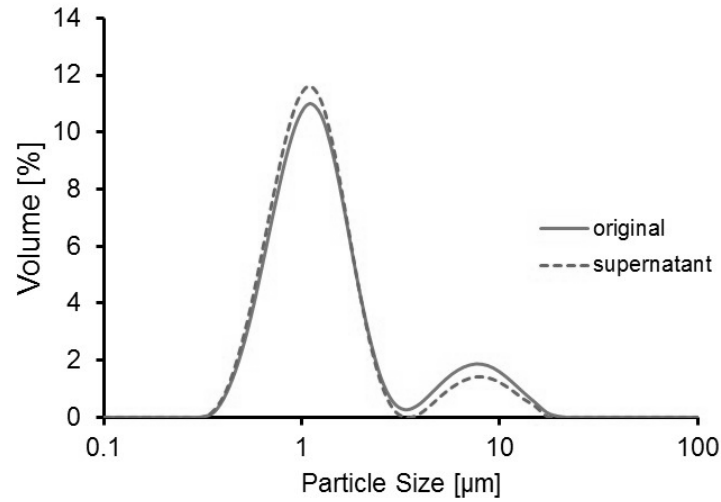

Figure 4.9 PSD of the polymer dispersions (0.25 wt.-%) before and after mixing with cement

If the specific surface area of latex particles is known, surface coverage could be calculated from Equation 4-1 and 4-2.

$$\varphi = \frac{S_{lat}}{S_{hex}} = \frac{\sum_{i=1}^{n} 4\pi \cdot R_i^2}{\sum_{i=1}^{n} 2\sqrt{3} \cdot R_i^2} = \frac{2\pi}{\sqrt{3}} \qquad \text{4-1}$$

$$\theta = \frac{m \cdot S_{hex}}{S_{cem}} = \frac{\sqrt{3} \cdot m \cdot S_{lat}}{2\pi \cdot S_{cem}} \qquad \text{4-2}$$

Where,

φ = ratio between SSA and equally occupied hexagonal area by projection of the particles;

R_i = radius of individual latex particle;

S_{lat} = specific surface area of latex particles, m^2/g;

S_{hex} = occupied hexagonal surface area by latex particles;

m = adsorbed amount, takes 19 mg/g cement for C, 18 mg/g for B, 6 mg/g for A;

S_{cem} = specific surface area of cement, m^2/g;

θ = surface coverage;

The calculated initial surface coverage of latex C on cement was ~35.4% with respect to SSA as determined by laser granulometry, ~19.4% by the Blaine test or ~7.6% by the BET method, respectively. The initial surface coverage between 7.6-19.4% was more consistent with literature [146], where a cationic polystyrene latex was adsorbed onto a mica surface under different ionic strength. Apparently, BET theory that works based on gas adsorption included

the internal surface of micropores, while the Blaine test determined merely the envelope surface of the particles [187]. Considering the size of the latex particle, available surface area for latex adsorption should be in between the surface areas measured by the BET and Blaine methods, as illustrated in Figure 4.10.
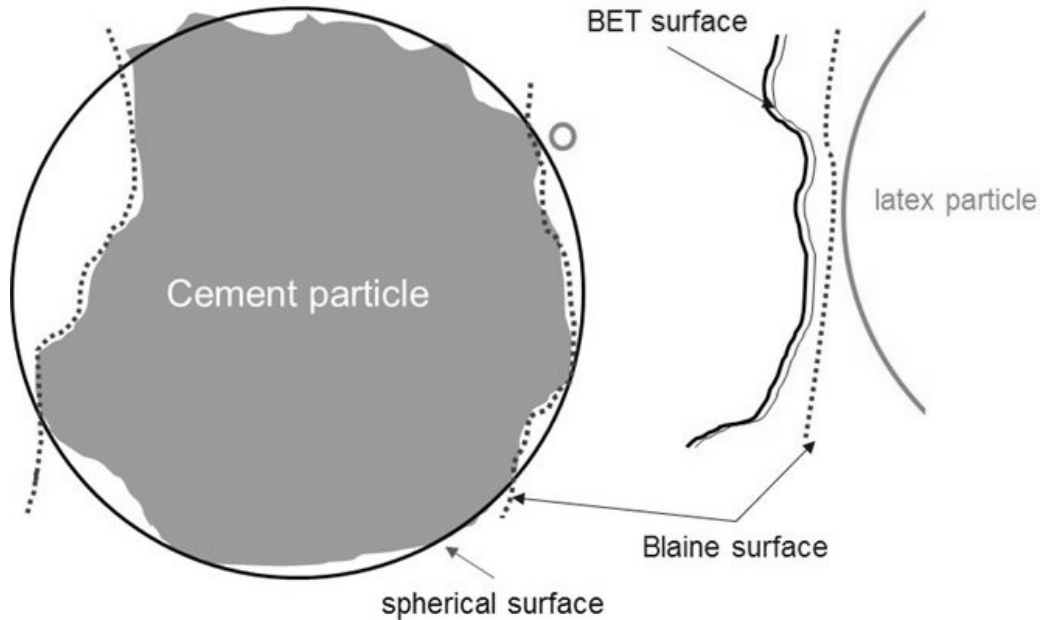

Figure 4.10 Schematic illustration of different specific surface area of cement particle with respect to latex adsorption

Accordingly, initial surface coverage was 1.2-3.0% for latex A and 3.5-8.8% for latex B at the concentration of the saturated adsorption, respectively. As the Blaine surface applied, little preferential adsorption on C_3S was found for non-ionic latices A and B (Figure 4.11). A similar result could be achieved while the BET surface is applied.
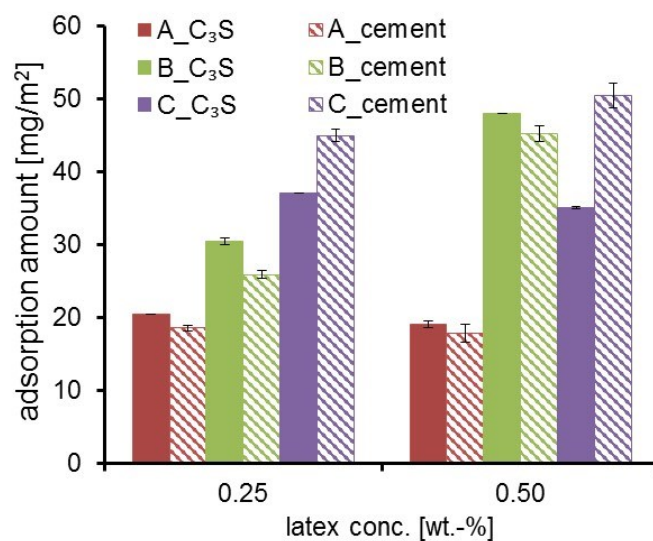
Figure 4.11 Calculated adsorption amount on cement and C_3S based on SSA by Blaine test

4.3 Initial interaction between PVOH and clinker phases

As presented in Table 3-2, approximately 4~5% PVOH could be separated from the latex physically by ultracentrifugation. Therefore, the possible PVOH-cement interaction was significant to elaborate the possible interaction mechanism between the VAE latex and cement. However, the separation of non-adsorbed polymer and mineral particles was not sufficient due to limited centrifugal force and the availability of materials. Thus, depleted amount of PVOH in the mineral-polymer suspension was measured, which can be an indication of the adsorption of PVOH on the mineral.
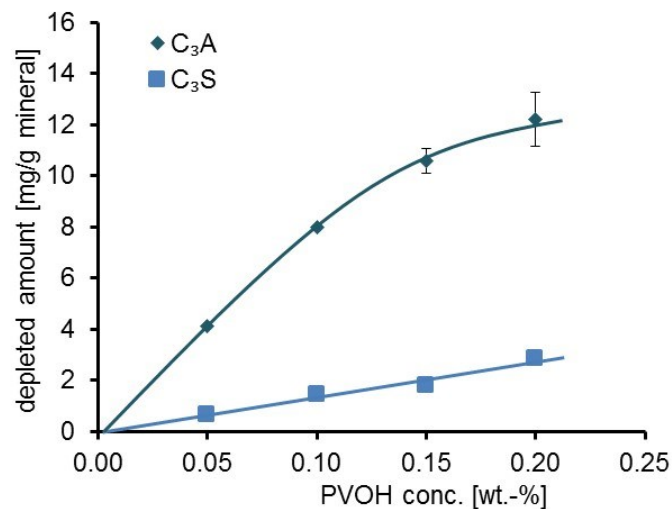
Figure 4.12 Depletion amount of PVOH on hydrating minerals

Figure 4.12 presents the depletion amount of PVOH on the hydrating minerals. Negligible adsorption was found on C_3S based on the approximate linear depletion versus polymer concentration as well as an almost constant depletion ratio (viz. ~ 25%).

In contrast, PVOH showed remarkably high depletion amount on C_3A, i.e. much stronger interaction with aluminate phase, in which adsorption or $Al(OH)_4^-$ crosslinking [188] should be dominant. Despite the inability to distinguish polymer aggregation due to $Al(OH)_4^-$ crosslinking, the high depletion amount indicated a higher adsorbed amount of the polymer. This implied that a higher surface area was available for PVOH adsorption, i.e. the possibility of PVOH – C-A-H complex formation. Furthermore, dilution of the original 20 wt.-% PVOH with different solution displayed no significant changes on the depletion amount, implying that the interaction between PVOH and C_3A was neither pH nor sulfate ion sensitive (Figure 4.13).
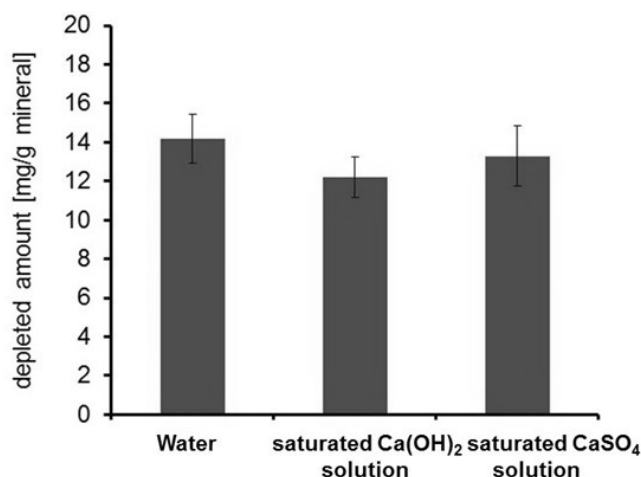
Figure 4.13 Depletion amount of PVOH (c = 0.20 wt.-%) on hydrating C_3A in different ionic environments

4.4   Initial interaction between the VAE latex and cement: the role of PVOH

This study was conducted with the aim of investigating the possible interaction between VAE latex stabilized by PVOH and cement. Although the possible adsorption mechanism was associated with surface and dissolved PVOH of the latex, considerable amount of latex was found to adsorb onto C_3S, relative to that for PVOH. From the same logic, Merlin *et al*. [19] attributed the adsorption of methacrylate butyl acrylate copolymer latex stabilized by polyethylene glycol φ-octylphenyl ether (Triton® X 405) on C_3S to the negative surface charge due to ionized carboxylate groups. However, if we take molecular weight into account, considerable adsorbed amounts of latex via surfactant was feasible. In that work, the saturated adsorption of TX 405 (molecular weight of 1966 g/mol) was less than 1 ± 0.5 µmol/g. Also, the saturation point of adsorption for the latex was 42 ± 3 mg/g, though the non-adsorbed amount in sediment was also included. Nevertheless, the ratio of adsorbed amount between latex and surfactant was about 22, which was comparable to that of the molecular weight ratio. Therefore, in this study, even when the adsorption of PVOH onto C_3S was negligible, a high adsorbed amount of VAE latex on the same mineral could be feasible. To clarify the possible relationship between electrostatic interaction and the adsorption of the non-ionic latex (A&B) onto cement minerals, DLVO theory will be applied to discuss the driving force for the adsorption further (In Appendix A).

In previous studies, VAE (most often abbreviated as EVA [5,15,20,189,190]) dispersible polymer powder was treated as a whole, with respect to the interaction between the polymer and the cement. In the form of latex, nearly half of the added PVOH during polymerization was freely dissolved in the solution [24], while even more PVOH is present in the dispersible polymer

powder [23]. In this way, the non-ionic VAE latex or its powder form is made up of two components regardless of their chemical similarity. This 'two components' concept explained the stabilization problem when low concentrations of VAE polymer dispersions were mixed with C_3A. The strong interaction between PVOH and C_3A led to desorption of PVOH (not the grafted one) from the surface of the VAE particle. This resulted in insufficient stabilization, especially at extremely low polymer concentrations. Thus, additional PVOH at these low polymer concentrations enhanced the colloidal stability, which was confirmed experimentally (Figure 4.14). Though the interaction between PVOH and C_3A phase in cement-latex suspension could not be as strong as that of pure C_3A - latex suspension, free PVOH should dominate the interaction with the aluminate phase. The influence of VAE latex on the hydration kinetics of aluminate phase has been reported by some workers [21,189], whereby similar alteration was also described in the sole presence of PVOH [170]. Thus, as discussed in section 4.2 and 4.3, cross-linking with $Al(OH)_4^-$, adsorption on the crystallites could also be the possible mode of interactions.
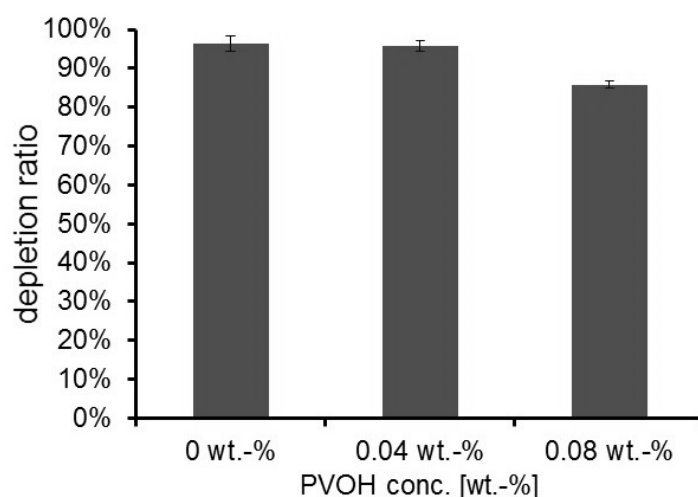

Figure 4.14 Depletion of 0.25 wt.-% latex A after interaction with C_3A in the presence of additional PVOH

The 'two components' concept was also verified by adding PVOH to the polymer dispersions (Figure 4.15). With an increasing amount of PVOH, the depletion ratio of latex B was less affected while that of latex A was decreased subsequently, i.e. the reduction in depletion ratio was more pronounced with the increase of additional PVOH for latex A. The inconsistent reduction in depletion ratio between latices A and B indicates that PVOH has a different effect on the adsorption behaviour of the studied latices.
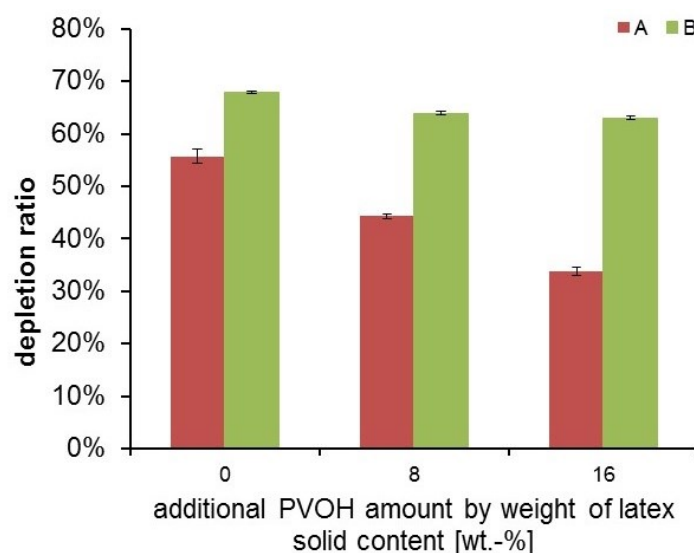
Figure 4.15 Depletion of 0.25 wt.-% latex A and B in the presence of additional PVOH

Since both the high and low molecular weight PVOH presents in latex B (from personal communication), a plausible explanation is that the high molecular weighted PVOH may appear on the surface of the latex particle and adsorb on the mineral surface, while less steric repulsion or osmotic pressure is exerted between the low molecular ones (Figure 4.16).
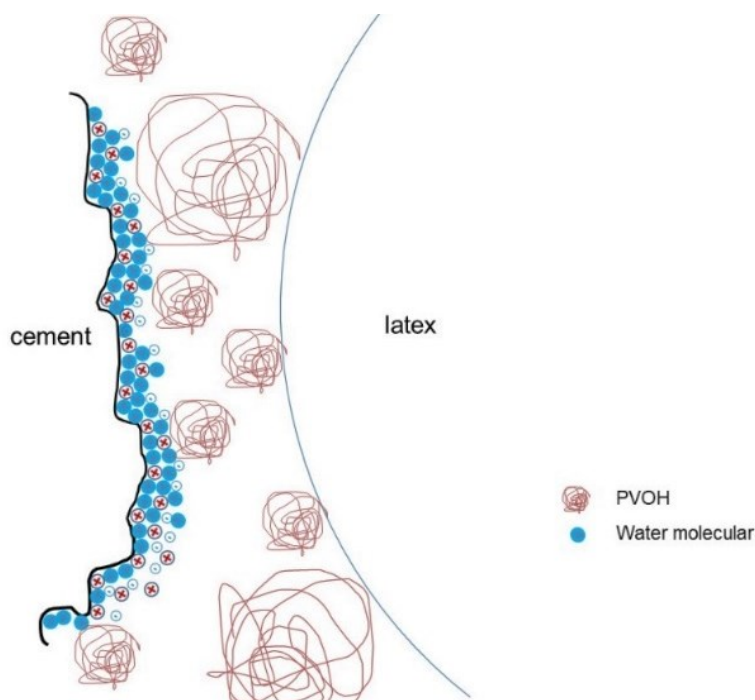

Figure 4.16 Schematic illustration of the interaction between latex possessed high molecular weight PVOH and cement

5 Hydration kinetics of cement affected by latex

Cement hydration can be considered as a dissolution-precipitation process [153]. Therefore, the adsorption of chemicals like polymers can affect the mineral dissolution. Meanwhile, since polymer colloids induce a huge surface area, the interaction between polymer particles and ions or hydration products from cement pore solution are not negligible. Consequently, the interaction (e.g. ion complexation) can also affect the precipitation process to some extent.

5.1 Rate of cement hydration affected by polymers

As revealed in chapter 4, latex particles can adsorb onto the cement mineral surfaces, resulting in different surface coverage. Thus, retardation of the hydration process could be expected. Cement hydration is a highly exothermic reaction that cannot be described by the ordinary chemical rate equations. Therefore, the rate of cement hydration should be studied by calorimetry ideally [191].

In Figure 5.1, the influence of latex A on the rate of cement hydration is presented. At p/c = 0.02, nearly no effect was observed for the non-ionic latex on silicate hydration, showing almost the same hydration rate as control cement specimen, whereas, only minor enhancement on sulfate depletion peak was shown. At p/c = 0.05 or 0.1, an extension of the induction period was observed, which increased with p/c ratio. At p/c = 0.05, almost no influence of the latex on the rate of silicate hydration was found. This rate was decreased when the p/c was further increased to 0.1. The hydration heat of the silicate phase was also impaired at p/c = 0.1. This observation, however, was not consistent with the initial adsorption amount. Nevertheless, as a complicated process, cement hydration could be influenced by the latex in various ways.

First, as a soft matter, the latex particle that was adsorbed on the cement surface can deform and increase its coverage, resulting in a change in the dissolution of surface mineral. Secondly, latex particles, which can interact with the ions from the interstitial pore solution (section 4.1), resulting in changes in the nucleation and precipitation process. Thirdly, the presence of PVOH can also alter the cement hydration due to its strong interaction with the aluminate phase, as discussed in section 4.3. Therefore, no distinct conclusion can be drawn independently from the heat flow curve, with respect to the interaction between latex and cement.
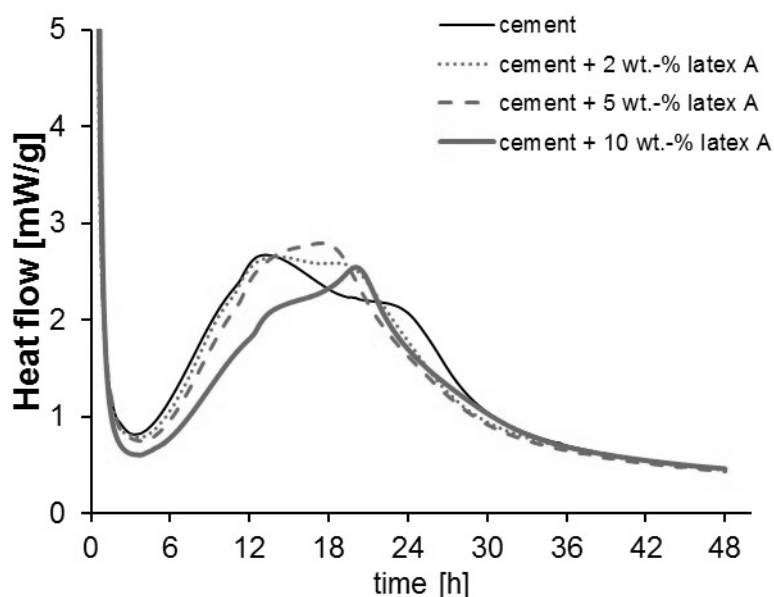
Figure 5.1 Heat of hydration during the first 48 h in the presence of latex A

Compared to latex A, latex B affected the rate of cement hydration in a similar way (Figure 5.2). The main difference is the occurrence of the sulfate depletion peak as well as the exothermic peak intensity. Cement hydrated with latex B showed a slightly lower sulfate depletion related, exothermic peak as compared to latex A. Moreover, at p/c = 0.10, the nucleation rate of C-S-H and portlandite was affected to a less extent compared with that of latex A. Again, these two non-ionic latices showed some differences in their interactions with cement. If initial adsorption matters, the dissolution of the minerals should be retarded more by latex B, since latex B covered more mineral surfaces.

However, this assumption is based on the precondition that both latices or at least latex A were stable in cement pore solution after 5 hours. With water consumption by cement hydration, latex particles should either deposit on mineral surface continuously (i.e. contact with each other gradually), or agglomerate due to stabilization failure in the high electrolytes concentration of the pore solution. Hence, mineral dissolution as well as nucleation and precipitation of hydration products should be subjected to the state of latex particles as time evolved. With regard to the chemical similarity between these latices, both had a slightly different influence on cement hydration.
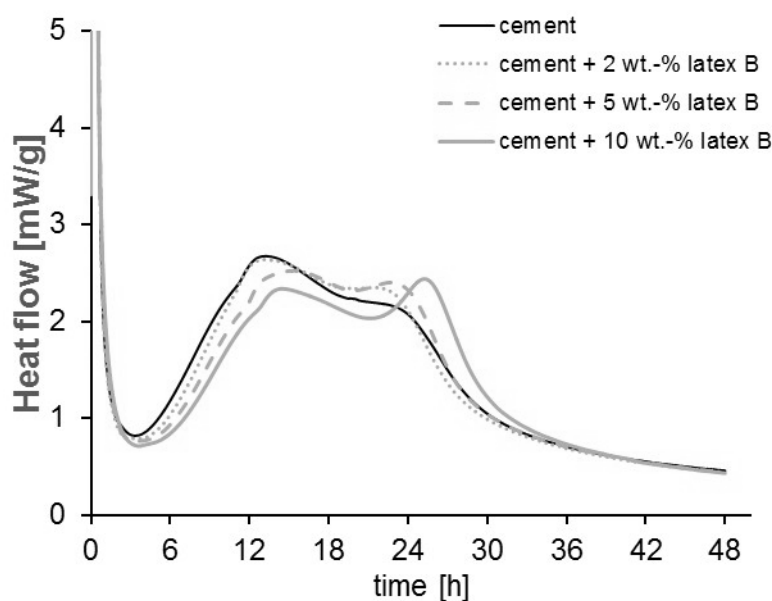
Figure 5.2 Heat of hydration during the first 48 h in the presence of latex B

Anionic latex C had a stronger influence on the rate of cement hydration even at p/c = 0.02, as shown in Figure 5.3. With the increasing in p/c ratio, both the rate of silicate hydration and the maximum of the exothermic peak was decreased. Similarly, the induction period was extended as a function of p/c ratio. Different to the non-ionic latex, latex C presented no enhanced sulfate depletion peak. Instead, an extension of the period of sulfate depletion resulting in the development of a shoulder was observed with increasing p/c ratio. Thus, the enhanced sulfate depletion peak could be attributed to the presence of PVOH in the VAE latex, whereas, this peak was present due to the rapid formation of ettringite in the presence of PVOH, as reported by Jansen *et al*. [170].

As discussed above, latex C presented much higher surface coverage on cement mineral. Doubtless, latex adsorption or deposition, particle coalescence as well as agglomeration can affect the available surface for mineral dissolution and crystallite precipitation. However, different to the water-soluble polymer, the latex particle itself is hardly related to the changed morphology or crystal orientation, which are commonly influenced by polymers during the crystallization process [192–194]. Latex particle, normally above 100 nm in diameter, can provide enough surfaces for the deposition of small entities, i.e. ions, nano-size crystallites etc., by which precipitation and nucleation processes may be affected. In this sense, latex should be distinguished from the water-soluble polymer.
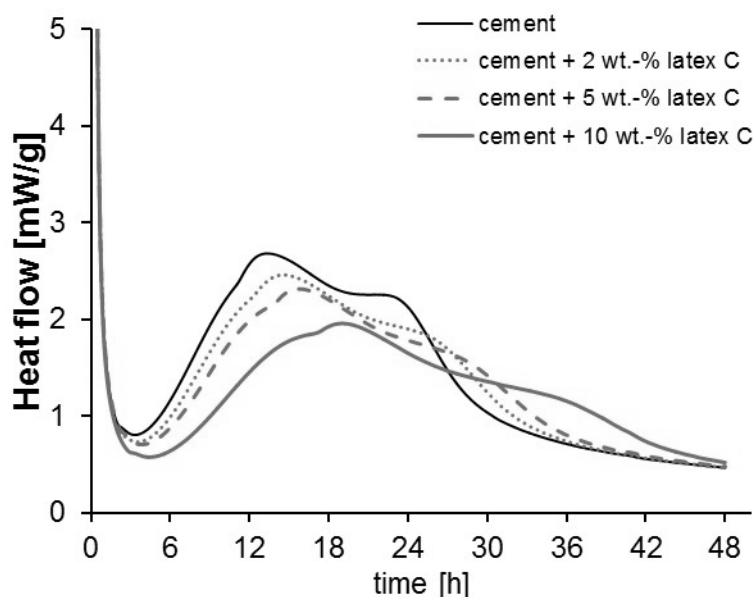
Figure 5.3 Heat of hydration during the first 48 h in the presence of latex C

As indicated previously, PVOH could affect the rate of cement hydration by enhancing the sulfate depletion peak (in Figure 5.4). However, the sulfate depletion peak was not postponed with the increase in p/c ratio, to which its intensity was related. At p/c = 0.05, no clear silicate hydration peak could be observed, indicating that there should be some synergetic effect between silicate and aluminate hydration. With the increase in p/c ratio, the induction period was slightly extended. However, the rate of silicate hydration was not affected, at least in the range of applied polymer dosage.
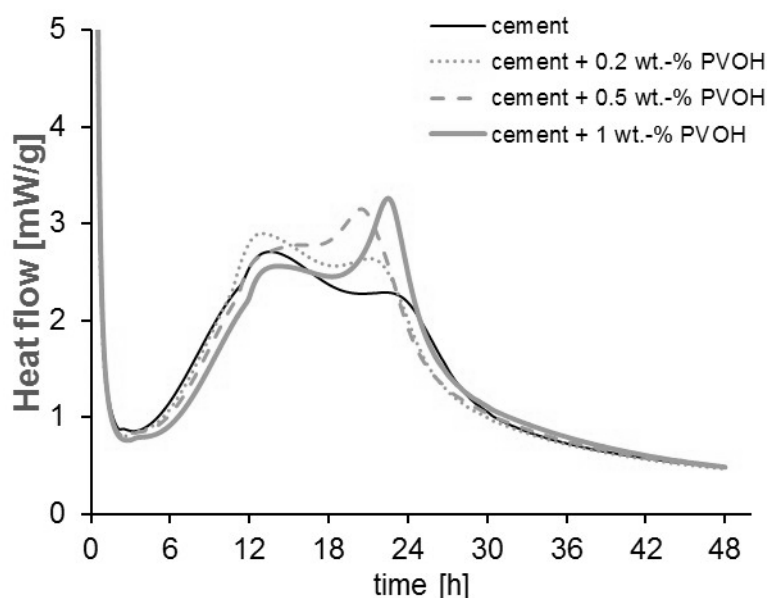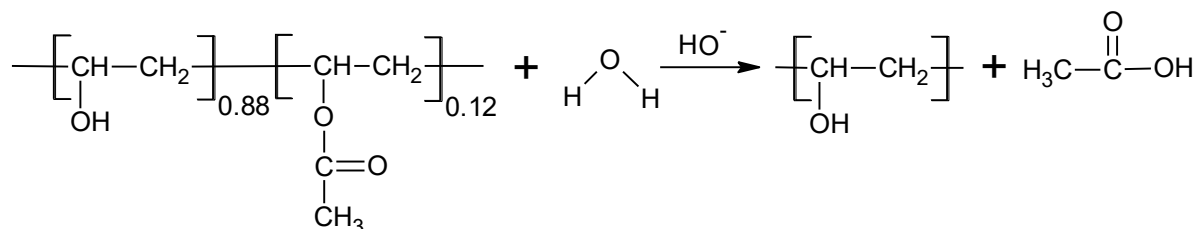

Figure 5.4 Heat of hydration during the first 48 h in the presence of PVOH

That PVOH shows a strong influence mainly on the hydration of the aluminate phase is in accordance with the initial interaction between PVOH and the mineral phases. As reported by

Jansen *et al*. [170], PVOH can influence initial dissolution of C_3A and promote ettringite formation after sulfate depletion. Also, it has only a minor influence on the induction period, which appears to exist as a distinct stage only when chemical retarders are added or materials have been annealed [152]. The PVOH used in this study is partially hydrolyzed poly (vinyl alcohol -co-vinyl acetate) copolymer, which could undergo further alkaline hydrolysis in cement pore solution as follows:

$$\left[\begin{matrix} CH-CH_2 \\ | \\ OH \end{matrix}\right]_{0.88} \left[\begin{matrix} CH-CH_2 \\ | \\ O \\ | \\ C=O \\ | \\ CH_3 \end{matrix}\right]_{0.12} + H \overset{O}{\diagup} H \xrightarrow{HO^-} \left[\begin{matrix} CH-CH_2 \\ | \\ OH \end{matrix}\right] + H_3C-\overset{O}{\underset{||}{C}}-OH$$

The solubility of $Ca(OH)_2$ in NaOH solution decayed exponentially in the range of 0 - 0.1 mol/L concentration [195] i.e. the pH of the solution approaches 13. Thus, the hydrolysis reaction should affect the degree of undersaturation through the change in the pH of the solution. Hence, it is of interest to discuss the possible influence of the hydrolysis reaction, since the rate controlling process of the alite dissolution (induction period) was highly related to undersaturation degree, which was proposed by recently developed dissolution theory [163].

To investigate the possible influence of hydrolysis reaction, the pH change of the pore solution extracted from cement/polymer mixes has been investigated. In Figure 5.5, a very slightly increase in the pH of the control cement specimen was observed between 10 and 180 min. Low dosages of latices A and B respectively showed a limited influence on pH of the pore solutions. In contrast, PVOH showed a considerable influence on the pH of the pore solution, especially during the initial hydration period. The relatively low pH of the pore solution in the presence of PVOH could be first maintained for at least 30 min, indicating that the hydrolysis reaction in cement paste is similar to a buffer system. Additionally, slower alkaline hydrolysis of the ester group from latex polymer is predicted here. This could explain why latices A and B showed less of an effect on the pH of the pore solutions at low dosages.
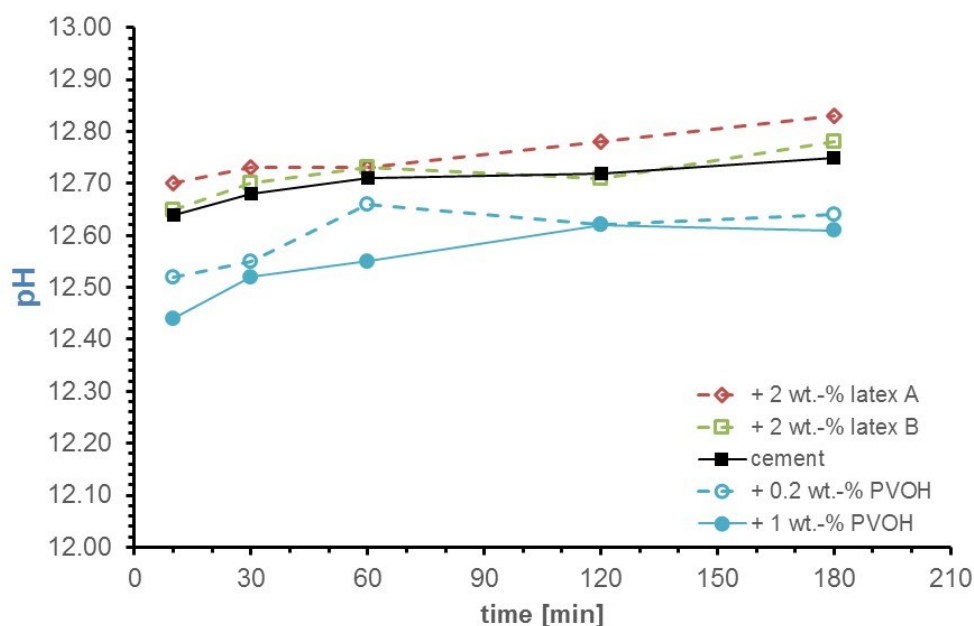
Figure 5.5 pH of filtered cement pore solution as a function of time

Despite that, employing a high dosage of the non-ionic latex in the cement pore solution showed a relatively longer induction period, relative to that of the PVOH. Thus, other ingredients in the latex may influence the undersaturation degree, e.g. acetic acid. The acidity may be due to the residual of vinyl acetate synthesis, showing a pH of about 4 for both undiluted latices. At 0.1 wt.-% concentration, both latices showed a pH about 4.7 – 5. Therefore, this acid should also contribute to the extension of the induction period.
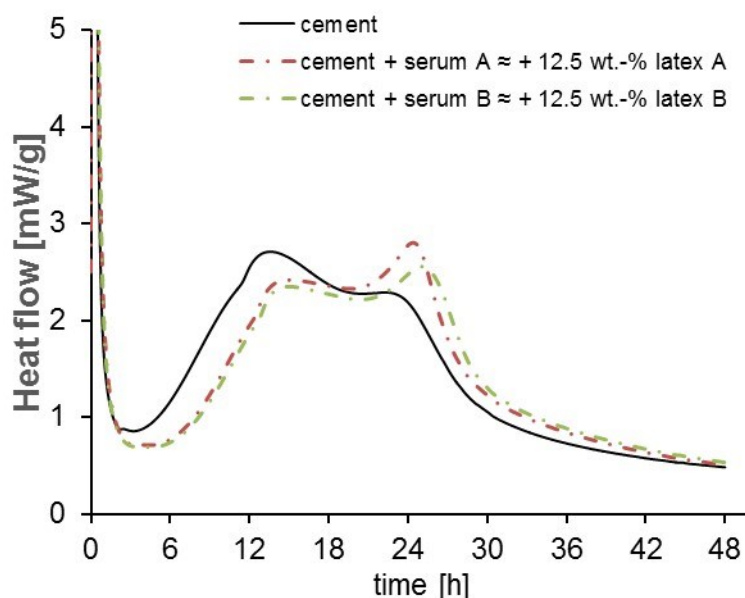

Figure 5.6 Heat of hydration during the first 48 h in the presence of serum from latex

To verify this assumption, the influence of serum from the upper supernatant of 20 wt.-% non-ionic latex by ultracentrifugation was determined. In Figure 5.6, both sera showed prolonged

induction periods, confirming the speculation. Both cement and sera mixtures showed a very similar rate of hydration before the acceleration period (due to silicate hydration) was over, showing a similar trend to that of the latices. Similarly, the two sera showed different behaviours in regard to enhanced sulfate depletion peak. This corresponded to the individual influence by different non-ionic latices, whereby the occurrence of the sulfate depletion peak was either accelerated or retarded. This result implied that latex particles had little effect on the late ettringite formation when the sulfate carrier was consumed.

5.2 Influence of polymers on the pore solution during induction period

As discussed in section 5.1, polymers influenced the rate of cement hydration by changing the degree of undersaturation of the pore solution. Therefore, equilibrium ion concentration should be altered to some extent.
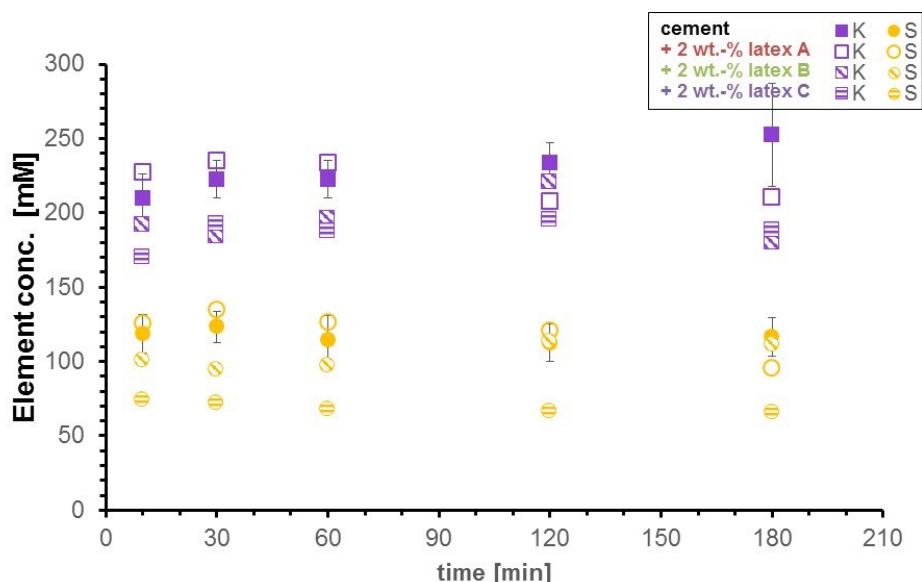

Figure 5.7 Ion concentration in cement pore solution in the presence of 2 wt.-% latex polymer

In Figure 5.7, two major ion species in cement pore solution (K^+, SO_4^{2-}) are presented, in the presence of different latices at p/c = 0.02. Both latices B and C influence the equilibrium concentration of both K^+ and SO_4^{2-}. Latex B affected the concentration within the first hour while latex C showed its impact throughout the investigated period. On the one hand, latex A showed less effect on the concentration. This observation may be linked to the initial adsorption as described in section 4.2. It should be noted here that the minor influence of latex A and B on the ion concentration in the pore solution corresponds to the results from isothermal calorimetry. As revealed in chapter 4, latex A showed less adsorption on cement minerals, i.e. more latex particles were left in the cement pore solution. As a result, extraction of filtrate from latex A was difficult within the first hour, which induced higher measured values

of Na$^+$ and Ca^{2+} concentrations (in Figure 5.8). Otherwise, a limited influence of the latices on the cement pore solution was observed, especially at low polymer concentrations. In the same sense, the influence of the latices on Si and Al concentration were not taken into account, since errors induced by extraction technique could not be distinguished in the range of µmol/L.
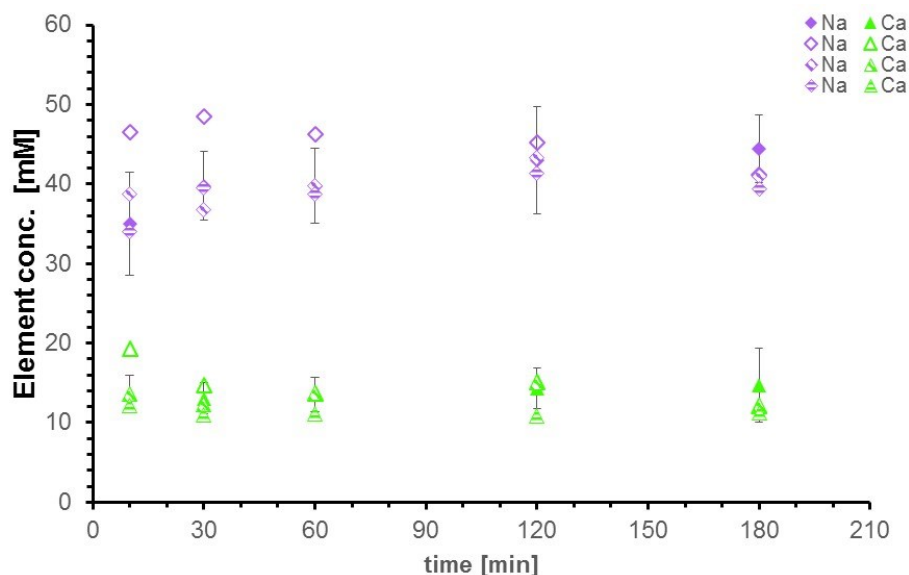

Figure 5.8 Ion concentration in cement pore solution in the presence of 2 wt.-% latex polymer

With the increase in polymer concentration, all latices reduced both K$^+$ and SO$_4^{2-}$ in the cement pore solution pronouncedly (Figure 5.9). However, differences among those latices were not noticeable except at the beginning (30 min). As discussed before, the differences in the first hour may be induced by the extraction procedure, i.e. time consumption, filtrate amount etc. Nevertheless, these results were not in accordance with the adsorption behaviour, nor the rate of hydration. There are two sources of SO$_4^{2-}$ in cement pore solution: dissolution of alkali sulfate or calcium sulfate (e.g. gypsum) added as a retarder. The adsorption of latex on gypsum lowers the dissolution of sulfate, while the latex in cement pore solution may act as a diffusion barrier. The latter may result in local supersaturation and slow down the dissolution of calcium sulfate. Actually, the reduction of K$^+$ and SO$_4^{2-}$ in the pore solution was inconsistent, i.e. ~25% reduction of K$^+$ but 50% of SO$_4^{2-}$ in the presence of latices. These results implied that dissolution of calcium sulfate was inhibited in the presence of latices. However, this speculation explains the prolonged sulfate depletion shoulder in the presence of latex C (Figure 5.3), while it cannot predict the enhanced sulfate depletion peak in the presence of PVOH for latex A (Figure 5.1) and B (Figure 5.2).
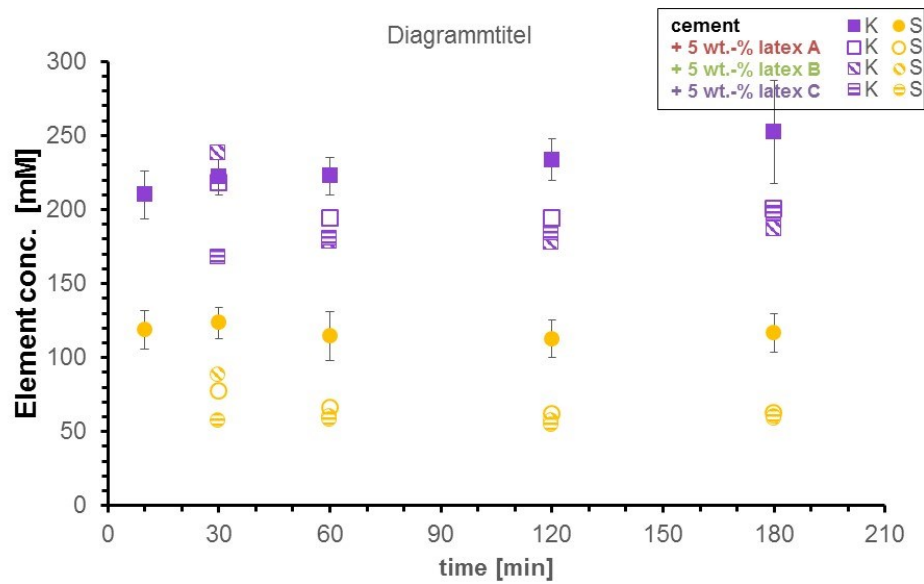
Figure 5.9 Ion concentration in cement pore solution in the presence of 5 wt.-% latex polymer

The influence of latex concentration on Na^+ or Ca^{2+} at higher latex dosages was not distinguishable (Figure 5.10), similar to that at lower concentrations of latex (Figure 5.8). The possible Ca^{2+} complexation cannot be confirmed by the change in Ca^{2+} concentration, though nearly half of the Ca is in the form of $Ca(OH)^+$ at pH ~ 13 [195]. One possible explanation is that Ca^{2+} complex compound may be retained with latex particles during the filtration.
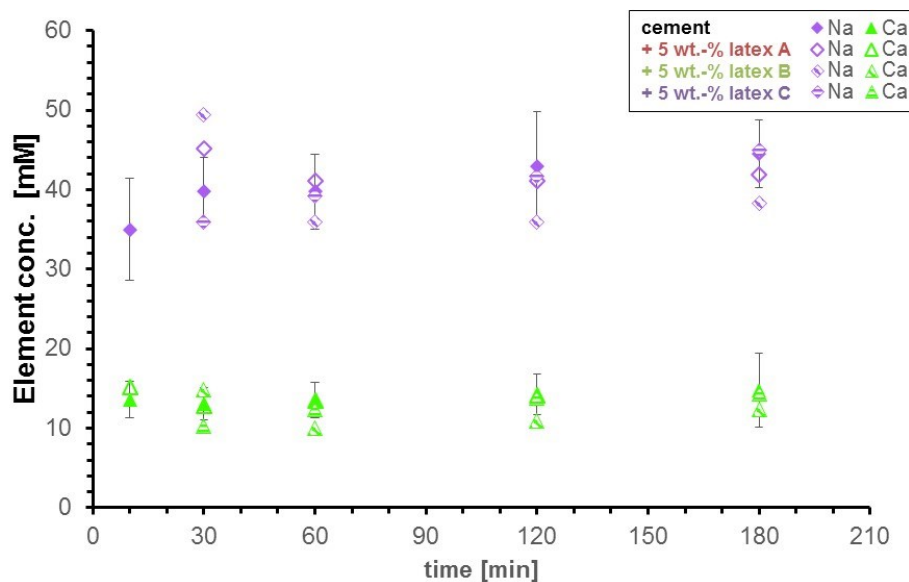

Figure 5.10 Ion concentration in cement pore solution in the presence of 5 wt.-% latex polymer

As discussed, the decrease in SO_4^{2-} concentration cannot explain the enhanced sulfate depletion peak for the latex stabilized with PVOH. Thus, the influence of the PVOH on the ion composition was further investigated.
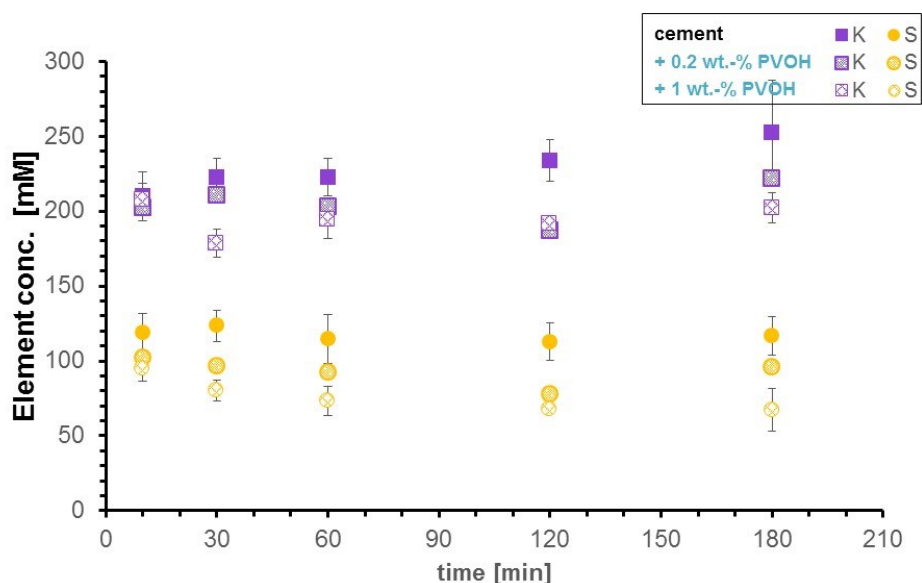

Figure 5.11 Ion concentration in cement pore solution in the presence of PVOH

In Figure 5.11, the concentrations of K^+ and SO_4^{2-} were reduced in the presence of the PVOH, which was quite similar to that of latices A and B. The inconsistent lowering of these ions indicated that PVOH may also affect the dissolution of calcium sulfate, while the effect may be attributed to the increase in the viscosity of the pore solution that was ascribed for the retardation of bassanite dissolution in the presence of cellulose ether [196]. When 1 % PVOH by weight of cement was present, the change in Ca^{2+} concentration was indistinct. Ca^{2+} complexation, if any, was not a dominant process with respect to the cement-polymer interaction. Accordingly, Ca^{2+} complexation by the non-ionic latex was limited as well. Though the change in pH can greatly affect the Ca^{2+} solubility [195], the concentration of soluble Ca^{2+} is limited in the high pH range. Owing to the indistinctive change in Ca^{2+} concentration, potential cement-polymer interaction via Ca^{2+} bridging could not be confirmed. Nevertheless, the influence of polymers on Ca^{2+} concentration could not be excluded.
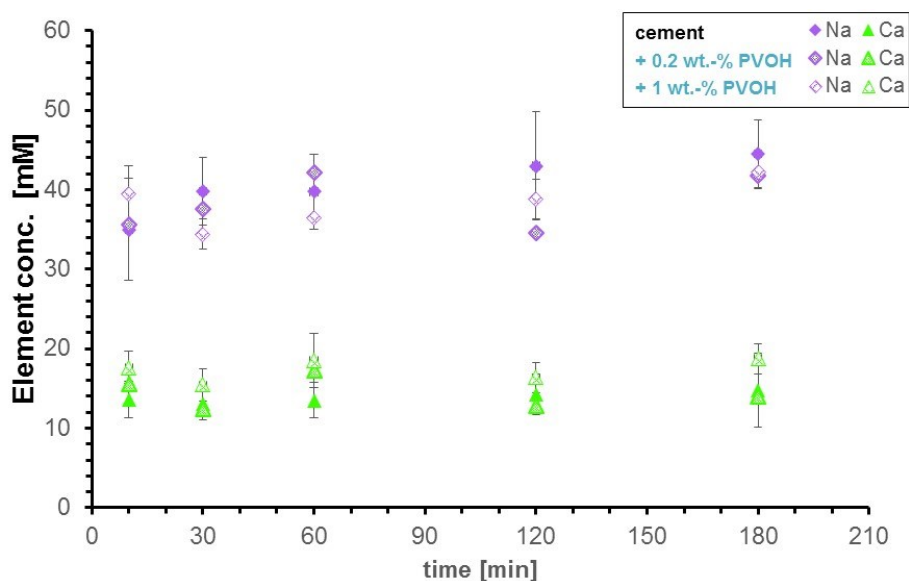
Figure 5.12 Ion concentration in cement pore solution in the presence of PVOH

The presence of the PVOH in the cement pore solution reduced the Si concentration, which might be attributed to the adsorption of PVOH as well as the change of the pH. However, no pronounced influence of the PVOH on Al concentration could be observed. Indeed, this observation cannot eliminate the possibility of potential $Al(OH)_4^-$ complexation, though the crosslinking via C-O-Al was not feasible when mechanochemical activation was absent [197].
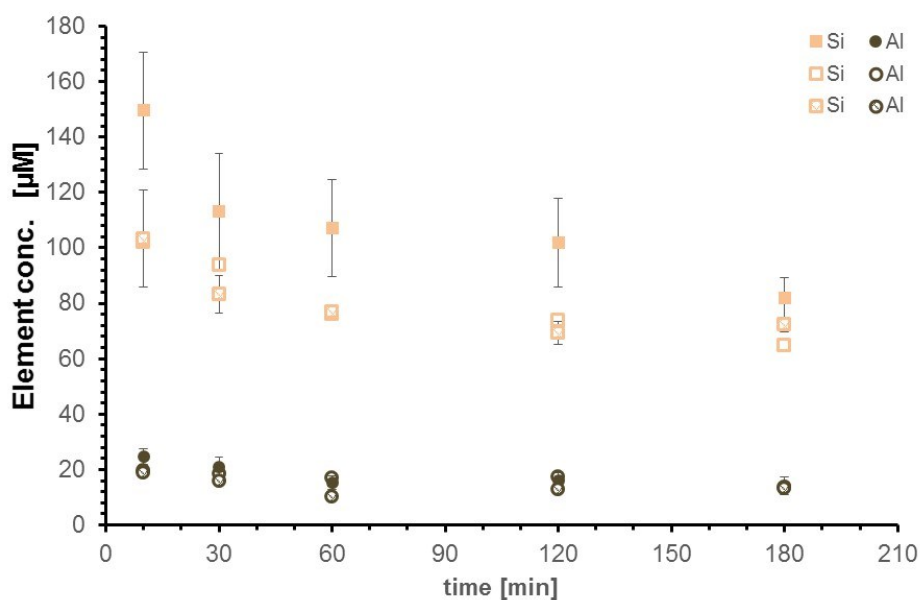

Figure 5.13 Ions concentration in cement pore solution in the presence of PVOH

Möschner *et al.* [198] reported that citric acid did not greatly change the composition of the pore solution, but cement hydration was retarded significantly. With the aid of a thermodynamic calculation, they speculated that crystalline citrate should be precipitated, which could be the cause of the severe retardation. In a similar way, the influence of PVOH on the precipitation

and nucleation process afterwards ought to be clarified. Accordingly, saturation indices during the first hours were calculated by using the Geochemical modelling program Phreeqc [199] (version 3.1.4-8929) with the CEMDATA07 [200] database. Saturation indices (SI) are given by log IAP/K_{sp} (IAP: ion activity product; K_{sp}: solubility product), while SI > 0 denotes supersaturation and SI < 0 for undersaturation. The thermodynamic modelling of saturation levels requires the assumption of local equilibrium, where rates of dissolution/precipitation are much faster than those of ionic transport, so that mineral solubility controls the chemistry of the aqueous phase [43]. Data used in the calculation are listed in Table 5-1.

Table 5-1 Composition of the pore solution during the first few hours (standard deviation ± 10-15%)

Minutes	Elemental concentration						pH
	K [mM]	Na [mM]	Ca [mM]	S [mM]	Al [µM]	Si [µM]	
Cement							
10	210	35	14	119	25	150	12.64
30	222	40	13	123	21	113	12.68
60	223	40	14	115	15	107	12.71
120	234	43	14	113	16	102	12.72
180	252	44	15	117	14	82	12.75
+ 1 wt.-% PVOH							
10	208	39	18	95	19	103	12.44
30	179	34	15	80	16	83	12.52
60	194	36	19	73	10	77	12.55
120	191	39	16	68	13	69	12.62
180	202	42	19	67	13	72	12.61

From Figure 5.14, no portlandite precipitation could be observed within 3 hours. Though PVOH influenced the saturation indices in the first hour, the difference was limited afterwards. Also, inhibition of anhydrite dissolution in the presence of the PVOH was not indicated. The saturation indices of gypsum and ettringite were very similar. No profound influence of the PVOH on precipitation process could be confirmed during the first 3 hours, which is in accordance with the calorimetry results (Figure 5.4).
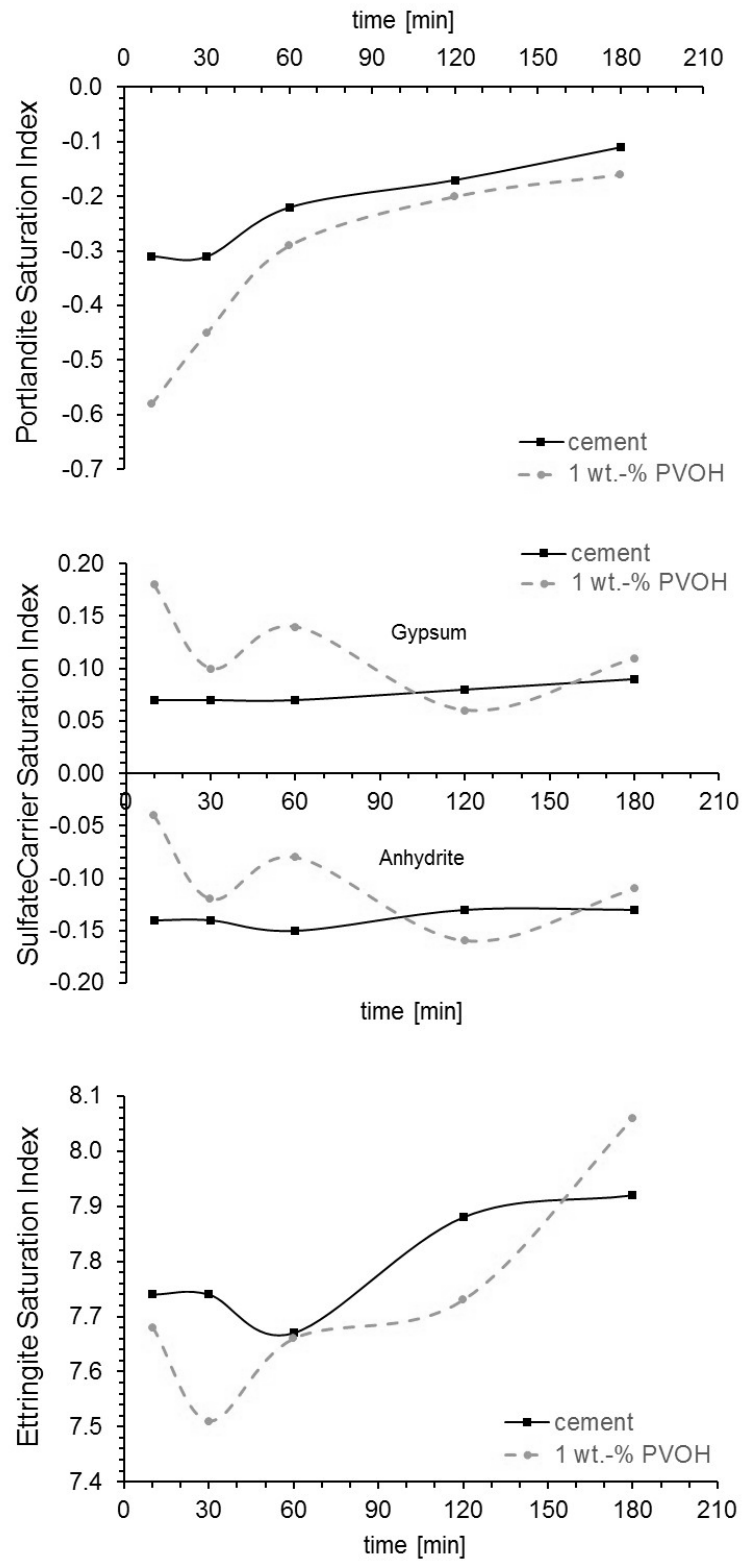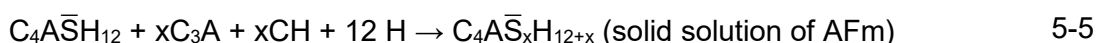
Figure 5.14 Saturation indices of portlandite, gypsum/anhydrite and ettringite calculated as a function of time at 25 °C

5.3 Hydration products formation affected by polymers

As discussed in previous sections, hydration kinetics were altered by the polymers. However, information about hydration products was not available, especially when both latex particles and PVOH were involved in the hydration. Therefore, quantitative or at least qualitative determination of the hydration product is necessary. In Portland cement, the following reactions commonly occurred [157]:

$C_3S + (3-x+n)H \rightarrow C_x\text{-}S\text{-}H_n + (3-x)CH$ (portlandite)   5-1

$2C_2S + 4.3H \rightarrow C_{1.7}\text{-}S\text{-}H_4 + 0.3CH$ 5-2

$C_3A + 3C\bar{S}H_2 + 26H \rightarrow C_6A\bar{S}_3H_{32}$ (ettringite)   5-3

$C_6A\bar{S}_3H_{32} + 2C_3A + 4H \rightarrow 3C_4A\bar{S}H_{12}$ (monosulphoaluminate)   5-4

$C_4A\bar{S}H_{12} + xC_3A + xCH + 12\,H \rightarrow C_4A\bar{S}_xH_{12+x}$ (solid solution of AFm)   5-5

As can be seen, the major hydration products of Portland cement are amorphous C-S-H gel, portlandite, ettringite, monosulphoaluminate, as well as the solid solution of AFm. Despite the complexity in the determination of C-S-H gel [201], other hydration products are crystalline and can be conveniently determined quantitatively by X-ray diffractometry [155,202]. However, the quantitative Rietveld analysis is often invalid for the crystal with preferential orientation unless correction is applied [111], e.g. portlandite [202] or anhydrite [155]. Moreover, with the increase in p/c ratio, the amorphous fraction increases as well. With respect to the complexity of quantitative analysis, where reliable analysis is highly dependent on the expertise, qualitative analysis can be an appropriate alternative. With the aid of in-situ XRD, qualitative analysis of early cement hydration is feasible with time resolution (Figure 5.15).
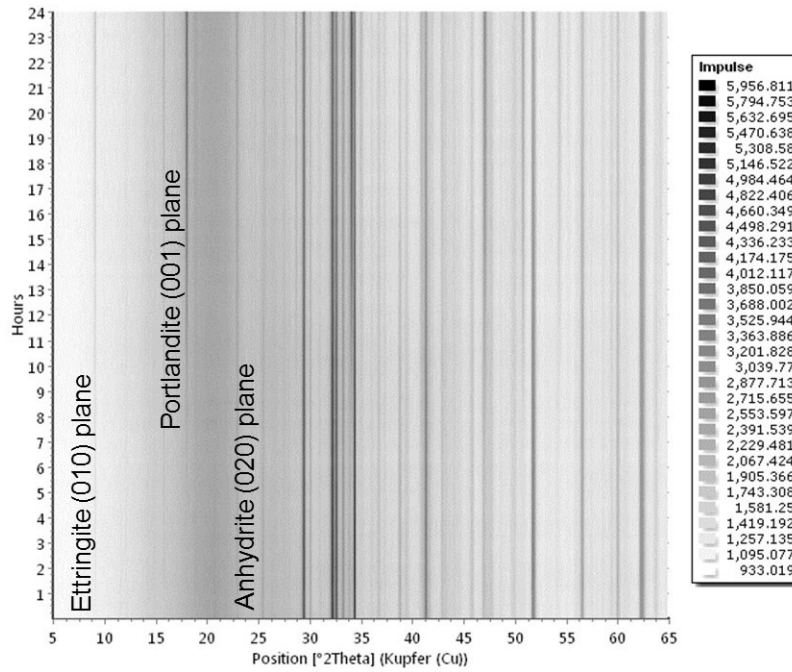
Figure 5.15 2D illustration of time-resolved XRD pattern

Table 5-2 lists the 2θ angle of characteristic peaks from some selected minerals. The 2 θ angles were converted from the d-spacings using the wavelength of incident ray (Cu Kα / 1.5406 Å). It is important to note that at about 25.5°, some characteristic peaks from ettringite and anhydrite might be overlapped, influencing the determination of time point (Table 5-2).

Table 5-2 2θ degree of specific crystal plane of some minerals

Minerals	2θ degree	Crystal plane	Reference
ettringite	9.086	(0 1 0)	ref.[203]
	15.772	(-1 2 0)	
	25.595	(-1 3 2) & (1 2 2)	
portlandite	18.066	(0 0 1)	ref. [204]
anhydrite	25.447	(0 2 0)	ref. [205]
	25.454	(2 0 0)	

wavelength of incident ray (Cu Kα) = 1.5406 Å

If kinetic information obtained from isotherm calorimetry and in-situ XRD are combined, further insights might be speculated. As discussed, two main characteristic peaks - silicate hydration and sulfate depletion – are related to the formation of portlandite and late ettringite formation, i.e. consumption of anhydrite. Therefore, time points of those peaks from either calorimetry or in-situ XRD are presented in Table 5-3.

Table 5-3 Time point [a] [h] of exothermic peak and specific phases occurrence

p/c	peak summit by calorimetry		in-situ XRD	
	primary silicate	sulfate depletion	portlandite occurrence	anhydrite disappearance
cement 0	13	22.5 [b]	5.5	22.5
Latex A 0.02	13	19	7.5	23
0.05	13.5	17.5	8	21
0.10	15	20	8.5	>24
Latex B 0.02	13	21.5	7.5	21.5
0.05	15.5	23	9	21.5
0.10	14.5	25.5	9.5	23
Latex C 0.02	14	26 [b]	6	>24
0.05	16	27.5 [b]	8	>24
0.10	19	37 [b]	10	>24
PVOH 0.002	13	20.5	8.0	>24
0.01	14	22.5	8.5	>24

a. accuracy: ± 0.5 h;
b. for control cement specimen or latex C specimens, sulfate depletion peak was the turn point of the sulfate depletion shoulder

As expected, the silicate hydration peak and portlandite formation showed little correlation. In section 5.1, a plausible speculation was made, in which continuous silicate hydration and later ettringite formation may occur simultaneously. With increased polymers content, portlandite formation was retarded gradually due to the interaction between polymers and ions in cement pore solution. Probably, the change in pH as well as the adsorption of ions or crystallites on latex surface played an important role.

The summit of the sulfate depletion peak and the disappearance of anhydrite as shown in XRD carried little relevance. It is obvious that anionic latex C retarded the dissolution of anhydrite, which resulted in a prolonged sulfate depletion shoulder, depending on the p/c ratio. This result is also in accordance with the initial ionic composition. By the presence of PVOH, late ettringite formation was enhanced which was attributed to the rapid dissolution of C_3A during the deceleration period when sulfate was used up [170]. However, either latex A or B barely exerted any influence on the depletion of anhydrite, which does not agree with the initial ionic composition. Nevertheless, the sulfate depletion peak was principally enhanced by the

presence of PVOH, while the rapid dissolution of the aluminate phase was affected by the latex particles as well (see Appendix B).

Crystallization of mineral could be altered in the presence of polymer [194]. Thus, it is also interesting to determine whether the ettringite crystal could be altered by the PVOH. As presented in Figure 5.16, crystal modification could not be confirmed. The only evidence here is that the relative intensity of the peak areas from both were smaller than the well crystallized ettringite mineral [206].
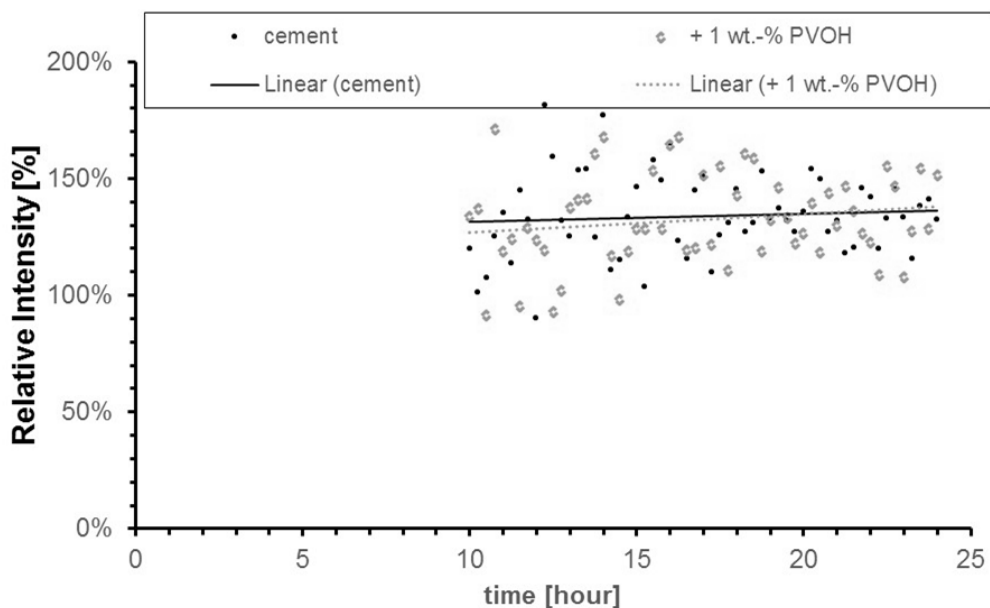
Figure 5.16 Relative intensity between peak area integral of crystal plane (0 1 0) and (-1 2 0) of ettringite

Other than the surface interaction, PVA intercalated calcium aluminate hydrate was also reported [207]. PVA polymer chains could intercalate into the AFm layered structure at 5 °C when the interlayer anion was OH^- [208]. To verify the possibility in cement-PVOH composite, C_3A hydration in the presence of PVOH was carried out at room temperature. As presented in Figure 5.17, the missing 5 ° 2θ peak indicated that no such structure can be confirmed. Besides, in the presence of PVOH, only a minor difference in the formation of hemicarbonate or hydroxyl-AFm could be observed. The carbonation probably occurred during the separation and drying process. Nevertheless, at ambient temperatures (>20 °C), the AFm type mineral is transformed into the more stable cubic katoite (C_3AH_6) in $CaO-Al_2O_3-H_2O$ system [209], on which PVOH showed no effect.
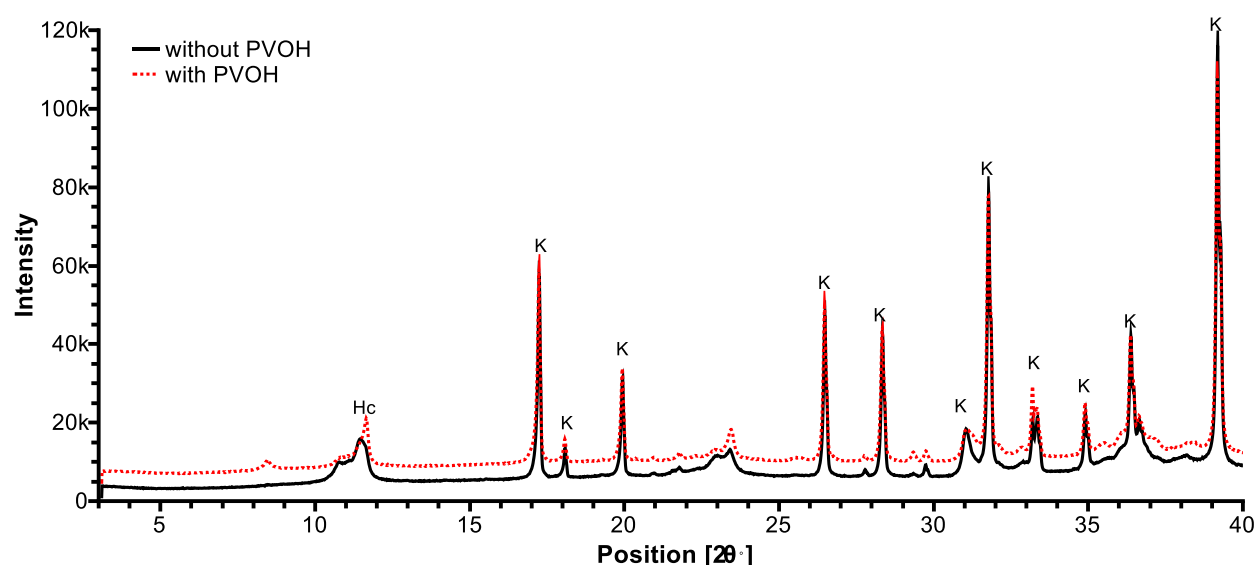
Figure 5.17 Powder X-ray diffractogram of C$_3$A – saturated Ca(OH)$_2$ solution hydration product (Hc: hemicarbonate; K: katoite)

In the presence of SO$_4^{2-}$, ettringite formation was the favoured mechanistic pathway. Well crystallized ettringite was formed regardless of the presence of PVOH, as shown inFigure 5.18. At the same time, no intercalated structure was indicated. This result elucidated that PVOH intercalations are hardly present in the Portland cement paste. In fact, the presence of anions other than OH$^-$ inhibited the formation of PVA-intercalated C-A-H compounds [208]. Thus, the strong interaction between PVOH and C$_3$A may be attributed to surface adsorption on both the aluminate surfaces of the nonhydrates and hydrates of the aluminate phase, where the latter constitutes a large effective surface area.
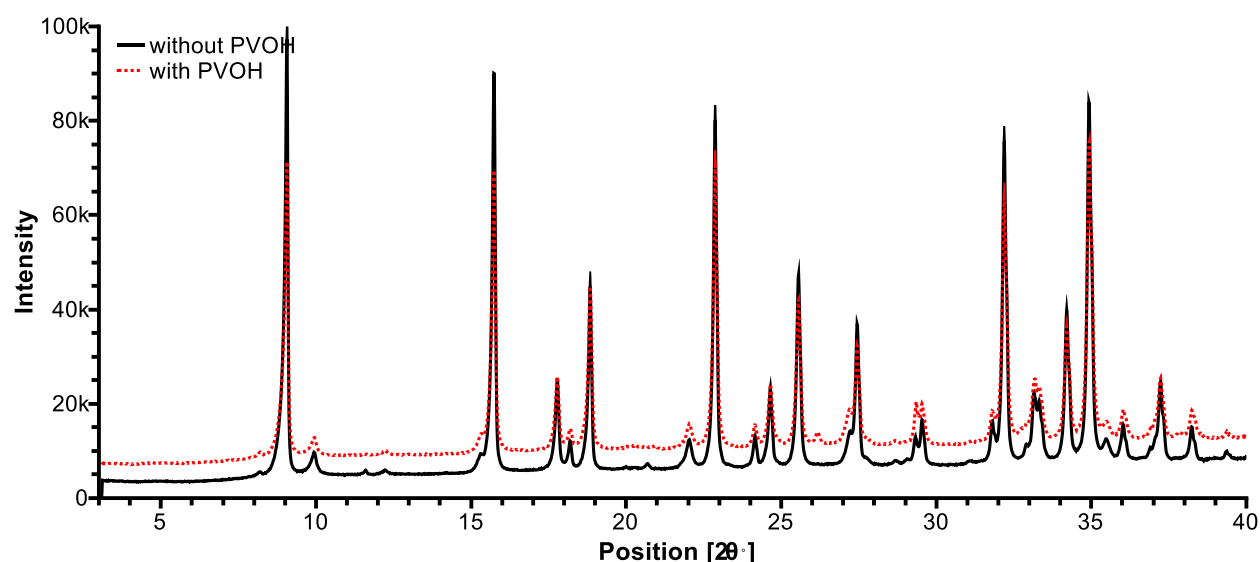

Figure 5.18 Powder X-ray diffractogram of C$_3$A – saturated CaSO$_4$ solution hydration product

6 Film formation of the VAE latex stabilized with PVOH in cement environment

When latex is mixed with cement, film formation is accompanied by cement hydration. Thus, the film-forming process is inevitably affected by the cementitious environment. High electrolyte concentration of cement pore solution [171], relative humidity [9] and p/c ratio [9,18] were found to be influential factors with respect to film formation in cement matrix. However, instead of the charge stabilized latices in previous studies, the film-forming process in cementitious environment is particularly of interest to PVOH stabilized latex in this study [23]. As revealed in chapters 4 and 5, PVOH interacts with cement minerals as well as ions from the pore solution, which changes the film-forming process.

6.1 Stability of the latex in high electrolytes concentration

Microscopy, especially ESEM is a very powerful tool to investigate film formation of latex [100]. However, it is difficult to distinguish the morphologies generated either by initial agglomeration (Figure 6.1) or by close-packing during the normal film-forming process. Apparently, particle identity of the agglomerate was distinct with a minor deformed morphology. Be that as it may, initial agglomeration does not mean the failure of the film formation.
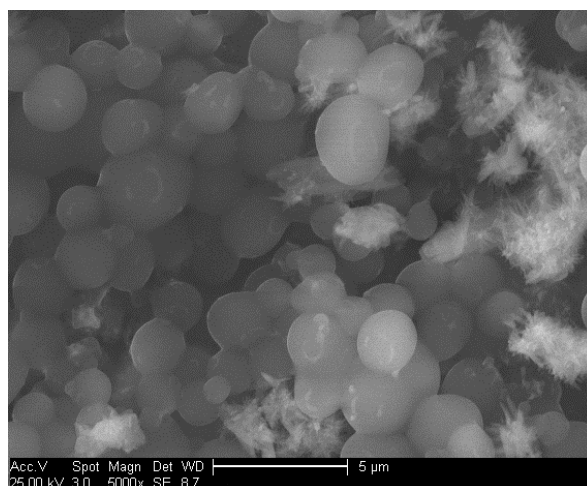

Figure 6.1 SEM image of VAE latex agglomeration formed immediately in cement pore solution

In cement paste, initial agglomeration can result in a change in the distribution of the polymer. Therefore, the stability of the latex in high electrolyte concentration, e.g. cement pore solution, should be considered prior to the film formation. Generally, stability of the medium in the presence of Ca^{2+} is of importance to charged polymer colloids. With regard to the VAE latex stabilized with PVOH, this condition is expected to be not critical. The results confirmed that

the two non-ionic latices showed good stability against Ca^{2+} in a nearly neutral solution (Figure 6.2).
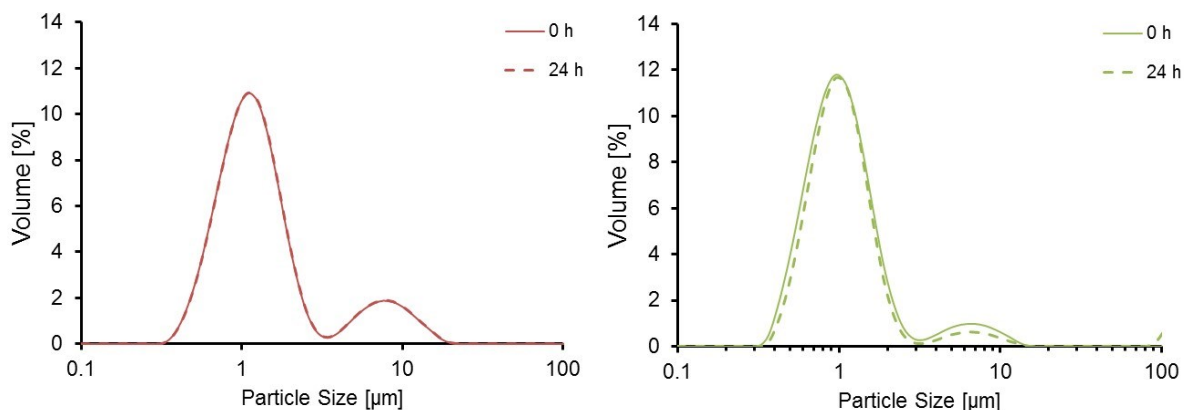

Figure 6.2 PSD of 0.1 wt.-% latex A (left) and latex B (right) in 0.1 mol/L $CaCl_2$ solution

However, if the polymer colloid was dispersed in SCPS, the stability against agglomeration decreased as a function of time (Figure 6.3). The measurements were conducted 5 min after the polymer dispersions were dispersed in SCPS. As can be seen, latex A showed trends of agglomeration immediately, while latex B showed relatively good stability even after 1 h. Until 3 h, both latices showed the tendency of agglomeration. After 24 h, both latices presented strong agglomeration while a new peak appeared at ~ 150 nm. To rule out the effects of carbonation, pure SCPS was conducted with the same protocol. However, no PSD could be determined. Thus, the smaller particle could be either due to the agglomeration of PVOH or complex of PVOH and inorganic salt. Alternatively, this effect could have arisen simply from model fitting by the software algorithm. Indeed, this highly diluted polymer dispersions may enlarge the effect of agglomeration in the real cement pore solution. However, if polymer agglomeration occurred, the film-forming process within cement paste will be altered.
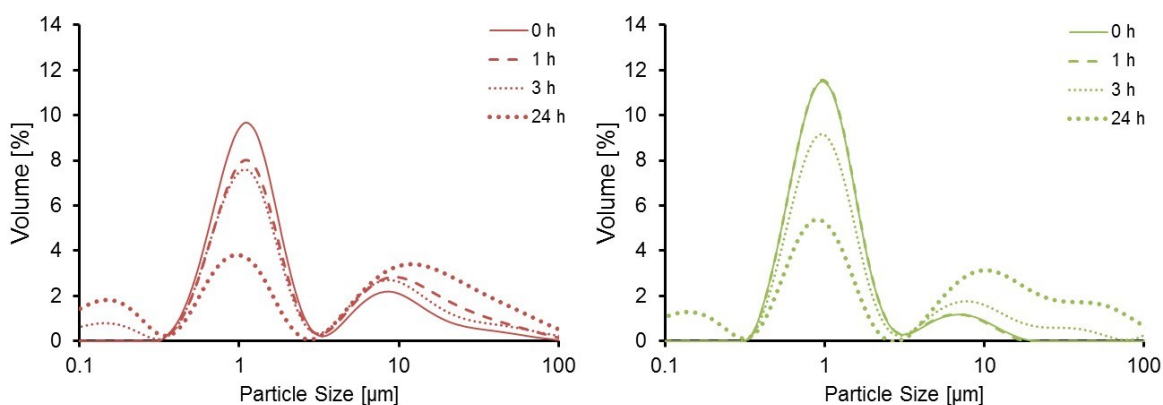

Figure 6.3 PSD of 0.1 wt.-% latex A (left) and latex B (right) in SCPS

6.2 Redispersibility of the VAE latex film

As revealed in previous studies [28,105], VAE latex stabilized with PVOH formed a unique structure (illustrated in Figure 6.4) instead of a continuous film in classic theory. Hydrophilic PVOH membrane in the vicinity of the latex particles hinders the interdiffusion of latex polymer and hence imparts the polymer domain redispersibility. Therefore, breakup of this PVOH membrane is the key for non-dispersible film formation. Meanwhile, this unique property indicates that polymer interdiffusion and coalescence have occurred, since the coalescence is irreversible under ambient conditions.
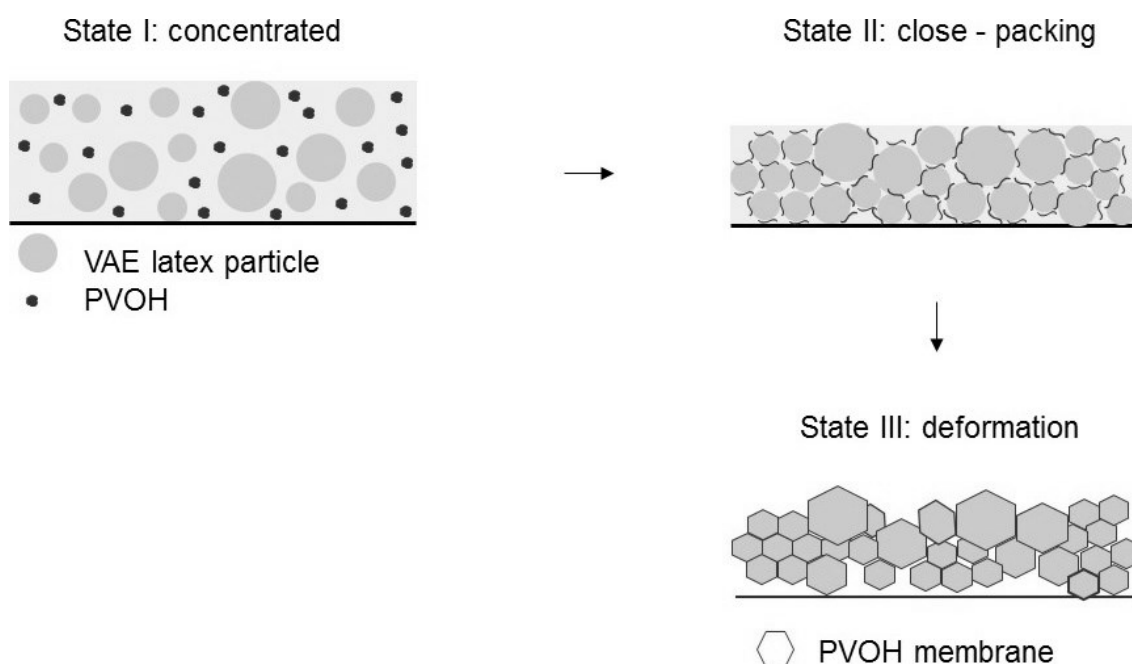

Figure 6.4 Schematic illustration of polymer domain formed by the VAE latex stabilized with PVOH

As presented in Table 6-1, 80% R.H. influenced the redispersibility of latex A, but displayed no such effect on latex B. Cement substrate as well as SCPS also influenced the redispersibility, in which the latter promoted the film-forming process additionally. These results also indicated that the kinetics of film formation were affected by different influential factors in various degrees. If film were formed in a cementitious matrix, the synergy effect should also be taken into consideration. Nevertheless, a cementitious environment can promote a non-dispersible film formation with regards to the VAE latex stabilized with PVOH.

Table 6-1 Redispersibility of the investigated films

	Aging [d]	80% relative humidity			on cement substrate	from SCPS
		dialyzed	original	add PVOH		
A	1	+	+	+	+/-	-
	7	-	-	+/-	-	-
B	1	+	+	+	+	-
	7	+	+	+	-	-

+ redispersible; - non-dispersible; +/- difficult to redisperse

6.3 Influence of high humidity on film formation

Prior to discussing the results related to surface morphology of the film as obtained from ESEM and AFM, it is important to note that uniform drying in the vertical direction may be achieved with slow evaporation rates and thin films [86]. Large particles and the relatively high viscosity of the VAE latex may result in some difference on top and bulk of the film. In this section, the interface between the film and glass slide was investigated, in order to gain information about the vertical uniformity.
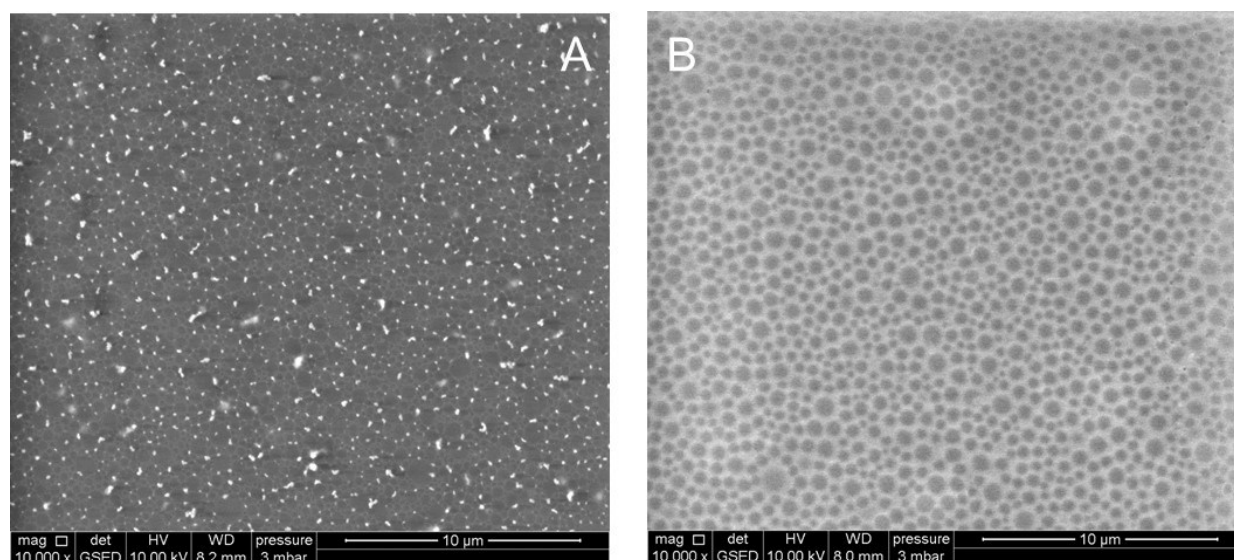

Figure 6.5 ESEM image of the films from latex A (left) and latex B (right) after 1 day under 23 °C and 85% R.H. (Interface to the glass slide)

After one day, both VAE latices showed some differences in the surface morphology (Figure 6.5). Many white spots or fibre like soft matters were distributed throughout the surface of the latex A film, while individual particles surrounded by a light grey membrane were observed for that of latex B. EDX measurement was not possible as the soft matter was too small. However, the white soft matter above the examined surface could be created by the electron beam, indicating that it should be organic matter, which effectively could be the PVOH according to

the latex composition. For latex B, unambiguous interpretation for the acquired image is quite difficult due to the limited information based on the image contrast.

High magnification images acquired by AFM (Figure 6.6) confirmed the results on surface morphology as obtained from ESEM imaging. Particles of latex A sample were covered by some curled fibrous soft matter, while those of latex B sample were isolated by the surrounding membrane. Budhlall *et al.* [106] described the morphology as latex particle hill and PVOH valley, indicating that the surrounding membrane should be PVOH. Besides, attention must be paid to the difference in height between the brightest and darkest spots of the image. The maximum difference that could be detected by AFM was around 120 nm, implying a relatively smooth surface.
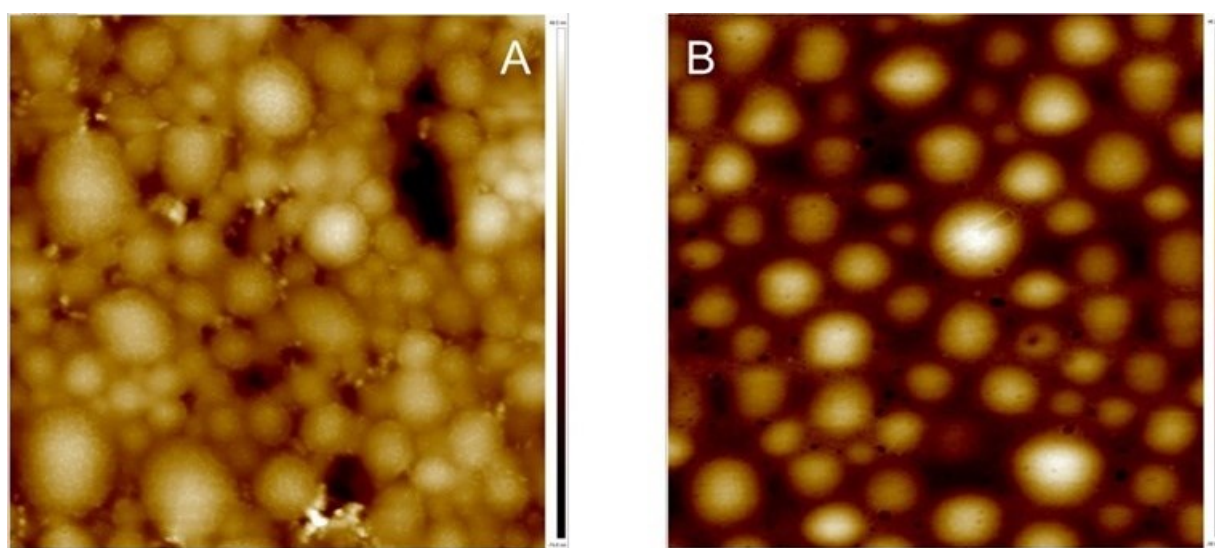

Figure 6.6 AFM image of the films from latex A (left, height difference 124 nm) and latex B (right, height difference 84 nm) after 1 day (5 x 5 µm scanning area)

While the latex was treated either by dialysis or with subsequent addition of PVOH, no pronounced differences in the surface morphology of the latex B film could be observed (Figure 6.7 right and Figure 6.8 right).
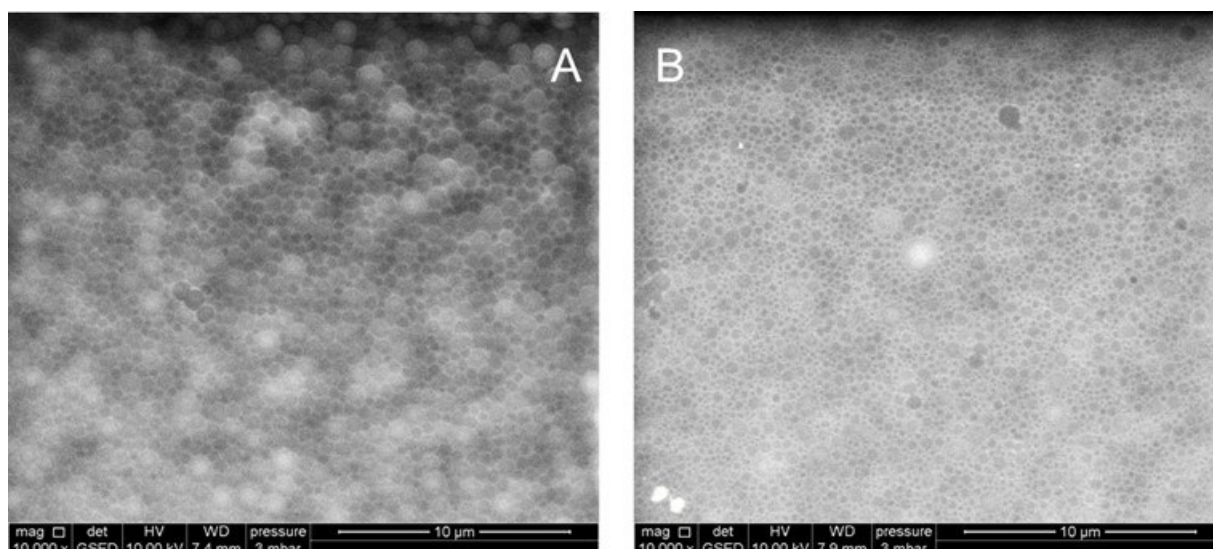
Figure 6.7 ESEM image of the films from dialyzed latex A (left) and latex B (right) after 1 day under 23 °C and 85% R.H. (Interface to the glass slide)

The differences in the image contrast should be attributed to the different PVOH amounts. Similarly, the higher the PVOH amount, the more pronounced were the phenomena whereby curled fibre like soft matter was above the surface of the latex A film (Figure 6.7 left and Figure 6.8 left).
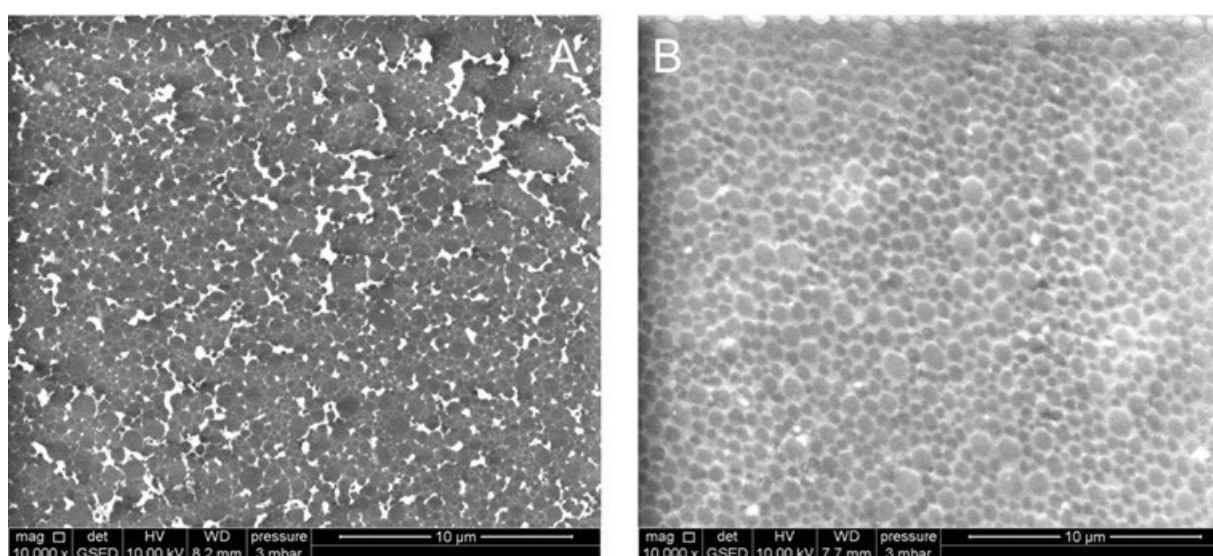

Figure 6.8 ESEM image of the films from latex A (left) and latex B (right) with additional PVOH after 1 day under 23 °C and 85% R.H. (Interface to the glass slide)
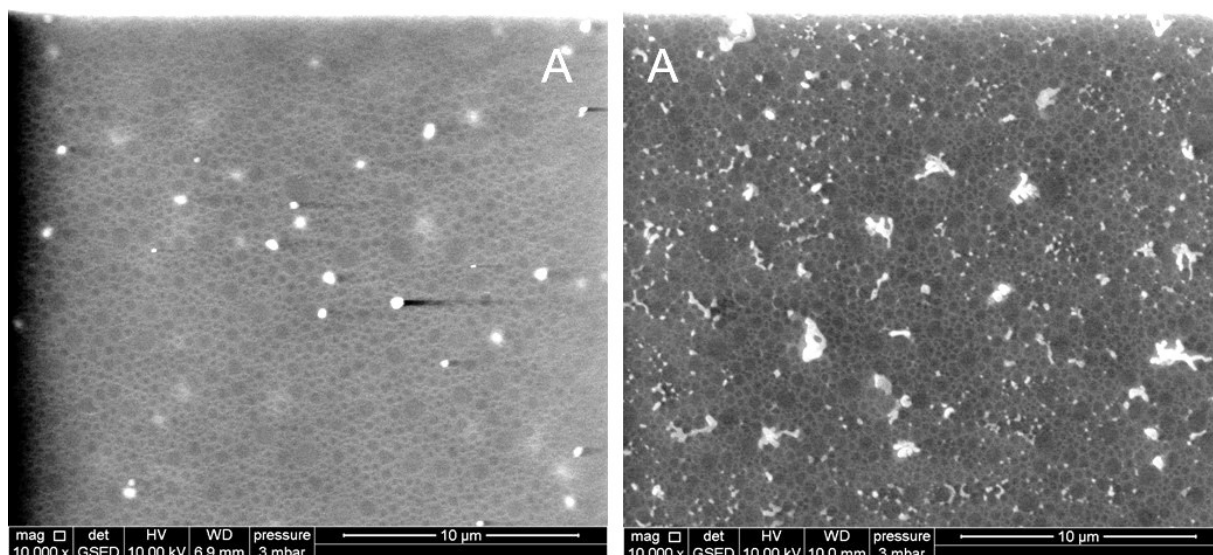
Figure 6.9 ESEM image of the films from latex A after 7 days under 23 °C and 85% R.H.
(left: surface towards air; right: interface to the glass slide)

Interestingly, no fibre-like soft matter was observed when the surface towards air was analyzed under ESEM. Conversely, the fibre-like soft matter was found if the interface to the glass slide was examined (Figure 6.9). Thus, PVOH was probably extruded during the film-forming process under 85% R.H. The reason why PVOH was extruded towards the bottom only in latex A film is unclear. If the negative capillary pressure is considered, two latices possessing similar surface tension (air-liquid) as well as contact angles [210] (solid-liquid) should result in quite similar capillary pressures. In the absence of water, temperature is a more decisive factor for particle deformation [95]. It elucidates that particle deformation ability depends on the polymer nature, i.e. T_g. Nonetheless, the residual capillary water that keeps the particles wet, can accelerate the particle deformation process [96]. Furthermore, the presence of water lowered the T_g of both polymers, since water is a plasticizer [52]. In the presence of water, T_g of latex polymer A decreased to -4 °C while that of latex polymer B decreased to 17 °C. Though it was not a decisive factor for the PVOH extrusion, capillary water played a positive role on particle deformation.

As reported by Budhlall et al. [106], VAc latex stabilized by PVOH showed a unique surface morphology. As a result, smooth and homogeneous surface morphology which is commonly used as the indicator for polymer coalescence is hardly applicable for the VAE latex stabilized by PVOH. Instead, the redispersibility originating from the interstitial PVOH membrane, can be the hint for polymer coalescence, since integrated polymer structure is non-dispersible in water. From the results in Table 6-1, films cast from latex B were dispersible in water regardless of pretreatment. On the other hand, the films cast with latex A were non-dispersible after seven days except when additional 5 wt.-% PVOH was present. On the one hand, increasing PVOH was efficient for the redispersibility; but otherwise, high humidity was positive

for the film formation. Linking the surface morphology to redispersibility, one could speculate that eliminating PVOH from the interstices of the particles is necessary for interdiffusion and coalescence. However, the surface morphology of latices at different ages (Figure 6.10) had nearly no differences but exhibited different mechanical properties, i.e. redispersibility in water.
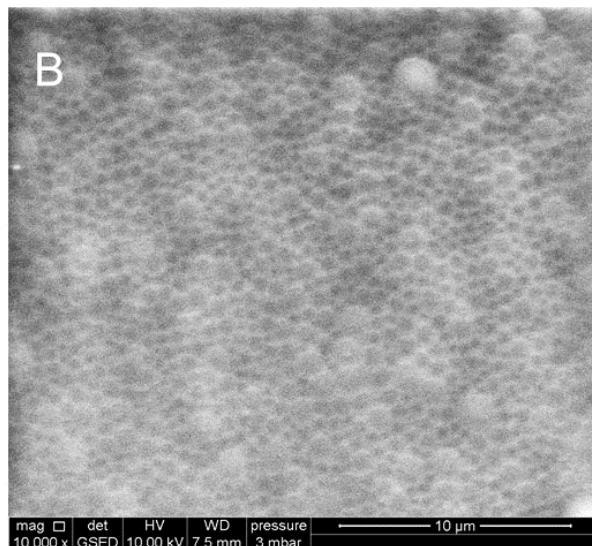

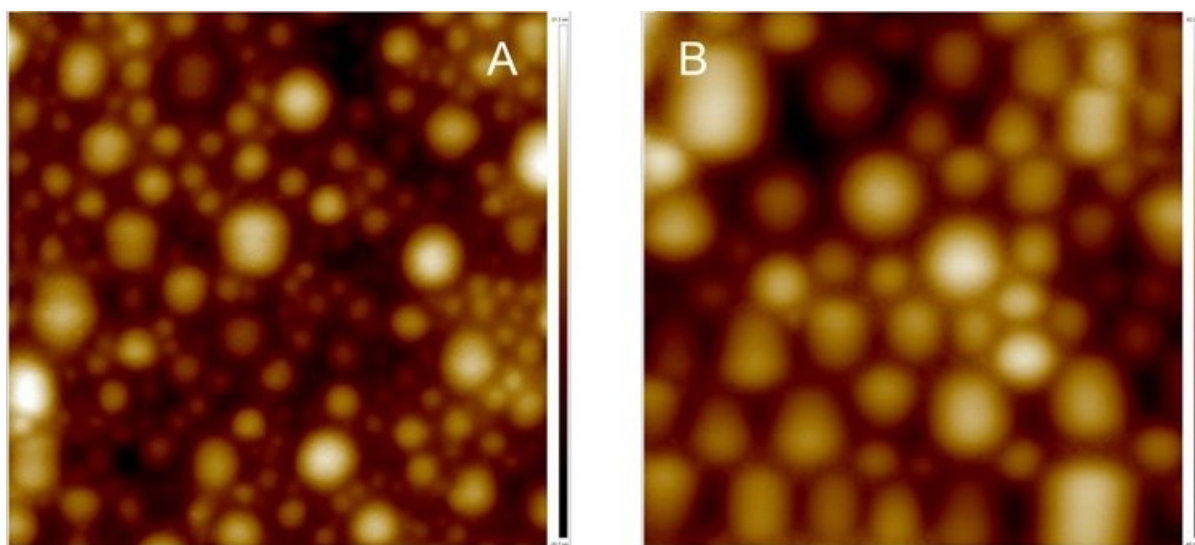Figure 6.10 ESEM image of the films from latex B after 7 days under 23 °C and 85% R.H. (surface to the air)

Figure 6.11 AFM image of the films from latex A (left, height difference 57 nm) and latex B (right, height difference 126 nm) after 7 days under 23 °C and 85% R.H. (5 x 5 μm area)

AFM results (Figure 6.11) also revealed that no pronounced differences were observed for films at different ages. The fluctuation of maximum height difference was dependent on the sampling area, since latex is not a mondisperse system.

6.4   Influence of cement matrix on film formation

Hardened cement paste possesses a porous structure especially at early age [211], in which PVOH could penetrate or even be adsorbed on the mineral phases. The advantage of this simulation is that the high contrast or resolution of the polymer film under ESEM could be guaranteed, without the interference of cement minerals. Obviously, interaction with cement minerals as well as ions is omitted by that, which could alter the film-forming kinetics.
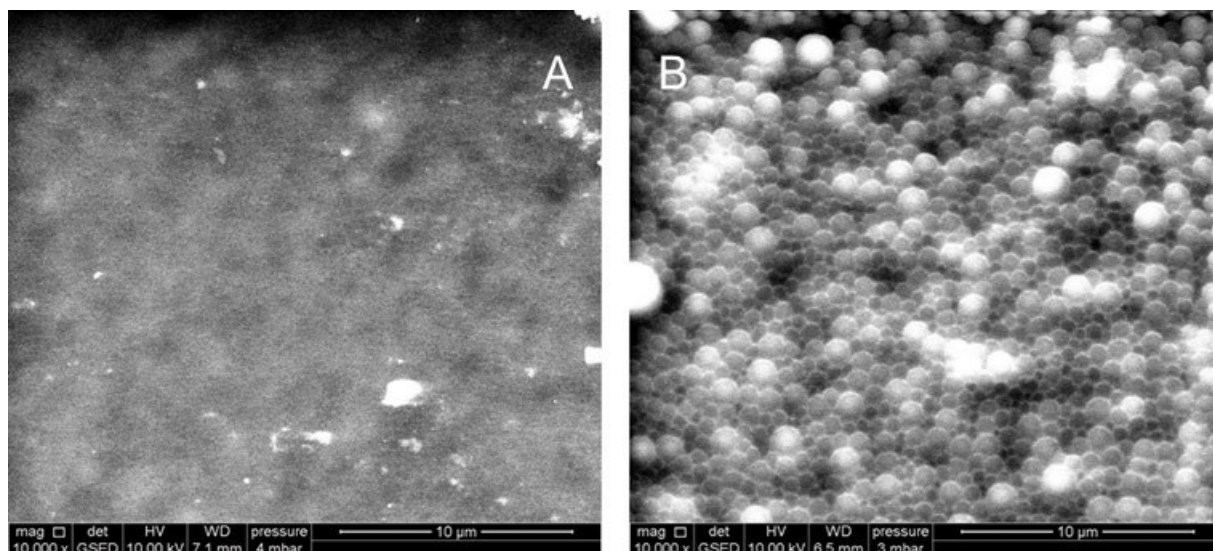

Figure 6.12 ESEM image of the films from latex A (left) and latex B (right) on cement substrate after 1 day under 23 °C and 50% R.H.

After one day of film formation, no sharp image for the latex A film could be acquired (Figure 6.12 left). The ambiguous boundary of the particles implied relative homogeneity on the surface. In contrast, spherical particles from the film of latex B (Figure 6.12, right) demonstrated that the film-forming process of latex B was between states 2 and 3. This corresponded to the redispersibility test results, where the latex A film was difficult to redisperse while that of latex B was still dispersible. The redispersibility test results also indicated that interdiffusion and coalescence took more than one day under the experimental conditions employed here.
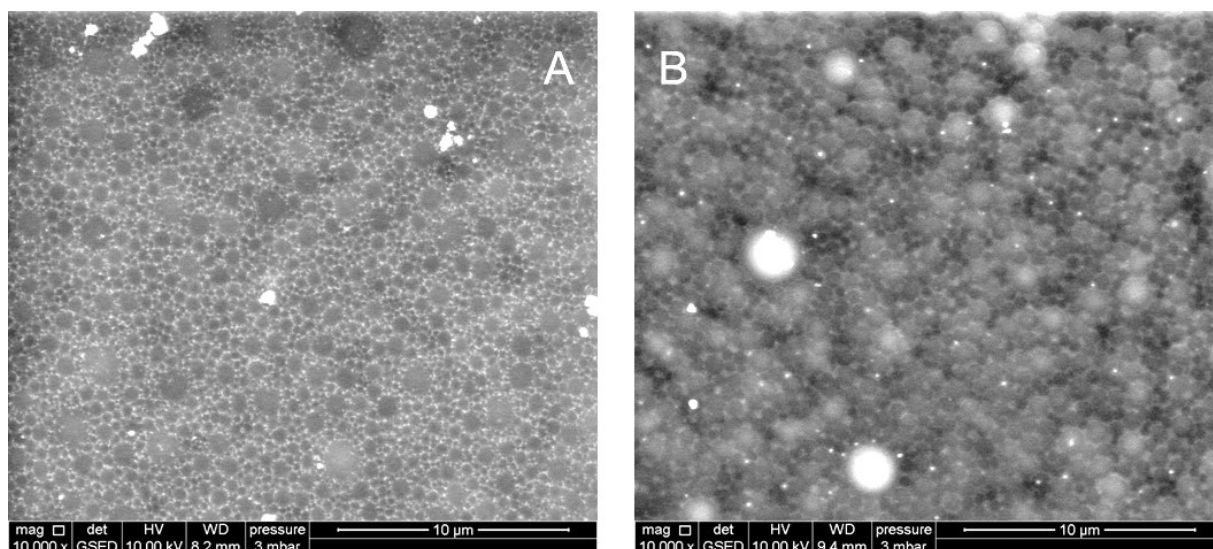
Figure 6.13 ESEM image of the films from latex A (left) and latex B (right) on cement substrate after 7 days under 23 °C and 50% R.H.

After seven days, a relatively sharp image of the latex A film was observed (Figure 6.13 left). Fusion of the particles was not observed from the surficial morphology; only particle deformation (stage 3) was confirmed. The particles' boundary was distinct, unlike that for the one-day samples. The redispersibility test revealed that the film of latex A was non-dispersible, indicating that interdiffusion and coalescence had probably occurred. Likewise, the film of latex B presented a deformed and compact morphology without the loss of the particle identity (Figure 6.13, right). The redispersibility test revealed that the film of latex B was non-dispersible, though film-forming state 3 should be specified accordingly. Actually, the ambient temperature in this study was quite critical for latex B while bulk water was adsorbed by the substrate, limiting its ability to deform.

However, polymer interdiffusion seems to be affected to a relatively low extent, in the respect that water could be located inside the polymer and thus relieve the polymer chains for the interdiffusion [91]. These results indicated once again that the elimination of PVOH within the interstices of particles was the key for the interdiffusion and coalescence of the VAE polymer, especially for the hard polymer. However, the difference between the simulation and the practice should be noticed with regard to the removal of PVOH. In this study, dissolved PVOH was removed either by penetration of the fluid into the pores or capillary suction; while in cement paste, PVOH was removed by the interaction with cement minerals [212].

6.5   Influence of cement pore solution on film formation

The surface morphology of the film can be affected by the salt concentration [171]. In general, the evaporation process could result in salt deposition on the surface of the film, counteracting the contrast within it. Therefore, interpretation of the acquired images should be cautious and

pretreatment of the specimens would be necessary, e.g., rinsing the samples with water. However, it is not always efficient since salt with low solubility is presented, e.g. $CaSO_4 \cdot 2H_2O$. Compared to those latices stabilized by ionic or nonionic surfactant, PVOH is a nonionic polymer with characteristics of saponification due to the residual acetate group [74]. It is therefore intriguing to investigate its behaviour in cement pore solution.
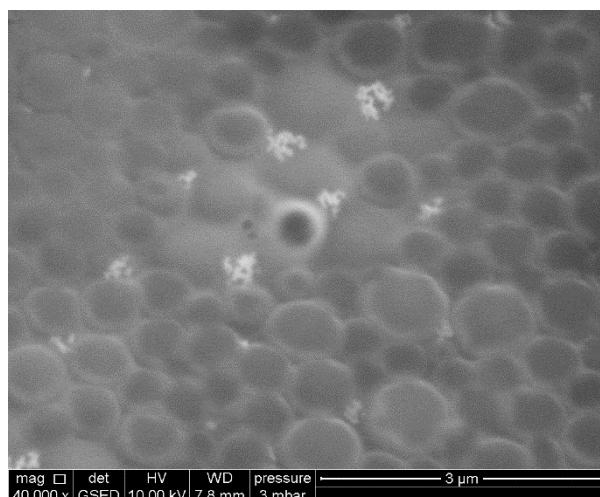

Figure 6.14 ESEM image of the latex B film formed from SCPS after 1 day under 23 °C and 50% R.H.

As presented in Figure 6.14, little fibre-like soft matter was observed in the interstices of particles. As argued in section 6.2, the soft matter identified was probably PVOH aggregates. Accordingly, elimination of PVOH can affect the film formation in two aspects. On the one hand, aggregation of PVOH results in more available interface for the interdiffusion of VAE polymer chains; whereas on the other hand, the hard PVOH inclusion acts as a spacer between particles that hinders the approach of the particles, as illustrated in Figure 6.14.
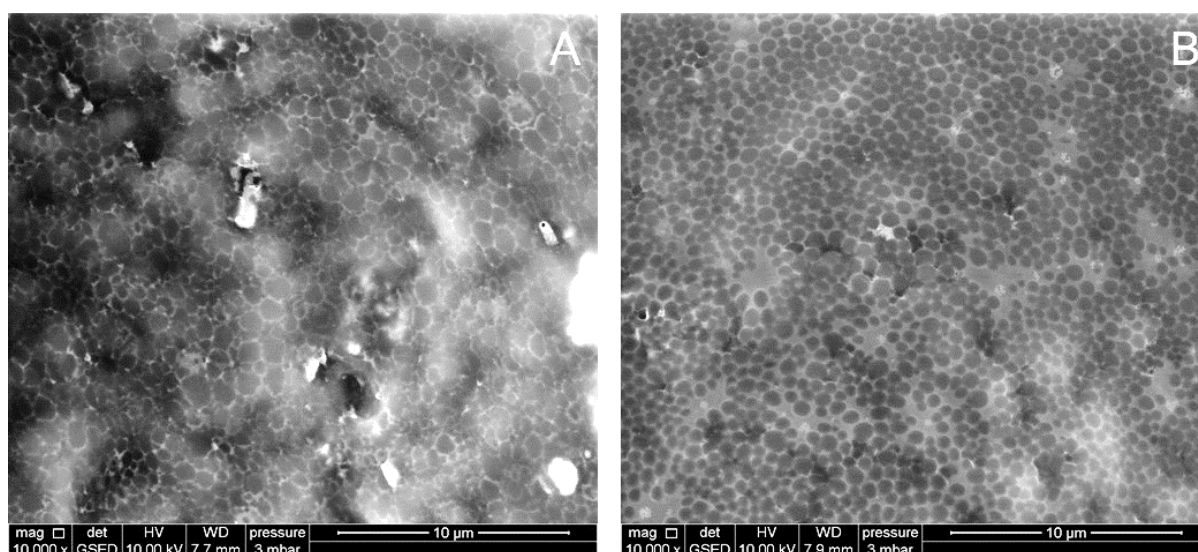

Figure 6.15 ESEM image of the latex A (left) and latex B (right) films formed from SCPS after 1 day under 23 °C and 50% R.H.

In Figure 6.15, surface morphologies of the two latex films were different, in which particle deformation of latex A film was more thorough. Routh *et al*. [93] proposed five mechanisms for the particle deformation during the film formation. In this study, wet sintering, capillary deformation and receding water front are the possible mechanisms. The wet sintering mechanism is dominated by the surface tension between the latex polymer and the aqueous phase, while the surface tension between the aqueous phase and air is significant for the other two mechanisms [86]. As discussed in section 3.1, surface tension and capillary force were nearly the same for both latices. Thus, though capillary force is sufficient for the elastic particle deformation [213], different surface morphologies between latices A and B were presented. This observation indicated that deformability of the particles should be responsible for the difference. In other words, T_g was again the decisive factor for the surface morphology of the film.

Compared to the film of latex B above the cement substrate (Figure 6.12), the film formed from SCPS exhibited prominent particle deformation. It was reasonable for attributing the observation to the saponification of PVOH which increased the surface tension (air-liquid) [74] and the capillary force. Also, the increased hydophilicity of the polymer allowed more water access. This deduction was applicable to the high humidity condition, when capillary force increased as a consequence of the high R.H. Thus, the cement environment is beneficial to the particle deformation, i.e. film-forming process could be accelerated in this condition. With reference to the redispersibility under this condition, both latex films cast from SCPS were non-dispersible after one day.

6.6 Film formation in cement matrix: influence of polymer/cement ratio

Although the circumstances in the cement paste are in favour of non-dispersible film formation, the adsorption of latex particles on mineral surface may lead to the failure of film formation at low p/c ratios. As discussed in section 4.2, higher amounts of particles of latex B were adsorbed on the surface of cement mineral at low p/c ratio (p/c ~ 0.023). This indicated that film formation was not favourable at this condition. In Figure 6.16, film formed within cement paste after 24 h was present.
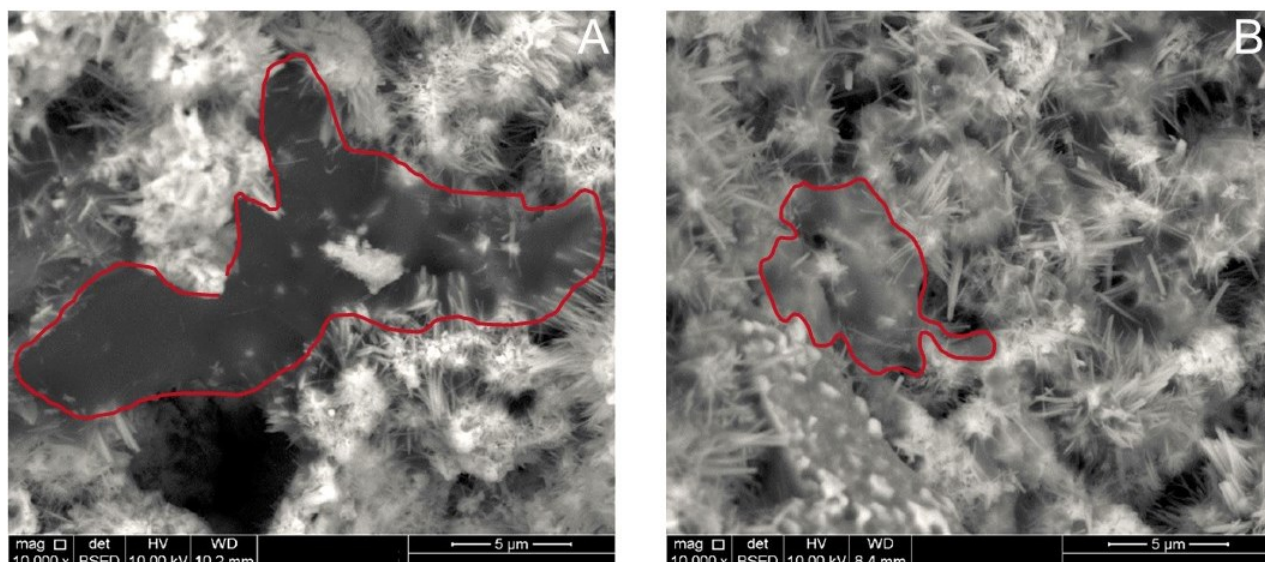
Figure 6.16 SEM image of latex-cement composite (p/c = 0.02) formed after 24 h

As expected, glue-like amorphous matter (dark image based on back-scattered secondary electrons) was more apparent in the cement paste with latex A, while it was almost invisible in the cement paste with latex B. Thus, film formation within cement paste is also linked to the adsorption on cement minerals.

At a p/c ratio of 0.1, the films were more perceptible as presented in Figure 6.17. Compared to the films of latex A, those of latex B were more fragmentary and low on occurrence. Indeed, these images had only qualitative significance. However, the location of the film was difficult to determine throughout the sample of latex B. It could be attributed to the continuous adsorption (i.e. deposition) of polymer particles on the growing mineral surface during cement hydration. Besides, the deformability difference between the two latices can result in this observation, since the film cast from low T_g latex A can spread and cover a larger area. Nevertheless, the result implied that latex adsorption (i.e. deposition) on cement minerals can obstruct film formation to some extent.
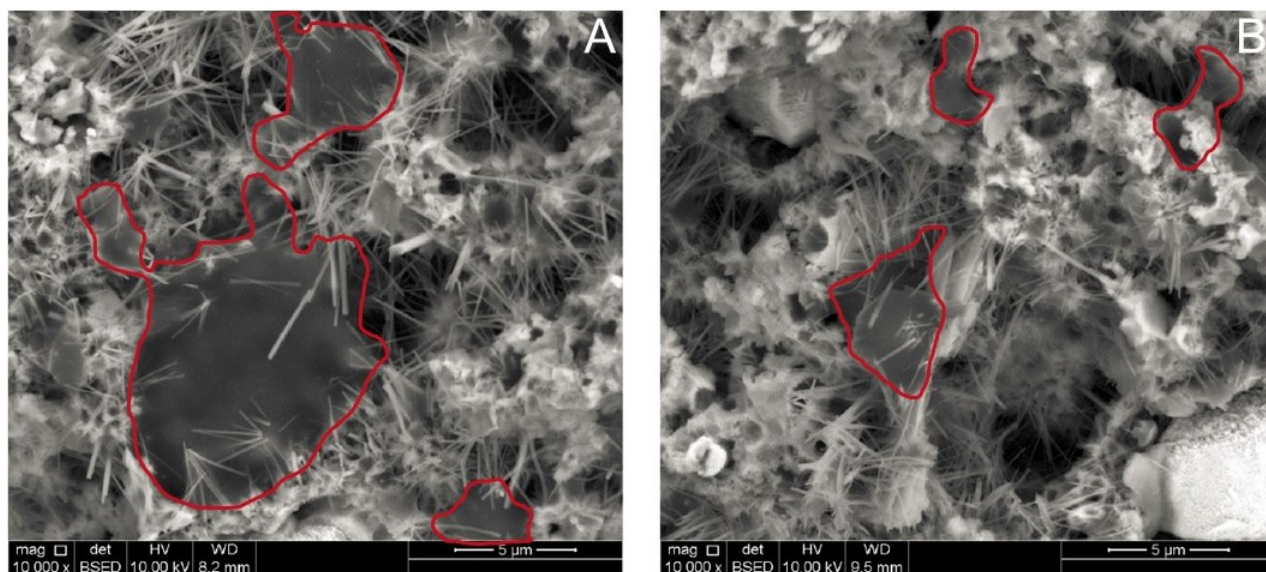
Figure 6.17 SEM image of latex-cement composite (p/c = 0.1) formed after 24 h

7 Conclusion and Outlook

Interaction between VAE latex stabilized with PVOH and Portland cement was studied in this work. To understand the role of ionic charge as well as PVOH, one surfactant stabilized anionic latex and a PVOH with an average molecular weight were employed. Here, the PVOH was also used as protective colloid during the emulsion polymerization of the VAE latex.

The first step involved identification of chemicals in the VAE latex. Two components of the VAE latex stabilized with PVOH were recognized: (1) the VAE copolymer colloid and (2) dissolved PVOH in the solution. By physical separation, part of the PVOH was isolated, while the rest remained adsorbed or grafted onto the surface of the latex particle. Dialysis of the latex indicated an adsorption - desorption equilibrium within the system. Although the colloid was sterically stabilized, the nominal non-ionic VAE latex possessed little anionic charge. Compared to the anionic latex C, the non-ionic VAE latices A and B possessed lower charge density. Charge titration by cations further confirmed that the non-ionic VAE latex had nearly no affinity to Ca^{2+}, both under neutral and alkaline conditions. In other words, the Ca^{2+} bridging effect was limited.

Normally, the adsorbed amount of adsorbate on the adsorbent at solid-liquid interface was assumed to be equal to the depleted amount in the liquid phase. However, from our results, the depletion ratio of the latex showed a plateau as a function of its concentration. Though polymer adsorption was not Langmuir type, the adsorption isotherm was analogous to the profile of a monolayer type of adsorption. Thus, the result contradicted the profile of a monolayer type. Due to the large particle size (> 800 nm), the short-range force does not work beyond this range. Based on this, a new assumption was proposed: depletion of latex from the solution was the combination of the adsorption and sedimentation (or trapped in the sediment). The amount of sedimentation was subtracted by regression from the total depletion amount. The calculated adsorption amount of the latex was very different when the two VAE latices were employed, whereby the adsorbed amount was higher for the VAE latex with a lower charge density.

This finding contradicted the conventional idea of polyelectrolytes adsorption on cement, whereby electrostatic force is principally responsible for the potential polymer-cement interaction. Indeed, the anionic latex showed the highest adsorption amount as well as the surface coverage on the mineral surface. However, in the presence of dissolved PVOH, adsorption (or more precisely as deposition) changed. The experiment proved that the depletion ratio decreased with an increased amount of PVOH. These findings confirmed that the adsorption of the VAE latex onto cement was dependent on both the PVOH corona on the surface of the latex particle and the dissolved PVOH, instead of the surface charge density of

latex particle. Simultaneously, PVOH interacted with cement and showed preferential interaction with C_3A.

Since the polymers interact with the cement, kinetics of cement hydration were altered. At low p/c ratios, both VAE latices showed little influence on the silicate hydration. Instead, an enhanced sulfate depletion peak was presented. Cement hydration with either the PVOH or the anionic latex proved that the phenomenen was attributed to the PVOH. In the presence of either latex or PVOH, K^+ and SO_4^{2-} concentrations in the cement pore solution decreased during the first few hours. This result indicated that latex particles acted as diffusion barriers for ion transportation in cement pore solution while the particles adsorbed cations from the pore solution. By means of in-situ XRD analysis, the complete dissolution of sulfate carrier was observed to be less affected by the non-ionic latex, but retarded by both PVOH and the anionic latex. Although the sulfate depletion peak was enhanced by the presence of PVOH with the non-ionic latex, the rapid dissolution of the aluminate phase was affected by the non-ionic latex polymer. At high p/c ratios, the induction period was extended. This was verified by the rate of cement hydration with the PVOH or serum of the latex. The duration of the induction period was related more to the solution chemistry (e.g. alkaline hydrolysis). Silicate hydration was affected more by the incorporation of latex particles.

As water is consumed by cement hydration, the concentration of polymer particles increased and film formation started consequently. In ambient conditions, VAE latex stabilized with PVOH formed a polymer domain with surrounding PVOH membrane. However, the unique structure resulted in the redispersibility of polymer film in water since the hydrophilic membrane destroyed the integral polymer structure by hindering the entanglement of polymer chains. The interaction between PVOH and cement eliminated the PVOH from the vicinity of VAE particles, thus promoting polymer interdiffusion and coalescence. The effect was simulated in this work and was found to be sufficient for the formation of integral film. High humidity as well as electrolyte solution within cement paste accelerated particle deformation during the film-forming process. In other words, fresh cement paste was an ideal environment for the non-dispersible film formation with regard to the VAE latex stabilized with PVOH. Moreover, this work also revealed that particle identity based on its surficial morphology was distinguishable even after the polymer coalesced. Therefore, interpretation of the state of film-forming according to electron microscopy images should be undertaken with cautiou.

The initial retention of the polymer particles on the mineral surface by adsorption (or deposition) influences their distribution throughout the matrix of PMC. This topic is significant since the film is desired to be located at the interface for certain applications, e.g. ceramic tile adhesives. Although this work revealed that the adsorption of latex particles onto the cement surface was the coaction of both surface and dissolved PVOH, it did not elaborate the mechanism behind

it. In the future, AFM may be employed with custom-built tip, which is covered by PVOH molecules to simulate the latex particle. Meanwhile, stable mineral substrate in different electrolytes solutions combined with different PVOH (amount, type etc.) shall be also applied. In this way, the initial interaction mechanism between the surface and dissolved PVOH may be revealed.

Furthermore, the adsorption was investigated at the initial time in the diluted state. The conditions here differed from the real state. As water is consumed or agglomeration of latex particles occurs, the particles or agglomerates can gradually deposit on cement surface. Thus, their influence on the dissolution of cement minerals will be altered. In fact, initial adsorption elaborated the changes in the ion composition of cement pore solution during the first few hours, but it was impossible to interpret the alteration of cement hydration later on. To overcome this shortcoming, the application of fluorescence-labelled polymer with confocal laser scanning microscopy may be an option in the future. With the aid of the confocal microscopy, surface coverage with time evolution will be available. Accompanying the 'squeeze out' apparatus, alteration of cement pore solution within a hardened cement paste can be analyzed. Hence, a more comprehensive understanding about the latex-cement interaction can be expected.

Finally, since ESEM and AFM pictures leave plenty of room for speculation, the results cannot be over-interpreted. Considering the importance of film formation in cement pore solution, it is quite necessary to investigate its film-forming kinetics further under such circumstances, especially for those latices stabilized with PVOH only. Other techniques based on molecular level rather than microscopy, such as small angle neutron scattering (SANS) or fluorescence resonance energy transfer (FRET) should be employed in future studies.

Appendix A

In chapter 4, the VAE latices with chemical similarity presented different adsorbed amounts onto the cement surface. To verify whether secondary minima played a role, interaction energy between the naked particle and cement surface was calculated according to DLVO theory.

1.   Debye Length

The concentration of Al, Si, Mg species ions is neglected because of their low concentrations. The experimental results from Schwenk CEM I 42.5 R (w/c = 0.5, see section 3.1.14) were employed. In which, OH⁻ concentration was calculated according to the charge balance.

Table 1 Ions composition of cement pore solution

	Concentration (mol/L)
K^+	0.228
Na^+	0.040
Ca^{2+}	0.014
SO_4^{2-}	0.117
OH^-	0.062

Thus, Debye length in cement pore solution could be calculated from Equation. A1.

$$\kappa^{-1} = \sqrt{\frac{\varepsilon_0 \varepsilon K_B T}{\sum_i N_A c_i z_i^2 e^2}} \tag{A1}$$

Where,

ε_0 permittivity of free space, 8.854 × 10⁻²⁰ C²/J·m

ε dieletric constant of water, e.g. 78.4

K_B Boltzmann's constant, 1.38 × 10⁻²³ J/K

T   absolute temperature, 298.15 K

N_A Avogadro's number, 6.02 × 10²³ /mol

c_i molarity of i th ion, mol/L

z_i valence of the i th ion

e   elementary charge, 1.60 × 10⁻¹⁹ C

Debye length (κ^{-1}) in the cement pore solution is calculated from Equation A1, as 0.48 nm. It must be noticed that this calculation assumes and treats the electrolyte solution as the ideal solution. Apparently, it is not true due to the high ionic strength in the cement pore solution, while the concentration should be expressed in molality instead of molarity. Nevertheless, for the purpose of the simplified calculation in following sections, κ^{-1} of 0,05 mol/L NaOH 1:1

symmetric electrolyte will be used, which is 1.36 nm. Besides, Flatt *et al*. reported [183] a more accurate Debye length with 0.67 nm in the pore solution (w/c = 0.45), applicable to the non-ideal electrolyte solution. Since the adsorption of latex particles onto cement was carried out in a diluted system at w/c of 9 (pH from 12.4-12.7), it is reasonable to estimate the Debye length κ^{-1} of the solution as ~1 nm.

2.   Surface potential and charge density (Grahame Equation)

Surface potential and charge density can be linked by the Grahame equation [42], though the equation below is suitable only for z:z electrolyte solution.

$$\sigma = \sqrt{8RT\varepsilon\varepsilon_0 c^\infty} \, sinh\left(\frac{ze\psi_0}{2k_BT}\right) \tag{A2}$$

Where,

σ Surface charge density, C/m^2

R   gas constant, 8.314 J/k·mol

Ψ_0 surface potential

T   absolute temperature, 298.15 K

c^∞ molarity of solute in bulk solution, mol/m^3

Surface charge density of both latices was determined by charge titration in pH=12.5 (see section 4.1). Therefore, surface potential is -138.74 mV for latex A (σ = 0.1936 C/m^2, negative) and -118.66 mV for latex B (σ = 0.1304 C/m^2, negative) in 0.05 mol/L NaOH solution.

Since Ca^{2+} might influence the surface potential greatly, a mixture of NaOH and Ca(OH)$_2$ solution is composed for the calculation, taking [Na$^+$] = 0.03 mol/L, [Ca^{2+}] = 0.01 mol/L and [OH$^-$] = 0.05 mol/L. Then, the equation could be written as follows [42]:

$$\sigma = \sqrt{8\varepsilon\varepsilon_0 K_BT} \, sinh\left(\frac{e\psi_0}{2k_BT}\right)\left\{[Na^+]_\infty + [Ca^{2+}]_\infty(2 + e^{\left(-e\psi_0/K_BT\right)})\right\}^{1/2} = \tag{A3}$$

$$0.117 \, sinh\left(\psi_0/51.4\right)\left\{[Na^+]_\infty + [Ca^{2+}]_\infty(2 + e^{\left(-\psi_0/25.7\right)})\right\}^{1/2} C \, m^{-2}$$

Then, a numerical calculation obtained a value of -88.89 mV for latex A and -78.28 mV for latex B. As a result, the divalent ion has a little influence on the surface potential of the latices.

It is quite difficult to estimate the surface potential of cement particle, either due to the heterogeneity of the irregular shape, or the dynamics during cement hydration as well as asymmetric non-ideal solution in its vicinity. Furthermore, the validity of the Poisson-Boltzmann approximation is still controversial [183,214], with respect to highly coupled systems in cement pore solution. Since DLVO theory is applied, co-ion and counter ion correlation is neglected in this calculation. Besides, only silicate surface of cement is considered for a simple

calculation. The Zeta potential of C_3S at [CaO] concentration of 10 mmol/L was reported as +10 mV, while that at 0.01 mmol/L was -40 mV [215]. In practice, the Zeta potential of cement suspension was measured at ~ +2 mV (w/c=9), which should be attributed mainly to the silicate surface. Meanwhile, in C_3S suspension, the surface charge at pH=12 was estimated to be 0.2-0.4 C/m^2 (negative) [214]. Thus, a crude estimate of a value of about -40 mV is applied to calculate the double layer interaction of the planar silicate surface, as schematically illustrated in Figure A1. Since the surface of a latex particle is negatively charged, the repulsive force between the spherical particle and planar silicate surface is presented. The force, however, should be weak because large separation distance inbetween is induced by the presence of PVOH and the electrical screening ought to arise in the high ionic strength environment.
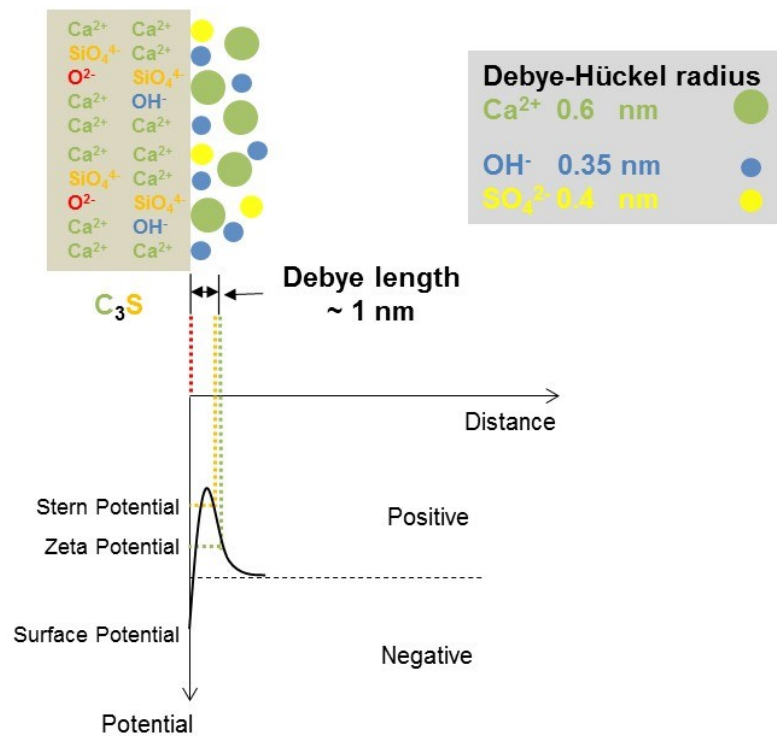

Figure A1 Schematic illustration of hydrated silicate surface (after the literature [216]), its ionic environment in cement pore solution and relation to the potential (water molecule is omitted, Debye-Hückel radius after the literature [217])

3.   Van der Waals interaction energy

Van der Waals interaction between cement and latex particle is simplified to sphere – flat surface interaction, expressed in Equation A4:

$$W(D) = -\frac{AR}{6D}$$

(A4)

Where,

D   separation distance, nm

R   Radius of sphere, nm

A   Hamaker constant, J

Since the origin of the van der Waals force is charge fluctuation [218], retardation of the pairwise interaction can come about. For the ease of calculation, only the non-retardation condition is considered, which is valid at zero separation. The non-retarded Hamaker constant was found to be proportional to the square of density difference within the system of inorganic minerals dispersed in water [180], where the screened Hamaker constant can be estimated to be about 0.44×10^{-20} J for the hydrated cement. In the cement-water-latex system, the combined relation of an unknown Hamaker constant can be crudely estimated in terms of the known values [42], using Equation A5:

$$A_{132} \approx \left(\sqrt{A_{11}} - \sqrt{A_{33}}\right)\left(\sqrt{A_{22}} - \sqrt{A_{33}}\right) \tag{A5}$$

Where,

A_{132} Hamaker constant for substance 1 and 2 via medium 3

A_{11} Hamaker constant of substance 1

A_{22} Hamaker constant of substance 2

A_{33} Hamaker constant of medium 3

The non-retarded Hamaker constant of the latex refers to the literature value [219] of 0.55×10^{-20} J. Importantly, this value is unscreened and the realistic value in cement suspension should be higher. Besides, the Hamaker constant of water is taken as 3.7×10^{-20} J [42]. Therefore, A_{132} is calculated to be 1.49×10^{-20} J.

4.   Electrical double layer interaction energy

The electrostatic double-layer interaction energy can be described by Equation A6, using sphere-flat approximation in z:z electrolytes:

$$W(D) = 64\pi\varepsilon\varepsilon_0 R \left(\frac{K_B T}{ze}\right)^2 tanh\left(\frac{ze\psi_1}{4K_B T}\right) tanh\left(\frac{ze\psi_2}{4K_B T}\right) e^{-\kappa D} \tag{A6}$$

Where,

R   Radius of the sphere

ψ_1 Surface potential of substance 1

Flatt *et al*. [183] proposed an equivalent symmetric noninteger parameter (z = 1.16) for cement suspension at w/c = 0.45, if the surface potential is in the range of -35-0 mV. In cement suspension, electrostatic interaction energy between silicate and latex surface can be expressed by Equations A7 and A8:

$$W(D) = 1.76 \times 10^{-12} Re^{-D/0.67} \ldots \text{latex A} \qquad (A7)$$

$$W(D) = 1.56 \times 10^{-12} Re^{-D/0.67} \ldots \text{latex B} \qquad (A8)$$

5.   DLVO interaction energy

Combining the Van der Waals interaction and electrostatic double-layer interaction, the DLVO interaction energy is obtained, as shown in Figure 2. The radius of both latices is taken as 430 nm, based on the number mean particle size by means of laser granulometry.
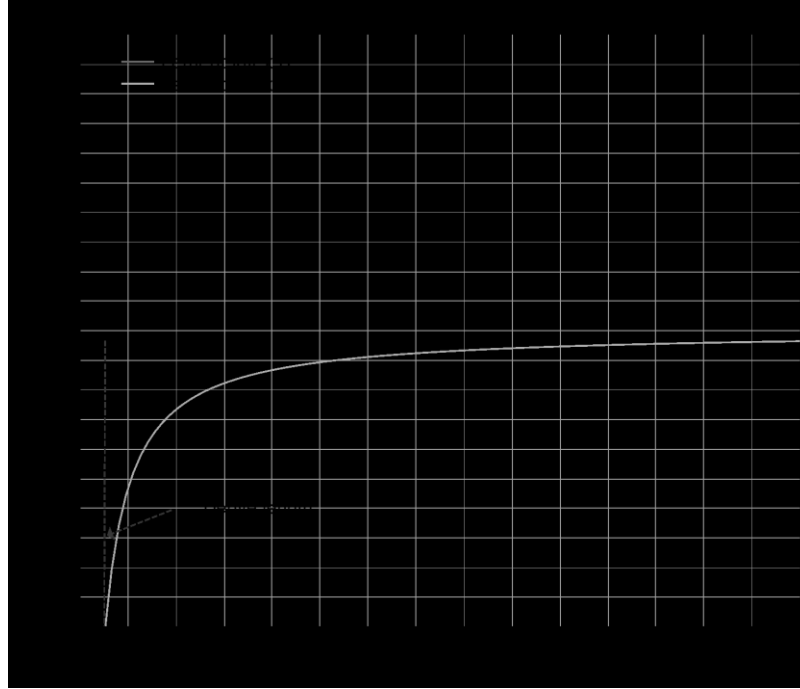

Figure A2 Computed DLVO interaction energy between naked spherical latex particle and planar silicate surface in cement suspension

As can be seen from the energy profile, the interaction energy is always favourable for the adsorption of polymer particles on the planar silicate surface in the specific conditions. The difference between the latices is negligible, indicating that the contribution of electrostatic forces can be neglected in this case. The interaction energy at a separation distance of 10 nm is 12×10^{-20} J (~30 K_BT), while that of 20 nm is 6×10^{-20} J (~15 K_BT). Since the retardation of the Hamaker constant was taken into account, which was decayed in accordance with the power law [218], the interaction energy was overestimated.

In summary, this simple theoretical calculation is quite crude. Nevertheless, it indicates that the adsorption of the latex particle onto the cement favours free energy reduction. However, the driven force for the different adsorbed amounts of latices A and B was unclear. One plausible explanation is that the surface and dissolved PVOH may play a significant role in the interaction between this kind of latex and the cement.

Appendix B

In chapter 5, the rate of cement hydration was compared in accordance with polymer dosage. In order to clarify the influence of different polymers further, additional comparisons were carried out as follows:
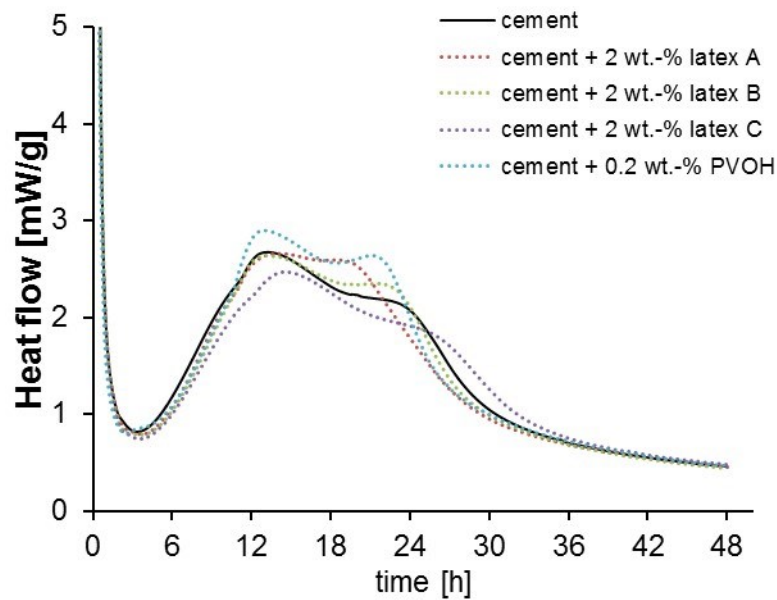

Figure B1 Heat of hydration during the first 48 h in the presence of 2 wt.-% latex
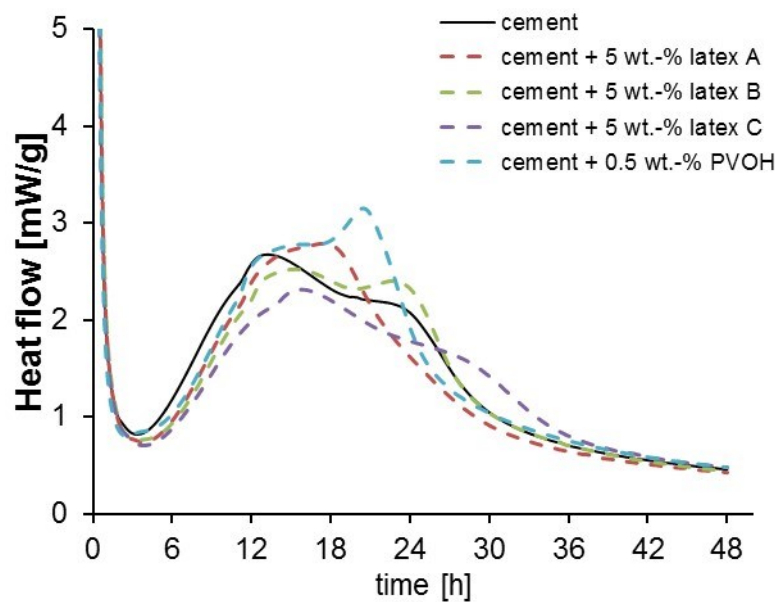

Figure B2 Heat of hydration during the first 48 h in the presence of 5 wt.-% latex
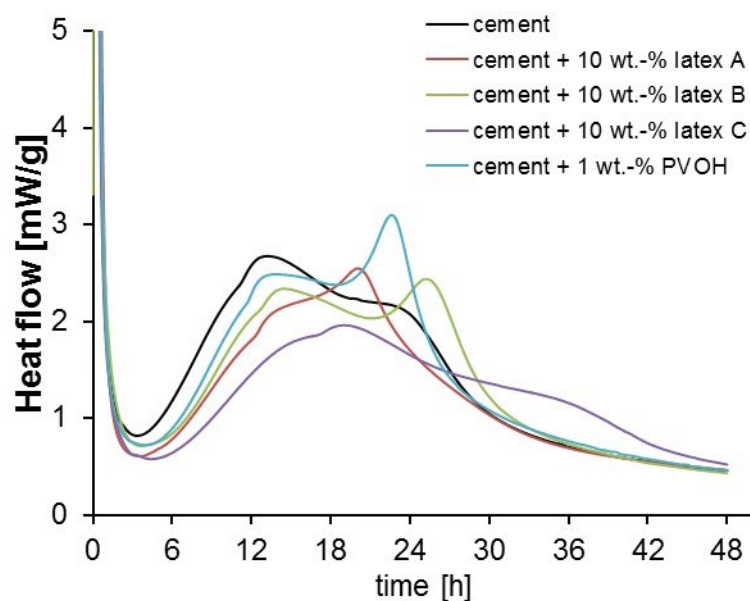
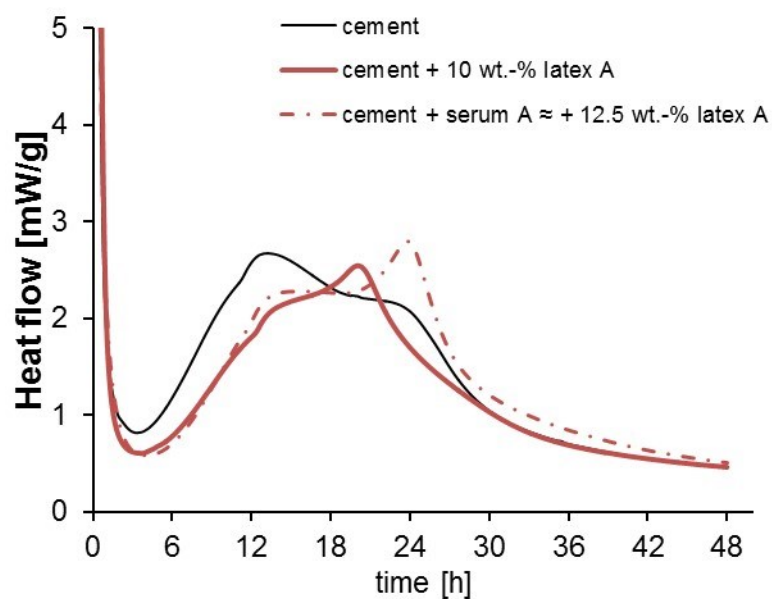Figure B3 Heat of hydration during the first 48 h in the presence of 10 wt.-% latex

Figure B4 Heat of hydration during the first 48 h in the presence of 10 wt.-% latex A or serum A
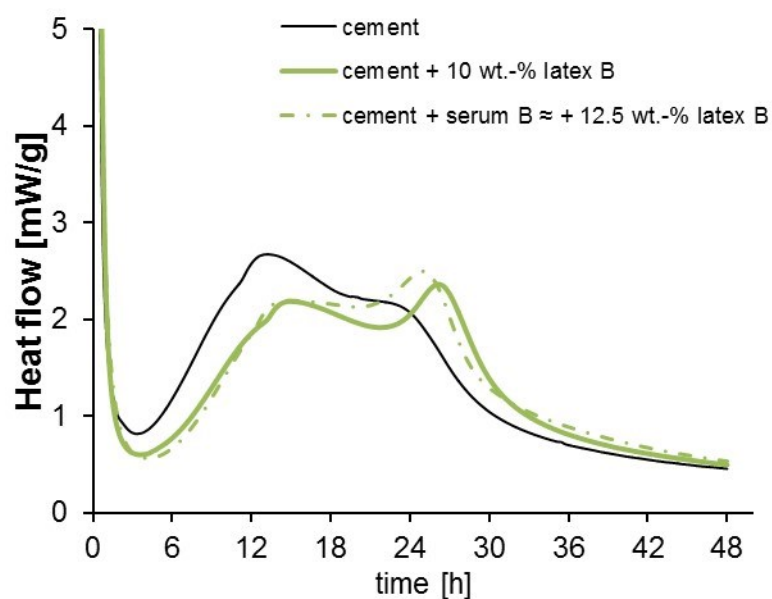
Figure B5 Heat of hydration during the first 48 h in the presence of 10 wt.-% latex B or serum B
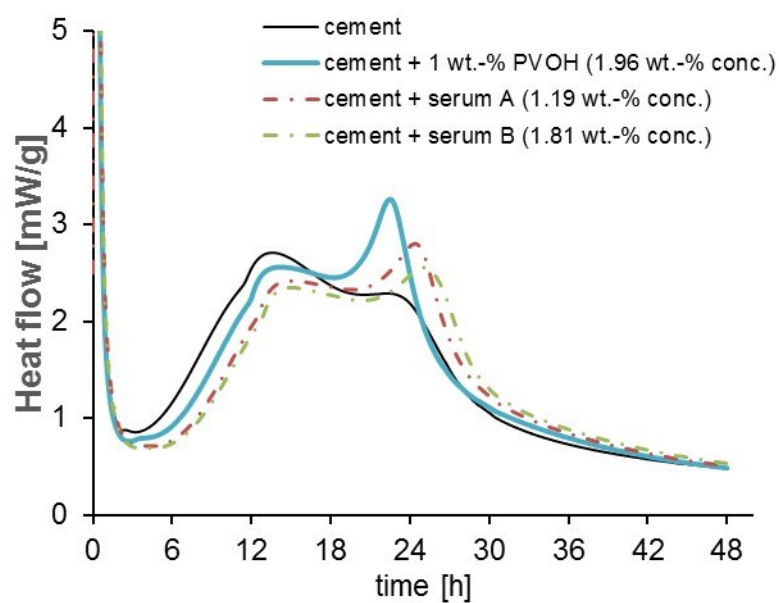

Figure B6 Heat of hydration during the first 48 h in the presence of PVOH or sera

References

[1] Ohama, Y., Handbook of polymer-modified concrete and mortars: Properties and process technology, Noyes Publications, Park Ridge, N.J, 1995.

[2] Miller, M., Polymers in Cementitious materials, Rapra Technology, Shawbury, Shrewsbury, Shropshire, U.K, 2005.

[3] van Gemert, D., Cement-Concrete and Concrete-Polymer Composites: Two Merging Worlds, in: Kyu-Seok, Y. (Ed.), Polymers in concrete, Kangwon National University, 2007, pp. 3–15.

[4] Ohama, Y., Polymer-based admixtures, Cement and Concrete Composites 20 (1998) 189–212.

[5] Sakai, E., Sugita, J., Composite mechanism of polymer modified cement, Cement and Concrete Research 25 (1995) 127–135.

[6] Su, Z., Sujata, K., Bijen, J., Jennings, H., Fraaij, A., The evolution of the microstructure in styrene acrylate polymer-modified cement pastes at the early stage of cement hydration, Advanced Cement Based Materials 3 (1996) 87–93.

[7] Nair, P.S., Thachil, E.T., Microstructural Studies of Cement Composites of Thermoplastics, Polymers & polymer composites 18 (2010) 75–83.

[8] Chandra, S., Ohama, Y., Polymers in concrete, CRC Press, Boca Raton, 1994.

[9] Beeldens, A., van Gemert, D., Schorn, H., Ohama, Y., Czarnecki, L., From microstructure to macrostructure: an integrated model of structure formation in polymer-modified concrete, Materials and Structures 38 (2005) 601–607.

[10] Do, J., Soh, Y., Performance of polymer-modified self-leveling mortars with high polymer–cement ratio for floor finishing, Cement and Concrete Research 33 (2003) 1497–1505.

[11] Betioli, A., Gleize, P., John, V., Pileggi, R., Effect of EVA on the fresh properties of cement paste, Cement and Concrete Composites 34 (2012) 255–260.

[12] Afridi, M., Ohama, Y., Demura, K., Iqbal, M., Development of polymer films by the coalescence of polymer particles in powdered and aqueous polymer-modified mortars, Cement and Concrete Research 33 (2003) 1715–1721.

[13] Baueregger, S., Perello, M., Plank, J., Influence of anti-caking agent kaolin on film formation of ethylene–vinylacetate and carboxylated styrene–butadiene latex polymers, Cement and Concrete Research 58 (2014) 112–120.

[14] Wang, R., Wang, P.-M., Formation of hydrates of calcium aluminates in cement pastes with different dosages of SBR powder, Construction and Building Materials 25 (2011) 736–741.

[15] Silva, D.A., Monteiro, P.J., The influence of polymers on the hydration of portland cement phases analyzed by soft X-ray transmission microscopy, Cement and Concrete Research 36 (2006) 1501–1507.

[16] Kaufmann, J., Winnefeld, F., Zurbriggen, R., Polymer dispersions and their interaction with mortar constituents and ceramic tile surfaces studied by zeta-potential measurements and atomic force microscopy, Cement and Concrete Composites 34 (2012) 604–611.

[17] Plank, J., Gretz, M., Study on the interaction between anionic and cationic latex particles and Portland cement, Colloids and Surfaces A: Physicochemical and Engineering Aspects 330 (2008) 227–233.

[18] Boutti, S., Urvoy, M., Dubois-Brugger, I., Graillat, C., Bourgeat-Lami, E., Spitz, R., Influence of Low Fractions of Styrene/Butyl Acrylate Polymer Latexes on Some Properties of Ordinary Portland Cement Mortars, Macromolecular Materials and Engineering 292 (2007) 33–45.

[19] Merlin, F., Guitouni, H., Mouhoubi, H., Mariot, S., Vallée, F., van Damme, H., Adsorption and heterocoagulation of nonionic surfactants and latex particles on cement hydrates, Journal of Colloid and Interface Science 281 (2005) 1–10.

[20] Betioli, A., Hoppe Filho, J., Cincotto, M., Gleize, P., Pileggi, R., Chemical interaction between EVA and Portland cement hydration at early-age, Construction and Building Materials 23 (2009) 3332–3336.

[21] Silva, D., Monteiro, P., Analysis of C_3A hydration using soft X-rays transmission microscopy: Effect of EVA copolymer, Cement and Concrete Research 35 (2005) 2026–2032.

[22] Silva, D., Monteiro, P., Hydration evolution of C_3S–EVA composites analyzed by soft X-ray microscopy, Cement and Concrete Research 35 (2005) 351–357.

[23] Lutz, H., Hahner, C., Applications of Redispersible Powders, in: Urban, D., Takamura, K. (Eds.), Polymer dispersions and their industrial applications, Wiley-VCH, Weinheim, 2002, pp. 329–354.

[24] Carrà, S., Sliepcevich, A., Canevarolo, A., Carrà, S., Grafting and adsorption of poly(vinyl) alcohol in vinyl acetate emulsion polymerization, Polymer 46 (2005) 1379–1384.

[25] Gilmore, C.M., Poehlein, G.W., Schork, F., Modeling poly(vinyl alcohol)-stabilized vinyl acetate emulsion polymerization. I. Theory, Journal of Applied Polymer Science 48 (1993) 1449–1460.

[26] Egret, H., Dimonie, V.L., Sudol, E.D., Klein, A., El-Aasser, M.S., Characterization of grafting in the emulsion polymerization of vinyl acetate using poly(vinyl alcohol) as stabilizer, Journal of Applied Polymer Science 82 (2001) 1739–1747.

[27] Yuki, K., Nakamae, M., Sato, T., Maruyama, H., Okaya, T., Physical properties of acrylic copolymer emulsions using poly(vinyl alcohol) as a protective colloid in comparison with those using surfactants, Polymer International 49 (2000) 1629–1635.

[28] Du Chesne, A., Bojkova, A., Gapinski, J., Seip, D., Fischer, P., Film Formation and Redispersion of Waterborne Latex Coatings, Journal of Colloid and Interface Science 224 (2000) 91–98.

[29] Urban, D., Distler, D., Introduction, in: Urban, D., Takamura, K. (Eds.), Polymer dispersions and their industrial applications, Wiley-VCH, Weinheim, 2002, pp. 1–14.

[30] Slomkowski, S., Alemán, J.V., Gilbert, R.G., Hess, M., Horie, K., Jones, R.G., Kubisa, P., Meisel, I., Mormann, W., Penczek, S., Stepto, R.F.T., Terminology of polymers and polymerization processes in dispersed systems (IUPAC Recommendations 2011), Pure and Applied Chemistry 83 (2011).

[31] Hiemenz, P.C., Rajagopalan, R., Principles of colloid and surface chemistry, 3rd ed., Marcel Dekker, New York, 1997.

[32] Ma, Y., Davis, H., Scriven, L., Microstructure development in drying latex coatings, Progress in Organic Coatings 52 (2005) 46–62.

[33] Warson, H., Finch, C.A., Fundamental chemistry of latices and applications in adhesives, Wiley, Chichester [u.a.], 2001.

[34] Sundberg, D.C., Durant, Y.G., Latex Particle Morphology, Fundamental Aspects: A Review, Polymer Reaction Engineering 11 (2003) 379–432.

[35] Elaissari, A. (Ed.), Colloidal polymers: Synthesis and characterization, M. Dekker, New York, 2003.

[36] Blackley, D.C., Polymer latices: Science and technology, 2nd ed., Chapman & Hall, London, New York, 1997.

[37] Collins, E.A., Measurement of Particle Size and Particle Size Distribution. Chapter 12, in: Lovell, P.A., El-Aasser, M.S. (Eds.), Emulsion polymerization and emulsion polymers, J. Wiley, New York, 1997, pp. 385–436.

[38] Hughes, R., An Introduction to Colloids, in: Cosgrove, T. (Ed.), Colloid science: Principles, methods and applications, 2nd ed., Wiley, Chichester, U.K, 2010, pp. 1–22.

[39] Gretz, M., Synthese und kolloidchemische Eigenschaften hydrider core shell Partikel und ihre mögliche Anwendung in der Bauchemie. Ph. D dissertation, Garching, Germany, 2010.

[40] Derjaguin, B., Landau, L., Theory of the stability of strongly charged lyophobic sols and of the adhesion of strongly charged particles in solutions of electrolytes, Progress in Surface Science 43 (1993) 30–59.

[41] Verwey, E. J. W., Overbeek, J. Th. G., Theory of the stability of lyophobic colloids: The interaction of sol particles having an electric double layer, Elsevier, Amsterdam, 1948.

[42] Israelachvili, J.N., Intermolecular and surface forces, 3rd ed., Academic Press, Burlington, MA, 2011.

[43] Rothstein, D., Thomas, J.J., Christensen, B.J., Jennings, H.M., Solubility behavior of Ca-, S-, Al-, and Si-bearing solid phases in Portland cement pore solutions as a function of hydration time, Cement and Concrete Research 32 (2002) 1663–1671.

[44] Kelzenberg, A.I., Tracy, S.L., Christiansen, B.J., Thomas, J.J., Clarage, M.E., Hodson, S., Jennings, H.M., Chemistry of the Aqueous Phase of Ordinary Portland, Journal of the American Ceramic Society 81 (1998) 2349–2359.

[45] Goto, T., Influence des paramètres moléculaires du latex sur l'hydratation, la rhéologie et les propriétés mécaniques des composites ciment/latex. Ph. D dissertation, Paris, France, 2006.

[46] Evans, R., Napper, D.H., Steric stabilization I: Comparison of theories with experiment, Kolloid-Zeitschrift und Zeitschrift für Polymere 251 (1973) 409–414.

[47] Hunter, R.J., Foundations of colloid science, Clarendon Press, New York, 1987.

[48] Teraoka, I., Polymer solutions: An introduction to physical properties, Wiley, New York, 2002.

[49] Klein, J., Interaction between surfaces with adsorbed polymers: poor solvents, Macromolecules 15 (1982) 1129–1135.

[50] Klein, J., Interactions between surfaces with adsorbed polymers: poor solvent: 2. Calculations and comparison with experiment 19 (1986) 1374–1381.

[51] Stenkamp, V.S., Steric and Electrosteric Stabilization of Colloids in Aqueous Salt Solutions. Ph. D dissertation, Washington, DC, 1999.

[52] Carraher, C.E., Seymour, R.B., Seymour/Carraher's polymer chemistry, 6th ed., M. Dekker, New York, 2003.

[53] German, A.L., van Herk, Alex M., Schoonbrood, Harold A. S., Aerdts, A.M., Latex Polymer Characterization. Chapter 11, in: Lovell, P.A., El-Aasser, M.S. (Eds.), Emulsion polymerization and emulsion polymers, J. Wiley, New York, 1997, pp. 343–384.

[54] Jones, R.G. (Ed.), Compendium of polymer terminology and nomenclature: IUPAC recommendations, 2008, Royal Society of Chemistry, Cambridge, 2009.

[55] Moad, G., Solomon, D.H., The chemistry of radical polymerization, 2nd ed., Elsevier, Amsterdam, Boston, 2006.

[56] Hiemenz, P.C., Lodge, T., Polymer chemistry, 2nd ed., CRC Press, Boca Raton, 2007.

[57] Odian, G.G., Principles of polymerization, 4th ed., Wiley, Hoboken, N.J, 2004.

[58] Vandezande, G.A., Smith, O.W., Bassett, D.R., Vinyl acetate Polymerization. Chapter 16, in: Lovell, P.A., El-Aasser, M.S. (Eds.), Emulsion polymerization and emulsion polymers, J. Wiley, New York, 1997, pp. 563–588.

[59] Erbil, H.Y., Vinyl acetate emulsion polymerization and copolymerization with acrylic monomers, CRC Press, Boca Raton, 2000.

[60] El-Aasser, M.S., Sudol, E.D., Features of Emulsion Polymerization. Chapter 2, in: Lovell, P.A., El-Aasser, M.S. (Eds.), Emulsion polymerization and emulsion polymers, J. Wiley, New York, 1997, pp. 36–58.

[61] Reynolds, G., Vinyl acetate-ethylene copolymer dispersions, British Polymer Journal 1 (1969) 233–238.

[62] Poljanšek, I., Fabjan, E., Burja, K., Kukanja, D., Emulsion copolymerization of vinyl acetate-ethylene in high pressure reactor-characterization by inline FTIR spectroscopy, Progress in Organic Coatings 76 (2013) 1798–1804.

[63] Chen, H., Lewis, M., Quantitative Determination of Vinyl Acetate Content of Ethylene-Vinyl Acetate Copolymers by High-Resolution Nuclear Magnetic Resonance, Analytical Chemistry 36 (1964) 1394–1396.

[64] Sung, H., Noggle, J., Carbon-13 NMR of poly(vinyl acetate) and ethylene-vinyl acetate copolymer, Journal of Polymer Science: Polymer Physics Edition 19 (1981) 1593–1602.

[65] Koopmans, R., Van der Linden, R., Vansant, E., Quantitative determination of the vinylacetate content in ethylene vinyl-acetate copolymers-a critical review, Polymer Engineering and Science 22 (1982) 878–882.

[66] Bugada, D.C., Rudin, A., Molecular structure and melting behaviour of ethylene-vinyl acetate copolymers, European Polymer Journal 28 (1992) 219–227.

[67] Scott, P., Penlidis, A., Rempel, G., Ethylene-vinyl acetate semi-batch emulsion copolymerization: Experimental design and preliminary screening experiments, Journal of Polymer Science Part A: Polymer Chemistry 31 (1993) 403–426.

[68] Scott, P., Penlidis, A., Rempel, G., Ethylene-vinyl acetate semi-batch emulsion copolymerization: Use of factorial experiments for improved process understanding, Journal of Polymer Science Part A: Polymer Chemistry 31 (1993) 2205–2230.

[69] Scott, P.J., Penlidis, A., Rempel, G.L., Lawrence, A.D., Ethylene-vinyl acetate semi-batch emulsion copolymerization: Use of factorial experiments for process optimization, Journal of Polymer Science Part A: Polymer Chemistry 32 (1994) 539–555.

[70] Gruber, B.A., Vratsanos, M.S., Smith, C.D., Effects of colloidal stabilizer on vinyl acetate-ethylene copolymer emulsions and films, Macromolecular Symposia 155 (2000) 163–170.

[71] Petrocelli, F.P., Cordeiro, C.F., Continuous process for the production of vinyl acetate-ethylene emulsion copolymers, Macromolecular Symposia 155 (2000) 39–52.

[72] Kim, N., Sudol, E.D., Dimonie, V.L., El-Aasser, M.S., Poly(vinyl alcohol) Stabilization of Acrylic Emulsion Polymers Using the Miniemulsion Approach, Macromolecules 36 (2003) 5573–5579.

[73] Noro, K., Emulsion polymerisation of vinyl acetate in relation to the chemical structure of polyvinyl alcohol, British Polymer Journal 2 (1970) 128–134.

[74] Marten, F.L., Vinyl Alcohol Polymers, in: Encyclopedia of Polymer Science and Technology, John Wiley & Sons, Inc, Hoboken, NJ, USA, 2002, pp. 399–437.

[75] Okaya, T., General Properties of Polyvinyl Alcohol in Relation to Its Applications. Chapter 1, in: Finch, C.A. (Ed.), Polyvinyl alcohol: Developments, Wiley, Chichester, New York, 1992, pp. 1–29.

[76] Clariant GmbH, Mowiol Polyvinyl Alcohol, 1999, http://www2.cbm.uam.es/confocal/Manuales/mowiol.pdf.

[77] He, J., Chen, J., Hellwich, K.-H., Hess, M., Horie, K., Jones, R.G., Kahovec, J., Kitayama, T., Kratochvíl, P., Meille, S.V., Mita, I., dos Santos, C., Vert, M., Vohlídal, J., Abbreviations of polymer names and guidelines for abbreviating polymer names (IUPAC Recommendations 2014), Pure and Applied Chemistry 86 (2014).

[78] Amiya, S., Tsuchiya, S., Qian, R., Nakajima, A., The Study of Microsturctures of Poly(vinyl alcohol) by NMR, Pure and Applied Chemistry 62 (1990) 2139–2146.

[79] Moritani, T., Kurama, I., Shibatani, K., Fujiwara, Y., Tacticity of Poly (vinyl alcohol) Studied by Nuclear Magnetic Resonance of Hydroxyl Protons, Macromolecules 5 (1972) 577–580.

[80] Budhlall, B.M., Landfester, K., Nagy, D., Sudol, E.D., Dimonie, V.L., Sagl, D., Klein, A., El-Aasser, M.S., Characterization of partially hydrolyzed poly(vinyl alcohol). I.: Sequence distribution via ^{1}H and ^{13}C-NMR and a reversed-phased gradient elution HPLC technique, Macromolecular Symposia 155 (2000) 63–84.

[81] Budhlall, B.M., Landfester, K., Sudol, E.D., Dimonie, V.L., Klein, A., El-Aasser, M.S., Characterization of Partially Hydrolyzed Poly(vinyl alcohol). Effect of Poly(vinyl alcohol) Molecular Architecture on Aqueous Phase Conformation, Macromolecules 36 (2003) 9477–9484.

[82] Toppet, S., Lemstra, P., Van der Velden, Geert, Nuclear magnetic resonance studies on sequence distributions in vinyl alcohol-vinyl acetate copolymers, Polymer 24 (1983) 507–512.

[83] Gilmore, C.M., Poehlein, G.W., Schork, F., Modeling poly(vinyl alcohol)-stabilized vinyl acetate emulsion polymerization. II. Comparison with experiment, Journal of Applied Polymer Science 48 (1993) 1461–1473.

[84] González, G. S. Magallanes, Dimonie, V.L., Sudol, E.D., Yue, H.J., Klein, A., El-Aasser, M.S., Characterization of poly(vinyl alcohol) during the emulsion polymerization of vinyl acetate using poly(vinyl alcohol) as emulsifier, Journal of Polymer Science Part A: Polymer Chemistry 34 (1996) 849–862.

[85] Budhlall, B.M., Sudol, E.D., Dimonie, V.L., Klein, A., El-Aasser, M.S., Role of grafting in the emulsion polymerization of vinyl acetate with poly(vinyl alcohol) as an emulsifier. I. Effect of the degree of blockiness on the kinetics and mechanism of grafting, Journal of Polymer Science Part A: Polymer Chemistry 39 (2001) 3633–3654.

[86] Keddie, J.L., Routh, A.F., Fundamentals of latex film formation: Processes and properties, Springer, Guildford, Berlin, 2010.

[87] Steward, P., Hearn, J., Wilkinson, M., An overview of polymer latex film formation and properties, Advances in Colloid and Interface Science 86 (2000) 195–267.

[88] Chen, X., Fischer, S., Men, Y., Temperature and Relative Humidity Dependency of Film Formation of Polymeric Latex Dispersions, Langmuir 27 (2011) 12807–12814.

[89] Baueregger, S., Perello, M., Plank, J., On the role of colloidal crystal-like domains in the film forming process of a carboxylated styrene-butadiene latex copolymer, Progress in Organic Coatings 77 (2014) 685–690.

[90] Ludwig, I., Schabel, W., Kind, M., Castaing, J.-C., Ferlin, P., Drying and film formation of industrial waterborne latices, AIChE Journal 53 (2007) 549–560.

[91] Rottstegge, J., Landfester, K., Wilhelm, M., Spiess, H., Heldmann, C., Different types of water in the film formation process of latex dispersions as detected by solid-state nuclear magnetic resonance spectroscopy, Colloid and Polymer Science 278 (2000) 236–244.

[92] Rottstegge, J., Traub, B., Wilhelm, M., Landfester, K., Heldmann, C., Spiess, H., Investigations on the Film-Formation Process of Latex Dispersions by Solid-State NMR Spectroscopy, Macromolecular Chemistry and Physics 204 (2003) 787–802.

[93] Routh, A.F., Russel, W.B., Deformation Mechanisms during Latex Film Formation: Experimental Evidence, Industrial & Engineering Chemistry Research 40 (2001) 4302–4308.

[94] Keddie, J.L., Film formation of latex, Materials Science and Engineering: R: Reports 21 (1997) 101–170.

[95] Sperry, P.R., Snyder, B.S., O'Dowd, M.L., Lesko, P.M., Role of Water in Particle Deformation and Compaction in Latex Film Formation, Langmiur 10 (1994) 2619–2628.

[96] Lin, F., Meier, D.J., A Study of Latex Film Formation by Atomic Force Microscopy. 1. A Comparison of Wet and Dry Conditions, Langmuir 11 (1995) 2726–2733.

[97] Jensen, O., Morgan, L., Particle size as it relates to the minimum film formation temperature of latices, Journal of Applied Polymer Science 42 (1991) 2845–2849.

[98] Keddie, J.L., Meredith, P., Jones, R. A. L., Donald, A.M., Rate-Limiting Steps in Film Formation of Acrylic Latices as Elucidated with Ellipsometry and Environmental Scanning Electron Microscopy, in: Provder, T., Winnik, M.A., Urban, M.W. (Eds.), Film formation in waterborne coatings, American Chemical Society, Washington, DC, 1996, pp. 332–348.

[99] Donald, A.M., He, C., Royall, C., Sferrazza, M., Stelmashenko, N.A., Thiel, B.L., Applications of environmental scanning electron microscopy to colloidal aggregation and film formation, Colloids and Surfaces A: Physicochemical and Engineering Aspects 174 (2000) 37–53.

[100] Keddie, J.L., Meredith, P., Jones, R. A. L., Donald, A.M., Kinetics of Film Formation in Acrylic Latices Studied with Multiple-Angle-of-Incidence Ellipsometry and Environmental SEM, Macromolecules 28 (1995) 2673–2682.

[101] Dragnevski, K., Donald, A., Taylor, P., Murray, M., Davies, S., Bone, E., Latex Film Formation in the Environmental Scanning Electron Microscope, Macromolecular Symposia 281 (2009) 119–125.

[102] Donald, A.M., The use of environmental scanning electron microscopy for imaging wet and insulating materials, Nature Materials 2 (2003) 511–516.

[103] Wang, Y., Winnik, M.A., Polymer diffusion across interfaces in latex films, Journal of Physical Chemistry B 97 (1993) 2507–2515.

[104] Urban, D., Takamura, K. (Eds.), Polymer dispersions and their industrial applications, Wiley-VCH, Weinheim, 2002.

[105] Kast, H., Aspects of film formation with emulsion copolymers, Die Makromolekulare Chemie 10 (1985) 447–461.

[106] Budhlall, B.M., Shaffer, O.L., Sudol, E.D., Dimonie, V.L., El-Aasser, M.S., Atomic Force Microscopy Studies of the Film Surface Characteristics of Poly(vinyl acetate) Latexes Prepared with Poly(vinyl alcohol), Langmuir 19 (2003) 9968–9972.

[107] Taylor, H. F. W, Cement chemistry, 2nd ed., T. Telford, London, 1997.

[108] Bishop, M., Bott, S.G., Barron, A.R., A New Mechanism for Cement Hydration Inhibition: Solid-State Chemistry of Calcium Nitrilotris(methylene)triphosphonate, Chemistry of Materials 15 (2003) 3074–3088.

[109] Holzer, L., Flatt, R.J., Erdoğan, S.T., Bullard, J.W., Garboczi, E.J., Shape Comparison between 0.4-2.0 and 20-60 μm Cement Particles, Journal of the American Ceramic Society (2010).

[110] Erdoğan, S., Nie, X., Stutzman, P., Garboczi, E., Micrometer-scale 3-D shape characterization of eight cements: Particle shape and cement chemistry, and the effect of particle shape on laser diffraction particle size measurement, Cement and Concrete Research 40 (2010) 731–739.

[111] Taylor, J., Aldridge, L., Matulis, C., Hinczak, I., Chapter 18 X-ray powder diffraction analysis of cements, in: Bensted, J., Barnes, P. (Eds.), Structure and performance of cements, 2nd ed., E & Fn Spon, London, 2002.

[112] Taylor, J., Hinczak, I., Matulis, C., Rietveld full-profile quantification of Portland cement clinker The importance of including a full crystallography of the major phase polymorphs, Powder Diffraction 15 (2000) 7–18.

[113] Snellings, R., Bazzoni, A., Scrivener, K., The existence of amorphous phase in Portland cements: Physical factors affecting Rietveld quantitative phase analysis, Cement and Concrete Research 59 (2014) 139–146.

[114] León-Reina, L., De la Torre,A. G., Porras-Vázquez, J.M., Cruz, M., Ordonez, L.M., Alcobé, X., Gispert-Guirado, F., Larrañaga-Varga, A., Paul, M., Fuellmann, T., Schmidt, R., Aranda, M.A.G., Round robin on Rietveld quantitative phase analysis of Portland cements, Journal of Applied Crystallography 42 (2009) 906–916.

[115] Whitfield, P., Mitchell, L., Quantitative Rietveld analysis of the amorphous content in cements and clinkers, Journal of Materials Science 38 (2003) 4415–4421.

[116] Stutzman, P., Scanning electron microscopy imaging of hydraulic cement microstructure, Cement and Concrete Composites 26 (2004) 957–966.

[117] Scrivener, K.L., The microstructure of anhydrous cement and its effect on hydration, MRS Proceedings 85 (1986) 39–46.

[118] Jeffery, J., The crystal structure of tricalcium silicate, Acta Crystallographica 5 (1952) 26–35.

[119]   Nishi, F., Takéuchi, Y., Maki, I., Tricalcium silicate $Ca_3O[SiO_4]$: The monoclinic superstructure, Zeitschrift für Kristallographie Supplements 172 (1985) 297–314.

[120]   Mumme, W.G., Crystal structure of tricalcium silicate from a Portland Cement clinker and its application to quantitative XRD analysis, Neues Jahrbuch für Mineralogie Monatsheft (1995) 145–160.

[121]   Noirfontaine, M.-N. de, Dunstetter, F., Courtial, M., Gasecki, G., Signes-Frehel, M., Polymorphism of tricalcium silicate, the major compound of Portland cement clinker: 2. Modelling alite for Rietveld analysis, an industrial challenge, Cement and Concrete Research 36 (2006) 54–64.

[122]   Dunstetter, F., Noirfontaine, M.-N. de, Courtial, M., Polymorphism of tricalcium silicate, the major compound of Portland cement clinker: 1. Structural data. review and unified analysis, Cement and Concrete Research 36 (2006) 39–53.

[123]   De la Torre, Ángeles G., Vera, R.N. de, Cuberos, A.J., Aranda, M.A., Crystal structure of low magnesium-content alite: Application to Rietveld quantitative phase analysis, Cement and Concrete Research 38 (2008) 1261–1269.

[124]   Ghosh, S.N., Rao, P. Bhaskara, Paul, A.K., Raina, K., The chemistry of dicalcium silicate mineral. Review, Journal of Materials Science 14 (1979) 1554–1566.

[125]   Mondal, P., Jeffery, J., The Crystal Structure of Tricalcium Aluminate, Ca3Al2O6, Structural Crystallography and Crystal Chemistry 31 (1975) 689–698.

[126]   Pöllmann, H., Chapter 2 Composition of cement phases, in: Bensted, J., Barnes, P. (Eds.), Structure and performance of cements, 2nd ed., E & Fn Spon, London, 2002, pp. 25–56.

[127]   Bensted, J., Gypsum in cements. Chapter 8, in: Bensted, J., Barnes, P. (Eds.), Structure and performance of cements, 2nd ed., E & Fn Spon, London, 2002, pp. 253–264.

[128]   Wade, L.G., Organic chemistry, 8th ed., Pearson Education; Pearson, Boston, 2013.

[129]   Atkins, K.M., Edmonds, R.N., Majumdar, A.J., The hydration of Portland and aluminous cements with added polymer dispersions, Journal of Materials Science 26 (1991) 2372–2378.

[130] Larbi, J., Bijen, J., Interaction of polymers with portland cement during hydration: A study of the chemistry of the pore solution of polymer-modified cement systems, Cement and Concrete Research 20 (1990) 139–147.

[131] Pöllmann, H., Sieksmeier, J., Dispersionspulver in zementären Systemen, ZKG International (2012) 56–61.

[132] Ma, H., Tian, Y., Li, Z., Interaction between Organic and Inorganic Phases in PA- and PU/PA-Modified-Cement-Based Materials, Journal of Materials in Civil Engineering 23 (2011) 1412–1421.

[133] Wang, R., Li, X.-G., Wang, P.-M., Influence of polymer on cement hydration in SBR-modified cement pastes, Cement and Concrete Research 36 (2006) 1744–1751.

[134] International Union of Pure and Applied Chemistry, Compendium of Chemical Terminology: Gold Book, 2014.

[135] Myers, D., Surfaces, interfaces, and colloids: Principles and applications, 2nd ed., Wiley-VCH, New York, 1999.

[136] Giles, C.H., Smith, D., Huitson, A., A general treatment and classification of the solute adsorption isotherm: I. Theoretical, Journal of Colloid and Interface Science 47 (1974) 755–765.

[137] Limousin, G., Gaudet, J.-P., Charlet, L., Szenknect, S., Barthès, V., Krimissa, M., Sorption isotherms: A review on physical bases, modeling and measurement, Applied Geochemistry 22 (2007) 249–275.

[138] Hinz, C., Description of sorption data with isotherm equations, Geoderma 99 (2001) 225–243.

[139] Adamczyk, Z., Adsorption of Particles: Theory, in: Encyclopedia of Surface and Colloid Science, Second Edition, Taylor & Francis, 2007, pp. 575-591.

[140] Pattanayek, S.K., Juvekar, V.A., Prediction of Adsorption of Nonionic Polymers from Aqueous Solutions to Solid Surfaces, Macromolecules 35 (2002) 9574–9585.

[141] Chibowski, Paszkiewicz, M., Studies of the Influence of Acetate Groups from Polyvinyl Alcohol on Adsorption and Electrochemical Properties of the TiO_2 – Polymer Solution Interface, Journal of Dispersion Science and Technology 22 (2001) 281–289.

[142] Backfolk, K., Rosenholm, J.B., Husband, J., Eklund, D., The influence of surface chemical properties of kaolin surfaces on the adsorption of poly(vinyl

alcohol), Colloids and Surfaces A: Physicochemical and Engineering Aspects 275 (2006) 133–141.

[143] Santhiya, D., Subramanian, S., Natarajan, K.A., Malghan, S.G., Surface Chemical Studies on the Competitive Adsorption of Poly(acrylic acid) and Poly(vinyl alcohol) onto Alumina, Journal of Colloid and Interface Science 216 (1999) 143–153.

[144] Labidi, N.S., Djebaili, A., Studies of The Mechanism of Polyvinyl Alcohol Adsorption on The Calcite/Water Interface in The Presence of Sodium Oleate, Journal of Minerals & materials Characterization & Engineering 7 (2008) 147–161.

[145] Feder, J., Random sequential adsorption, Journal of Theoretical Biology 87 (1980) 237–254.

[146] Johnson, C.A., Lenhoff, A.M., Adsorption of Charged Latex Particles on Mica Studied by Atomic Force Microscopy, Journal of Colloid and Interface Science 179 (1996) 587–599.

[147] Filby, A., Plaschke, M., Geckeis, H., AFM force spectroscopy study of carboxylated latex colloids interacting with mineral surfaces, Colloids and Surfaces A: Physicochemical and Engineering Aspects 414 (2012) 400–414.

[148] Adamczyk, Z., Particle adsorption and deposition: role of electrostatic interactions, Advances in Colloid and Interface Science 100-102 (2003) 267–347.

[149] Adamczyk, Z., Siwek, B., Musiał, E., Latex particle adsorption at heterogeneous surfaces, Colloids and Surfaces A: Physicochemical and Engineering Aspects 214 (2003) 219–229.

[150] Shen, C., Lazouskaya, V., Zhang, H., Li, B., Jin, Y., Huang, Y., Influence of surface chemical heterogeneity on attachment and detachment of microparticles, Colloids and Surfaces A: Physicochemical and Engineering Aspects 433 (2013) 14–29.

[151] Ramachandran, V.S. (Ed.), Handbook of thermal analysis of construction materials, Noyes Publications/William Andrew Pub., Norwich, N.Y, 2003.

[152] Bullard, J.W., Jennings, H.M., Livingston, R.A., Nonat, A., Scherer, G.W., Schweitzer, J.S., Scrivener, K.L., Thomas, J.J., Mechanisms of cement hydration, Cement and Concrete Research 41 (2011) 1208–1223.

[153] Scrivener, K.L., Nonat, A., Hydration of cementitious materials, present and future, Cement and Concrete Research 41 (2011) 651–665.

[154] Hesse, C., Goetz-Neunhoeffer, F., Neubauer, J., A new approach in quantitative in-situ XRD of cement pastes: Correlation of heat flow curves with early hydration reactions, Cement and Concrete Research 41 (2011) 123–128.

[155] Hesse, C., Goetz-Neunhoeffer, F., Neubauer, J., Braeu, M., Gaeberlein, P., Quantitative in situ X-ray diffraction analysis of early hydration of Portland cement at defined temperatures, Powder Diffraction 24 (2009) 112–115.

[156] Jansen, D., Goetz-Neunhoeffer, F., Lothenbach, B., Neubauer, J., The early hydration of Ordinary Portland Cement (OPC): An approach comparing measured heat flow with calculated heat flow from QXRD, Cement and Concrete Research 42 (2012) 134–138.

[157] Gartner, E.M., Young, J.F., Damidot, D., Jawed, I., Chapter 3 Hydration of Portland cement, in: Bensted, J., Barnes, P. (Eds.), Structure and performance of cements, 2nd ed., E & Fn Spon, London, 2002, pp. 57–113.

[158] Taylor, H.F.W., Barret, P., Brown, P.W., Double, D.D., Frohnsdorff, G., Johansen, V., Ménétrier-Sorrentino, D., Odler, I., Parrott, L.J., Pommersheim, J.M., Regourd, M., Young, J.F., The hydration of tricalcium silicate, Matériaux et Constructions 17 (1984) 457–468.

[159] Schlegel, M.-C., Sarfraz, A., Müller, U., Panne, U., Emmerling, F., First Seconds in a Building's Life-In Situ Synchrotron X-Ray Diffraction Study of Cement Hydration on the Millisecond Timescale, Angewandte Chemie International Edition 51 (2012) 4993–4996.

[160] Zingg, A., Holzer, L., Kaech, A., Winnefeld, F., Pakusch, J., Becker, S., Gauckler, L., The microstructure of dispersed and non-dispersed fresh cement pastes — New insight by cryo-microscopy, Cement and Concrete Research 38 (2008) 522–529.

[161] Matschei, T., Lothenbach, B., Glasser, F.P., Thermodynamic properties of Portland cement hydrates in the system $CaO–Al_2O_3–SiO_2–CaSO_4–CaCO_3–H_2O$, Cement and Concrete Research 37 (2007) 1379–1410.

[162] Bullard, J.W., Flatt, R.J., New Insights Into the Effect of Calcium Hydroxide Precipitation on the Kinetics of Tricalcium Silicate Hydration, Journal of the American Ceramic Society (2010).

[163] Juilland, P., Gallucci, E., Flatt, R., Scrivener, K., Dissolution theory applied to the induction period in alite hydration, Cement and Concrete Research 40 (2010) 831–844.

[164] Gartner, E., Discussion of the paper "Dissolution theory applied to the induction period in alite hydration" by P. Juilland et al., Cem. Concr. Res. 40 (2010) 831–844, Cement and Concrete Research 41 (2011) 560–562.

[165] Nicoleau, L., Schreiner, E., Nonat, A., Ion-specific effects influencing the dissolution of tricalcium silicate, Cement and Concrete Research 59 (2014) 118–138.

[166] Minard, H., Garrault, S., Regnaud, L., Nonat, A., Mechanisms and parameters controlling the tricalcium aluminate reactivity in the presence of gypsum, Cement and Concrete Research 37 (2007) 1418–1426.

[167] Pourchet, S., Regnaud, L., Perez, J., Nonat, A., Early C_3A hydration in the presence of different kinds of calcium sulfate, Cement and Concrete Research 39 (2009) 989–996.

[168] Quennoz, A., Scrivener, K.L., Hydration of C_3A–gypsum systems, Cement and Concrete Research 42 (2012) 1032–1041.

[169] Quennoz, A., Scrivener, K.L., Interactions between alite and C_3A-gypsum hydrations in model cements, Cement and Concrete Research 44 (2013) 46–54.

[170] Jansen, D., Götz-Neunhoeffer, F., Neubauer, J., Hergeth, W., Influence of polyvinyl alcohol on phase development during the hydration of Portland cement, ZKG International (2010) 100–107.

[171] Gretz, M., Plank, J., An ESEM investigation of latex film formation in cement pore solution, Cement and Concrete Research 41 (2011) 184–190.

[172] Dukhin, A.S., Goetz, P.J., Ultrasound for characterizing colloids: Particle sizing, zeta potential, rheology, Elsevier, Amstedam [u.a.], 2002.

[173] Kämmer, S.B., Introduction to Bruker's ScanAsyst and PeakForce Tapping Atomic Force Microscopy Technology, http://www.bruker.com/products/surface-analysis/atomic-force-microscopy/modes/modes-techniques/primary-modes/peakforce-tapping.html.

[174] Silverstein, R.M., Webster, F.X., Kiemle, D.J., Spectrometric identification of organic compounds, 7th ed., John Wiley & Sons, Hoboken, NJ, 2005.

[175] ASTM D2354-10, Test Method for Minimum Film Formation Temperature (MFFT) of Emulsion Vehicles, ASTM International, West Conshohocken, PA.

[176] Chui, J., Application of Thermogravimetry to the Study of High Polymers, Applied Polymer Symposia 2 (1966) 25–43.

[177] Böckenhoff, K., Fischer, W.R., Determination of electrokinetic charge with a particle-charge detector, and its relationship to the total charge, Fresenius' Journal of Analytical Chemistry 371 (2001) 670–674.

[178] Medala, M., Labbez, C., Pochard, I., Nonat, A., Ettringite surface chemistry: Interplay of electrostatic and ion specificity, Journal of Colloid and Interface Science 354 (2011) 765–770.

[179] Turesson, M., Labbez, C., Nonat, A., Calcium Mediated Polyelectrolyte Adsorption on Like-Charged Surfaces, Langmuir 27 (2011) 13572–13581.

[180] Flatt, R.J., Dispersion forces in cement suspensions, Cement and Concrete Research 34 (2004) 399–408.

[181] Walker, C.A., Kirby, J.T., Dentel, S.K., The Streaming Current Detector: A Quantitative Model, Journal of Colloid and Interface Science 182 (1996) 71–81.

[182] Chen, J., Heitmann, J.A., Hubbe, M.A., Dependency of polyelectrolyte complex stoichiometry on the order of addition. 1. Effect of salt concentration during streaming current titrations with strong poly-acid and poly-base, Colloids and Surfaces A: Physicochemical and Engineering Aspects 223 (2003) 215–230.

[183] Flatt, R.J., Bowen, P., Electrostatic repulsion between particles in cement suspensions: Domain of validity of linearized Poisson–Boltzmann equation for nonideal electrolytes, Cement and Concrete Research 33 (2003) 781–791.

[184] Koopal, L., Lyklema, J., Characterization of adsorbed polymers from double layer experiments, Journal of Electroanalytical Chemistry and Interfacial Electrochemistry 100 (1979) 895–912.

[185] Holmberg, K., Surfactants and polymers in aqueous solution, 2nd ed., John Wiley & Sons, Chichester [etc.], op. 2003.

[186] Yamada, K., Basics of analytical methods used for the investigation of interaction mechanism between cements and superplasticizers, Cement and Concrete Research 41 (2011) 793–798.

[187] Allen, T., Particle size measurement, 5th ed., Chapman & Hall, London, New York, 1997.

[188]   Edmonds, R.N., Majumdar, A.J., The hydration of an aluminous cement with added polyvinyl alcohol-acetate, Journal of Materials Science 24 (1989) 3813–3818.

[189]   Kotwica, Ł., Małolepszy, J., Chemical aspects of EVA redispersible powders influence on the hydration of tricalcium aluminate, in: Siasa Congresos S.A., Palomo, A., Zaragoza, A., López Agüí, Juan Carlos (Eds.), Cementing a sustainable future: XIII ICCC International Congress on the Chemistry of Cement, Madrid, 3-8 July, 2011 Abstracts and Proceedings, Instituto de Ciencias de la Construcción, Madrid, 2011.

[190]   Mansur, A.A., Nascimento, O.L.d., Mansur, H.S., Physico-chemical characterization of EVA-modified mortar and porcelain tiles interfaces, Cement and Concrete Research 39 (2009) 1199–1208.

[191]   Wadsö, L., Applications of an eight-channel isothermal conduction calorimeter for cement hydration studies, Cement International (2005) 94–101.

[192]   Keller, H., Plank, J., Mineralisation of $CaCO_3$ in the presence of polycarboxylate comb polymers, Cement and Concrete Research 54 (2013) 1–11.

[193]   Hosoda, N., Sugawara, A., Kato, T., Template Effect of Crystalline Poly(vinyl alcohol) for Selective Formation of Aragonite and Vaterite $CaCO_3$ Thin Films, Macromolecules 36 (2003) 6449–6452.

[194]   Marentette, J.M., Norwig, J., Stöckelmann, E., Meyer, W.H., Wegner, G., Crystallization of $CaCO_3$ in the presence of PEO-block-PMAA copolymers, Advanced Materials 9 (1997) 647–651.

[195]   Yuan, T., Wang, J., Li, Z., Measurement and modelling of solubility for calcium sulfate dihydrate and calcium hydroxide in NaOH/KOH solutions, Fluid Phase Equilibria 297 (2010) 129–137.

[196]   Brandt, F., Bosbach, D., Bassanite ($CaSO_4 \cdot 0.5H_2O$) dissolution and gypsum ($CaSO_4 \cdot 2H_2O$) precipitation in the presence of cellulose ethers, Journal of Crystal Growth 233 (2001) 837–845.

[197]   Kalina, L., Másilko, J., Koplík, J., Šoukal, F., XPS characterization of polymer–monocalcium aluminate interface, Cement and Concrete Research 66 (2014) 110–114.

[198] Möschner, G., Lothenbach, B., Figi, R., Kretzschmar, R., Influence of citric acid on the hydration of Portland cement, Cement and Concrete Research 39 (2009) 275–282.

[199] Parkhurst, D.L., Appelo, C., User's guide to PHREEQC—a computer program for speciation, reaction-path, advective transport, and inverse geochemical calculations: Water-Resources Investigations Report 99-4259, 1999.

[200] Jacques, D., Benchmarking of the cement model and detrimental chemical reactions including temperature dependent parameters, 2009, http://science.sckcen.be/en/Disposal_radioactive_waste/Safety_assessment_near_surface_disposal/concrete_durability_assessment.

[201] Richardson, I., The calcium silicate hydrates, Cement and Concrete Research 38 (2008) 137–158.

[202] Mitchell, L.D., Margeson, J.C., Whitfield, P.S., Quantitative Rietveld analysis of hydrated cementitious systems, Powder Diffraction 21 (2006) 111–113.

[203] Goetz-Neunhoeffer, F., Neubauer, J., Schwesig, P., Mineralogical characteristics of Ettringites synthesized from solutions and suspensions, Cement and Concrete Research 36 (2006) 65–70.

[204] Chaix-Pluchery, O., Pannetier, J., Bouillot, J., Niepce, J., Structural prereactional transformations in $Ca(OH)_2$, Journal of Solid State Chemistry 67 (1987) 225–234.

[205] Hawthorne, F., Ferguson, R., Anhydrous Sulphates II Refinement of the Crystal Structure of Anhydrite, Canadian Mineralogist 13 (1975) 289–292.

[206] Goetz-Neunhoeffer, F., Neubauer, J., Refined ettringite $(Ca_6Al_2(SO_4)_3(OH)_{12}\cdot26H_2O)$ structure for quantitative X-ray diffraction analysis, Powder Diffraction 21 (2006) 4–11.

[207] Messersmith, P.B., Stupp, S.I., Synthesis and Properties of Poly(Vinyl Alcohol)/Calcium Aluminate Nanocomposites, MRS Proceedings 245 (1991).

[208] Messersmith, P.B., Synthesis and characterization of novel polymer ceramic nanocomposites Organoceramics. Ph. D dissertation, Urbana-Champaign, United States of America, 1993.

[209] Lothenbach, B., Pelletier-Chaignat, L., Winnefeld, F., Stability in the system CaO–Al2O3–H2O, Cement and Concrete Research 42 (2012) 1621–1634.

[210] Ucar, I., Doganci, M., Cansoy, C., Erbil, H., Avramova, I., Suzer, S., Combined XPS and contact angle studies of ethylene vinyl acetate and polyvinyl acetate blends, Applied Surface Science 257 (2011) 9587–9594.

[211] Beaudoin, J.J., Marchand, J., Pore Sturcture, in: Ramachandran, V.S., Beaudoin, J.J. (Eds.), Handbook of analytical techniques in concrete science and technology: Principles, techniques, and applications, Noyes Publications; William Andrew Pub., Park Ridge, N.J, Norwich, N.Y, 2001, pp. 528–628.

[212] Rottstegge, J., Arnold, M., Herschke, L., Glasser, G., Wilhelm, M., Spiess, H., Hergeth, W., Solid state NMR and LVSEM studies on the hardening of latex modified tile mortar systems, Cement and Concrete Research 35 (2005) 2233–2243.

[213] Visschers, M., Laven, J., van der Linde, R., Forces operative during film formation from latex dispersions, Progress in Organic Coatings 31 (1997) 311–323.

[214] Jönsson, B., Nonat, A., Labbez, C., Cabane, B., Wennerström, H., Controlling the Cohesion of Cement Paste, Langmuir 21 (2005) 9211–9221.

[215] Nachbaur, L., Nkinamubanz, P.-C., Nonat, A., Mutin, J.-C., Electrokinetic Properties which Control the Coagulation of Silicate Cement Suspensions during Early Age Hydration, Journal of Colloid and Interface Science 202 (1998) 261–268.

[216] Mishra, R.K., Flatt, R.J., Heinz, H., Force Field for Tricalcium Silicate and Insight into Nanoscale Properties: Cleavage, Initial Hydration, and Adsorption of Organic Molecules, The Journal of Physical Chemistry C 117 (2013) 10417–10432.

[217] Dean, J.A., Lange, N.A., Lange's handbook of chemistry, 15th ed., McGraw-Hill, New York, NY [u.a.], 1999.

[218] Parsegian, V.A., Van der Waals forces: A handbook for biologists, chemists, engineers, and physicists, Cambridge University Press, New York, 2006.

[219] Melis, S., Kemmere, M., Meuldijk, J., Storti, G., Morbidelli, M., A model for the coagulation of polyvinyl acetate particles in emulsion, Chemical Engineering Science 55 (2000) 3101–3111.